國 立 交 通 大 學

電控工程研究所

博 士 論 文

基於傳遞函數比與非線性 H_∞ 濾波器之穩健適應性語音純化波束形成器

Robust Adaptive Beamformer for Speech Enhancement based on the Transfer Function Ratio and Nonlinear H_∞ Filter

研究生：楊佳興

指導教授：胡竹生

中華民國九十九年十二月

基於傳遞函數比與非線性 H_∞ 濾波器之穩健適應性語音純化波束形成器

Robust Adaptive Beamformer for Speech Enhancement based on the Transfer Function Ratio and Nonlinear H_∞ Filter

研 究 生：楊 佳 興　　Student：Chia-Hsin Yang

指導教授：胡 竹 生　　Advisor：Jwu-Sheng Hu

國立交通大學

電控工程研究所

博 士 論 文

A Dissertation

Submitted to Institute of Electrical Control Engineering

College of Electrical and Computer Engineering

National Chiao Tung University

in partial Fulfillment of the Requirements

for the Degree of

Doctor of Philosophy

in

Institute of Electrical Control Engineering

Dec. 2010

Hsinchu, Taiwan, Republic of China

中華民國九十九年十二月

基於傳遞函數比與非線性 H_∞ 濾波器之穩健適應性語音純化波束形成器

研究生：楊佳興　　指導教授：胡竹生 教授

國立交通大學電控工程研究所博士班

摘要

在過去三十年中，利用麥克風陣列純化語音的技巧已受到許多研究者的專注。在許多現實環境中，目標語音訊號通常受穩態雜訊與多個非穩態雜訊所干擾。本論文的目標為利用均勻線性麥克風陣列提供一滿意的波束形成器(亦稱空間濾波器)效能與穩健度對抗背景雜訊與空間響應效應。本論文提出兩種適應性空間濾波器：以傳遞函數比為基礎之適應性空間濾波器與以二階延伸 H_∞ 濾波器為基礎之穩健最小變異無失真響應空間濾波器。

在第一類適應性空間濾波器中，傳遞函數比為事先利用系統識別方法來模型。本論文提出的以傳遞函數比為基礎之適應性空間濾波器由傳遞函數比空間濾波器與多通道適應性濾波器所構成。傳遞函數比空間濾波器用以消除多個非穩態訊號中的主要部分，而目標語音訊號的通道效應則由傳遞函數比的資訊來同化。由於 H_∞ 濾波器能較穩健於模型誤差，因此從傳遞函數比空間濾波器輸出的剩餘雜訊訊號則由限制 H_∞ 濾波器來消除。此外，本論文提出虛擬聲源的觀念用以簡化多個非穩態訊號的空間複雜度。

在第二類適應性空間濾波器中，傳遞函數假設為一單純延遲模型與一不確定數的組合。本論文提出一新的方法用來實現穩健最小變異無失真響應空間濾波器。穩健最小變異無失真響應空間濾波器是設計在最差效能下最佳化的結果，此濾波器對於目標訊號方向向量誤差提供了絕佳的穩健度。為了方便即時性的實現，此種空間濾波器曾轉化為狀態空間模型並利用二階延伸 Kalman 濾波器來實現。然而，二階延伸 Kalman 濾波器假設系統動態為已知並假設雜訊為零平均與已知變異量。此類假設會影響穩健最小變異無失真響應空間濾波器的效能。本論文發展與推導二階延伸 H_∞ 濾波器並用以實現穩健最小變異無失真響應空間濾波器。二階延伸 H_∞ 濾波器是在最差情況下最小化估測誤差並對雜訊統計特性並無假設。最後，本論文提供模擬與真實環境實驗結果用以驗證演算法效能。

Robust Adaptive Beamformer for Speech Enhancement based on the Transfer Function Ratio and Nonlinear H_∞ Filter

Graduate Student: Chia-Hsin Yang Advisor: Prof. Jwu-Sheng Hu

Institute of Electrical Control Engineering
National Chiao-Tung University

Abstract

Speech enhancement techniques, utilizing microphone array, have attracted attentions of many researchers for the last thirty years. In many practical environments, the desired speech signal is usually contaminated not only by stationary noise but also multiple nonstationay interferences, such as competing speech signals. The objective of this dissertation is to design robust adaptive beamfromers to reduce background noise and compensate channel effects using a uniform linear microphone array. Two adaptive beamformers, the transfer function ratio (TFR)-based adaptive beamformer and the robust adaptive beamformer based on the second-order extended (SOE) H_∞ filter, are proposed in this dissertation.

In the first adaptive beamformer, the TFR is obtained using the system identification method in advance. The proposed TFR-based adaptive beamformer consists of the TFR beamformer and multi-channel adaptive filter algorithm. The TFR beamformer is used to block the major component of the multiple interference signals and the associated information is then used to equalize the channel effect of the desired speech. The residual noise from the TFR beamformer output is suppressed by the constrained H_∞ filter due to its robustness to the modeling error. In addition, the

virtual sound source concept is proposed to simplify the theoretical treatment for multiple competing speech signals.

In the second adaptive beamformer, a novel approach to implement the robust minimum variance distortionless response (MVDR) beamformer is proposed where the acoustic transfer function is assumed to be delay-only propagation with uncertainty. The robust MVDR beamformer is to optimize the worst-case performance for an arbitrary but norm-bounded desired signal steering vector mismatch. For real-time consideration, the beamformer was formulated into a state-space observer form and the SOE Kalman filter was derived. However, the SOE Kalman filter assumes an accurate system dynamic and known statistics of the noise signals. These assumptions limit the performance under various uncertainties. This dissertation develops the SOE H_∞ filter for the implementation of the robust MVDR beamformer. The estimation criterion in the SOE H_∞ filter design is to minimize the worst possible effects of the disturbance signals on the signal estimation errors without a priori knowledge of the disturbance signals statistics. Finally, the results from simulations and practical experiments are provided as proof of the performance of these proposed approaches.

致 謝

對於本論文的完成，首先要感謝的是指導教授胡竹生教授對我多年的辛勤指導。在碩士與博士班七年多中，我感受到胡教授對研究的熱忱與豐富的學問。在我博士班期間，投稿被退件的次數已經多到我數不出來，但老師總是能不斷的鼓勵我，開始舉例某位大師當年也是沒人要他的論文，最後才被發現是曠世傑作.....等等，希望我不要灰心，雖然我的論文應該稱不上什麼千古文章，但老師對我的永不放棄，讓我非常窩心與感動。也謝謝老師讓我參與各種計畫與競賽，讓我在理論與實作之間都有更深入的了解。此外，我非常感謝老師能推薦我在博士班期間去加州大學柏克萊分校從事七個月的短期研究，等於圓了我從小想出國讀書的夢，謝謝老師!

在這些日子，感謝實驗室同伴的陪伴。首先感謝學長們，立偉、价呈、宗敏、維瀚、昊群、憶如、Angel、鳥哥、家瑋、俊德、pazz 與康康，感謝你們在研究上的幫助與人生道路上的指引。感謝一起做計畫的麥克風陣列組所有的同伴，价呈、維瀚、晏榮、經展、papa、高手啟揚與辛苦的明唐，跟你們一起奮鬥，讓我感覺非常光榮。當然，感謝實驗室所有的同學與學弟妹們，一起讀博班的鏗元、不帥的士奇、去當美國人的岑思、群棋、硬體設計超強的育德、沒大沒小的朱木、螞蟻、鳥蕙、佩靜、耀賢、恆嘉、當爸爸的永融、做主任的弘齡、天才楷祥、長官 Alpha、認真的勁源、瓊文、超強助教阿吉、古意的俊宇、超愛唱歌的 Gun、英文超好的嘟嘟、超壯又不怕冷的 Judo、一起去深圳比賽的 Lundy、肉鬆、很會做甜點的小蔡、中文講得很好的阿 him、中文講得不錯的 Rodolfo、沛錡、愛跳傘的 Simon、客氣的 Artis、一起搞 H_∞的育成、不小心當主長的新文、冷靜的昀軒、小畫家很強的 macaca、湘筑、學文、建安、前兩名畢業的昭男與耕維。有了你們大家的陪伴、讓研究生生活充滿了許多歡樂。

感謝這幾年一路陪我走來的淑伶，謝謝妳平日的包容與付出並對我讀博士班期間不離不棄的鼓勵，妳的陪伴讓我的人生更完美。感謝從國中一路陪伴到現在

的好友們，當爸爸的貝克漢、當媽媽的齡尹、帥又有錢的英傑、毅修、鳥佐、Bellavita 首席公關凱玲、丁丁丁及胖子，謝謝你們的陪伴，讓我們大家 keep walking。

當然，最感謝的就是我的家人，老爸楊忠民先生、老媽李碧雪女士、哥哥佳元及大嫂雅芳，因為有你們無條件的支持與鼓勵，並且給我一個溫暖的家，我才能無後顧之憂進行我的學業，謝謝你們。也感謝我的叔叔楊孝志先生及楊仁祥先生還有姑姑楊雪娥女士，謝謝你們在生活上的幫助與精神上的鼓勵，讓我的人生能更有信心與方向。謹以本論文向家人獻上最誠摯的謝意。

從小到大，老爸總是不斷得講一些人生大道理，像是「物不經寒暑者必不堅凝，人不歷酸辛者必不諳練」，不然就是麥帥位子祈禱文「願你引導他不求安逸、舒適，相反的，經過壓力、艱難和挑戰，學習在風暴中挺身站立，學會憐恤那些在重壓之下失敗的人」...等等諸如此類的話。或許老天爺真的有感受到我爸的期望，讓我深深體會到讀博士班這段期間真的很辛苦，也因為這樣的體會讓我能堅強的認識到自己的軟弱並對未來無限大的挑戰能更具信心與勇氣。今天，我總算完成了生命中我給自己的階段性任務，願在未來的日子能夠不忘過去教訓，勇敢地實現理想，祝福大家順心如意，謝謝。

Contents

List of Tables

List of Figures

Index

Chapter 1

Introduction

Background noise and reverberation could seriously deteriorate the quality of speech signals received by sensors. Speech enhancement algorithms have therefore attracted a great deal of interest in the past three decades. For removing unwanted interference and noise from the desired signal, microphone array processing techniques are widely used. Speech enhancement algorithms using microphone array typically incorporate both spatial and spectral information. Hence, they have the potential to outrun methods using a single microphone where only the spectral information can be used. Among several existing microphone-array-based enhancement algorithms, beamformer is one of the most popular methods and was extensively studied for hands-free speech communication or recognition.

1.1 Overview of Beamformers

In speech communication, if the desired signal and the interfering signals occupy the same frequency band, it is difficult for temporal or spectral filtering methods to

separate the signal from the interferences. However the desired and the interfering signals are usually emitted from different spatial locations. This location difference can be exploited to separate them using a beamformer. A beamformer is an array of microphones which provide spatial information regarding acoustic dynamics of the sources. Typically, a beamformer linearly combines the spatially sampled waveform from each microphone in the same way as the finite impulse response (FIR) filter combines the temporally sampled data. The diagram of a beamformer with M microphones is shown in Fig. 1-1.

In the following, the existing beamformers are explained in two categories: fix beamformers and adaptive beamformers.

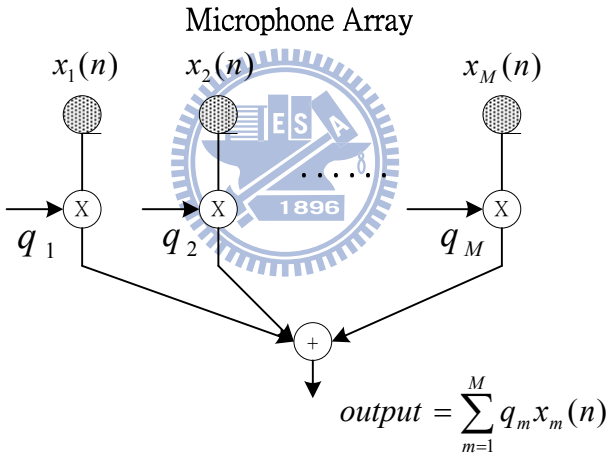

Figure 1-1 Diagram of the beamformer

1.1.1 Fix Beamformers

Fix beamformers includes delay-and-sum beamformer (DSB) [1], constant directivity beamformer (CDB) [2-4] and fixed superdirective beamformers [5-7]. They utilize fixed coefficients to achieve a desired spatial response. The DSB is the simplest structure in fixed beamformer and it first compensates for the relative time delay between distinct microphone signals and then sums the steered signal to form a single output. Jan and Flanagan [8] explicitly modeled the transfer function from source to

sensors to replace the simple delay assumption. Further, they extended the DSB concept by introducing the matched filter array beamformer. CDB is designed such that the spatial response is the same over a wide frequency band while the fixed superdirective beamformer attempts to suppress noise coming from all directions without affecting the desired speech signal from a principal direction. Fix beamformers generally assume the desired sound source, interference signals, and noises are slowly varying and at known locations. Therefore, these algorithms are sensitive to steering errors which limit their noises suppression performance and cause the desired signal distortion or cancellation. Furthermore, these algorithms also have limited performance under highly reverberation environments.

1.1.2 Adaptive Beamformers

Instead of using fixed coefficients to suppress noises and interference signals, an adaptive beamformer [9-14] can adaptively forms its directivity beam-pattern to the desired signal and its null beam-pattern to the undesired signals. In the fixed beamformers, the null beam-pattern exists when the noise's direction is known and remains unchanged. To cope with environmental changes, various adaptive beamformers were proposed to improve the performance. One of the key issues in adaptive beamformers is the sensitivity due to the mismatch between the actual desired signal steering vector and the presumed one [11], [12]. The mismatch can be induced by signal point errors [13], imperfect array calibration [14], or the channel effect (e.g., near-far problem [15], environment heterogeneity [16] and source local scattering [17]). In the presence of these effects, an adaptive beamformer can easily mix up the desired signal and interference components; that is, it suppress the desired signal instead of maintaining distortionless response. This phenomenon is commonly

referred to as *signal self-nulling* [18]. As a result, much effort has been devoted to the robustness issues [11].

Modifications to adaptive beamformer techniques for robustness were extensively studied. The linearly constrained minimum variance (LCMV) beamformer was proposed in [9] to minimize the array output power under a look-direction constraint. Another popular technique is the generalized sidelobe canceler (GSC) algorithm which essentially transforms the LCMV constrained minimization problem into an unconstrained one [10]. In the last decade, several techniques addressing this problem of the mismatch of the steering vector in the LCMV or GSC structure were developed [19]-[23]. For example, Hoshuyama *et al* [20] proposed two robust constraints on blocking matrix design. Spriet *et al* [22] proposed a robust adaptive beamformer called the spatially pre-processed speech distortion weighted multichannel Wiener filter which takes speech distortion into account in its optimization criterion and encompasses the standard GSC as a special case. Further, some *ad hoc* approaches were discussed to overcome the arbitrary desired signal mismatches, such as the diagonal loading of the sample covariance matrix [24], [25] and the eigenspace-based beamformer [26], [27].

1.1.3 Explicit Transfer Function Modeling for Adaptive beamformers

The other method to mitigate the problem of signal steering vector mismatch for adaptive beamformer is to abandon the delay-only propagation assumption and explicitly model the sound signal propagation from the source to the microphones by an arbitrary transfer function (TF) [28]. Affes and Grenier presented GSC-based near-field beamformer [29] using matched filters with signal subspace tracking. The matched filters which can be identified by the proposed signal subspace tracking

algorithm under the assumption of the FIR model and small displacements of the talker is used to design the fixed beamformer (FB) of the GSC.

Rather than estimating the TF, Gannot *et al.* [30] proposed the transfer function ratio (TFR) concept and applied to the GSC algorithm. The TFR can be estimated by exploiting the nonstationary characteristics of the desired signal. The suboptimal speech enhancement algorithm that can be implemented by using TFR to design the FB and blocking matrix (BM) of GSC is proposed. Several adaptive beamformer algorithms based on the GSC structure using TF ratio information have been proposed [31]-[33]. Dahl *et al.* [34] proposed a reference signal based adaptive beamformer which can suppress the nonstationary and stationary noise as well as recover the reverberation at the same time. This method uses FIR based normalized least-mean-square (NLMS) filtering approach to perform noise suppression and speech dereverberation by using pre-recorded speech signals and the desired signal acquired when the environment is quiet. Improvements on the finite number of taps in the FIR filters and relaxation on the disturbance assumption were studied [35]. Huang *et al.* [36], [37] treated a microphone array as a multiple-input multiple-output (MIMO) system and proposed a two-stage procedure for separation and dereverberation of speech signals. The interference signals can be removed by using two microphones with known TFs and the separated reverberant speech can be dereverberated by using the multiple-input/output inverse theorem. However, the stationary noise is neglected in this work and the transfer function of each speech source should be identified in advance during each single-talk interval which also limits its applications in practice.

1.1.4 Uncertainty of the Steering Vector for Adaptive beamformers

Most of the early methods of making the adaptive beamformers more robust to the steering vector errors are rather *as hoc* in that the choice of their parameters or the structural modifications is not directly related to the uncertainty of the steering vector [11]. Recently, Vorobyov *et al* proposed a new approach to robust adaptive beamforming in the presence of an arbitrary unknown steering vector mismatch [38]. This approach is based on the optimization of worst-case performance. They also showed that the robust minimum variance distortionless response (MVDR) beamformer using worst-case performance optimization can be formulated as a second-order cone program and solved in polynomial time via the interior point method. In further works, [40]-[44], several extensions of the robust MVDR beamformer of [38] have been considered.

1.2 Outline of Proposed Beamformers

The objective of this dissertation is to provide satisfactory beamfromer performance and robustness to background noise and channel effects using a uniform linear microphone array. Two adaptive beamformers, TFR-based adaptive beamformer and robust adaptive beamformer based on the second-order extended (SOE) H_∞ filter, which can be categorized into Section 1.1.3 and 1.1.4 are proposed in this dissertation.

1.2.1 Transfer Function Ratio-Based Adaptive Beamformer

The first beamformer, TFR-based adaptive beamformer, belongs to the category of Section 1.1.3 since a pre-training procedure is needed to explicitly model the TFR. The TFR-based adaptive beamformer is designed to extract the desired speech signal

while attenuating multiple competing speeches in a reverberant and noisy environment. The proposed method uses TFR beamformer and multi-channel adaptive filter algorithm to perform speech enhancement. The TFR beamformer is utilized to block the major component of the interference signals and the channel effect of the desired speech is adjusted by the TFR information. The residual noise signals from the TFR beamformer output are suppressed by the constrained H_∞ filter. In addition, the virtual sound source concept is proposed to simplify the treatment for multiple competing speeches.

1.2.2 Robust Adaptive Beamformer Based on the Second-Order Extended H_∞ Filter

The second beamformer, robust adaptive beamformer based on the SOE H_∞ filter, belongs to the category of Section 1.1.4 since the beamformer structure is based on the robust MVDR beamformer of [38] which assumes that the transfer function is a delay-only propagation with an uncertainty. This dissertation develops the SOE H_∞ filter for the implementation of the robust MVDR beamformer and the SOE H_∞ filter is derived by the game theory approach. The estimation criterion in the SOE H_∞ filter design is to minimize the worst possible effects of the disturbance signals on the signal estimation errors without priori knowledge. The proposed beamformer is compared with the existing robust adaptive beamformer based on the SOE Kalman filter.

1.3 Contribution of this Dissertation

The contribution of this dissertation is to propose and implement innovative

algorithms for speech enhancement. This dissertation proposes two adaptive beamformers, TFR-based adaptive beamformer and robust adaptive beamformer based on the SOE H_∞ filter.

1. Speech enhancement in a reverberant noisy environment with multiple competing speech signals is still a difficult problem. The challenge lies in the coexistence of spatial interference from competing sources and temporal echoes due to room reverberation in the received signals. In the TFR-based adaptive beamformer, a novel beamformer structure is proposed and the constrained H_∞ filter is applied to overcome the problem above. In addition, the virtual sound source concept is proposed to simplify the multiple competing speech signals and explain the component blocked by the TFR beamformer.
2. Many efforts have been considered to expand the H_∞ filter to different domains and to improve performance. However, no work has been done on considering the second-order extended case similar to that of the SOE Kalman filter. In this dissertation, a SOE H_∞ filter for a nonlinear discrete time system is derived based on the game theory approach. A numerical example is given to compare the proposed SOE H_∞ filter with the first-order extended H_∞ filter, and the SOE Kalman filter.
3. The robust MVDR beamformer of [38] has been implemented by the SOE Kalman filter [44]. However, the assumptions of the SOE Kalman filter about the disturbance limit the beamformer performance. The proposed SOE H_∞ filter is applied to implement the robust MVDR beamformer of [38] for speech enhancement to improve the issue above.

1.4 Dissertation Organization

The remainder of this dissertation is organized as follows. The TFR-based adaptive beamformer is introduced in Chapter 2. Chapter 3 presents the robust adaptive beamformer based on the SOE H_∞ filter. Also, the SOE H_∞ filter solution of a general nonlinear discrete-time system is provided and the detail derivation is given in the Appendix I-IV. Chapter 4 shows the experimental results in both simulated room and real environment. Finally, conclusion and future work are drawn in Chapter 5.

Chapter 2

Transfer Function Ratio-Based Adaptive Beamformer

2.1 Introduction

Speech enhancement in the presence of multiple competing speech signals under a reverberant and noisy environment is still a difficult problem. The challenge lies in the coexistence of spatial competing sources and temporal echoes from room reverberation [74]. This dissertation considers speech enhancement problem under multiple speech sources in a reverberant and noisy environment condition and we focus on reconstructing the desired speech while suppressing competing speech sources and stationary noise. To deal with this problem, the most commonly used algorithm is the LCMV [9] algorithm where the adaptive weight is trained to satisfy certain constraints for a set of directions while minimizing the array response in all other directions. Therefore, the adaptive weight in LCMV-based structure [9], [34] has two objectives: to minimize the interference signal and noises, and to equalize the channel effect of the desired speech (e.g. room acoustics). However, in practical environment, existing adaptive filter algorithms (e.g. least-mean-square) are unlikely to achieve these two objectives fully at the same time [45].

Hence, it serves as the motivation for this work to separate these two objectives using different beamformer weights.

This dissertation proposes a two-stage speech enhancement algorithm using the TFR beamformer and the multi-channel adaptive filter algorithm. As discussed in Section 1.1.3, the TFR is originally used to design the FB and BM of GSC [30] and this work uses it to equalize the channel effect and block the interference signals. In channel equalization part, the channel effect of the desired speech is adjusted by the TFR information. In noise suppression part, the TFR beamformer is employed to reduce certain noise level in advance. In multiple competing speech sources environment, it is cumbersome and impractical to analyze the TFR of each competing speech source. Hence, the virtual sound source perspective explained by singular value decomposition (SVD) method is proposed to simplify the complexity of multiple interference signals environment. The TFR beamformer can be considered a pre-filter to remove the major component of the virtual sound source first and the residual noise from TFR beamformer output can be suppressed by multi-channel adaptive filter. However, the residual noise signals could be nonstationary or hard to model ,and common adaptive filter algorithms (e.g. NLMS algorithm or Kalman filter) may not completely characterize uncertainty under the complexity of acoustic dynamics [35], [46], [47], Therefore, the assumption of bounded disturbances could be a better strategy than others such as certain statistical properties. Hence, this dissertation adopts the H_∞ filter as the multi-channel adaptive filter since it makes no further assumption regarding the disturbances and can be more robust to the model uncertainty problems [48].

The remainder of this chapter is organized as follows. Section 2.2 describes the problem formulation and the virtual sound source concept. Section 2.3 introduces the proposed system architecture and the performances of each noise cancellation block are also analyzed. The method to estimate the TFR information is presented in Section 2.4.

Finally, the summary is given in Section 2.5.

2.2 Problem Formulation

2.2.1 Problem Description

Consider P speech sources and M microphones in the reverberant and noisy environment ($M > P$). The received signal of the m-th microphone at discrete-time index t can be written as:

$$x_m(t) = \sum_{p=1}^{P} a_{mp}(t) \otimes s_p(t) + n_m(t) \tag{2-1}$$

where each symbol in (2-1) represents:

$\otimes$ convolution operation;

$a_{mp}(t)$ the transfer function from the p-th sound source to the m-th microphone;

$s_1(t)$ the desired speech signal;

$s_2(t) \sim s_P(t)$ the nonstationary interfering speech signals (competing speech signals);

$n_m(t)$ the (directional or omni-directional) stationary noise of the m-th microphone.

Typically, the transfer function $a_{mp}(t)$ is assumed to be time-invariant over the observation period. In this dissertation, the competing speech signals, $s_2(t) \sim s_P(t)$, are regarded as interference signals. Applying the short time Fourier transform (STFT) operation to (2-1) yields:

$$X_m(k,\omega) = \sum_{p=1}^{P} A_{mp}(\omega) S_p(k,\omega) + N_m(k,\omega) \tag{2-2}$$

where k is the frame number and ω is the frequency band. $X_m(k,\omega)$, $S_p(k,\omega)$ and

$N_m(k,\omega)$ are the STFT of $x_m(t)$, $s_p(t)$ and $n_m(t)$, respectively. $A_{mp}(\omega)$ is the time-invariant transfer function from the p-th source to the m-th microphone. The objective of this work is to reconstruct the desired speech signal from the received contaminated signals, while suppressing the nonstationary interfering speech signals and the stationary noise signals in a reverberant environment.

2.2.2 *Virtual Sound Source Perspective*

It is impractical to estimate the transfer function for each interference signal in real practice. To simplify the complexity involved in multiple interference signals, a virtual sound source perspective is proposed. The idea of virtual sound source comes from that the multiple interference signals may be able to be transferred to one virtual sound source. When the desired speech signal and the stationary noise are absent, the received microphone signal can be expressed as the matrix form:

$$\boldsymbol{X}_{\mathrm{I}}(k,\omega) = \mathbf{A}_{\mathrm{I}}(\omega)\boldsymbol{S}_{\mathrm{I}}(k,\omega) \tag{2-3}$$

where

$$\boldsymbol{X}_{\mathrm{I}}(k,\omega) = \begin{bmatrix} X_1(k,\omega) \\ X_2(k,\omega) \\ \vdots \\ X_M(k,\omega) \end{bmatrix} \in C^{M\times 1} \quad , \quad \boldsymbol{S}_{\mathrm{I}}(k,\omega) = \begin{bmatrix} S_2(k,\omega) \\ S_3(k,\omega) \\ \vdots \\ S_P(k,\omega) \end{bmatrix} \in C^{(P-1)\times 1}$$

$$\mathbf{A}_{\mathrm{I}}(\omega) = \begin{bmatrix} A_{12}(\omega) & A_{13}(\omega) & \cdots & A_{1P}(\omega) \\ A_{22}(\omega) & A_{23}(\omega) & & A_{2P}(\omega) \\ \vdots & \vdots & & \vdots \\ A_{M2}(\omega) & A_{M3}(\omega) & \cdots & A_{MP}(\omega) \end{bmatrix} \in C^{M\times(P-1)}$$

Assume the rank of the transfer function matrix $\mathbf{A}_{\mathrm{I}}(\omega)$ is R and $\mathbf{A}_{\mathrm{I}}(\omega)$ can be decomposed by SVD:

$$\mathbf{A}_{\mathrm{I}}(\omega)=\mathbf{U}(\omega)\mathbf{D}(\omega)\mathbf{V}^{\mathrm{H}}(\omega) \tag{2-4}$$

where

$$\mathbf{U}(\omega)=\begin{bmatrix}\boldsymbol{u}_1(\omega) & \boldsymbol{u}_2(\omega) & \cdots & \boldsymbol{u}_R(\omega)\end{bmatrix}\in C^{M\times R}$$
$$\mathbf{V}(\omega)=\begin{bmatrix}\boldsymbol{v}_1(\omega) & \boldsymbol{v}_2(\omega) & \cdots & \boldsymbol{v}_R(\omega)\end{bmatrix}\in C^{(P-1)\times R}$$
$$\mathbf{D}(\omega)=\begin{bmatrix}\sigma_1(\omega) & 0 & \cdots & 0\\ 0 & \sigma_2(\omega) & \cdots & 0\\ \vdots & \vdots & \ddots & \vdots\\ 0 & 0 & \cdots & \sigma_R(\omega)\end{bmatrix}\in C^{R\times R}$$

$\sigma_r(\omega)$ are the nonzero singular values of $\mathbf{A}_{\mathrm{I}}(\omega)$ with $\sigma_1(\omega)\geq\sigma_2(\omega)\geq\cdots\geq\sigma_R(\omega)>0$. $\boldsymbol{v}_{\mathrm{r}}(\omega)$ and $\boldsymbol{u}_r(\omega)$ are the input and output singular vectors of $\mathbf{A}_{\mathrm{I}}(\omega)$ respectively which construct the interference subspace. The idea of virtual sound source is characterized as follows. From (2-4), equation (2-3) can be rewritten as:

$$\begin{aligned}\boldsymbol{X}_{\mathrm{I}}(k,\omega)&=\sum_{i=1}^{R}\sigma_i(\omega)\boldsymbol{u}_i(\omega)\boldsymbol{v}_i^{\mathrm{H}}(\omega)\boldsymbol{S}_{\mathrm{I}}(k,\omega)\\&=\left(\boldsymbol{A}_V(\omega)+\boldsymbol{\Delta}_V(k,\omega)\right)S_V(k,\omega)\end{aligned} \tag{2-5}$$

where

$$S_V(k,\omega)=\sigma_1(\omega)\boldsymbol{v}_1^{H}(\omega)\boldsymbol{S}_{\mathrm{I}}(k,\omega)$$
$$\boldsymbol{A}_V(\omega)=\begin{bmatrix}A_{1V}(\omega)\\ A_{2V}(\omega)\\ \vdots\\ A_{MV}(\omega)\end{bmatrix}=\boldsymbol{u}_1(\omega),\quad \boldsymbol{\Delta}_V(k,\omega)=\begin{bmatrix}\Delta_{1V}(k,\omega)\\ \Delta_{2V}(k,\omega)\\ \vdots\\ \Delta_{MV}(k,\omega)\end{bmatrix}=\sum_{i=2}^{R}\alpha_i(k,\omega)\boldsymbol{u}_i(\omega)$$
$$\alpha_i(k,\omega)=\frac{\sigma_i(\omega)\boldsymbol{v}_i^{\mathrm{H}}(\omega)\boldsymbol{S}_{\mathrm{I}}(k,\omega)}{\sigma_1(\omega)\boldsymbol{v}_1^{H}(\omega)\boldsymbol{S}_{\mathrm{I}}(k,\omega)}$$

Observing (2-5), we can find that the MIMO acoustic system of (2-3) is treated as the single-input multiple-output (SIMO) acoustic system. The single input is the virtual sound source $S_V(k,\omega)$ with the TF $\boldsymbol{A}_V(\omega)+\boldsymbol{\Delta}_V(k,\omega)$. The virtual sound source is formed by mapping the interference signals $\boldsymbol{S}_{\mathrm{I}}(k,\omega)$ along the most sensitive input direction $\boldsymbol{v}_1(\omega)$

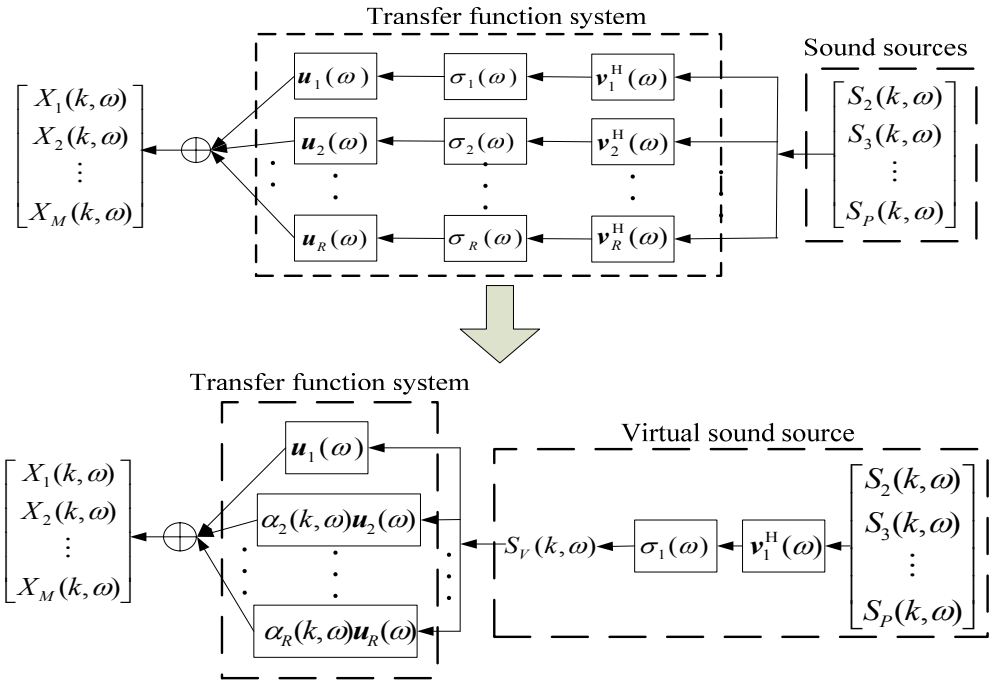

Figure 2-1 Illustration of virtual sound source transformation

which in turn is scaled by the maximum singular value $\sigma_1(\omega)$. The TF of the virtual sound source consists of two parts, time-invariant part $\boldsymbol{A}_V(\omega)$ and time-varying part $\boldsymbol{\Delta}_V(k,\omega)$. This dissertation considers that $\boldsymbol{A}_V(\omega)$ is constructed by the highest gain output direction $\boldsymbol{u}_1(\omega)$ and $\boldsymbol{\Delta}_V(k,\omega)$ is the linear combination of $\boldsymbol{u}_2(\omega) \sim \boldsymbol{u}_R(\omega)$ with time-varying coefficients $\alpha_i(k,\omega)$. The transformation from multiple sound sources to the virtual sound source is illustrated in Fig. 2-1.

2.3 System Architecture

The proposed system architecture of the TFR-based adaptive beamformer is shown in Fig. 2-2. The proposed beamformer uses the TFR-based beamformer to block the principal part of the virtual sound source and the residual noise signals from the TFR-based beamformer outputs are suppressed by the multi-channel adaptive filter.

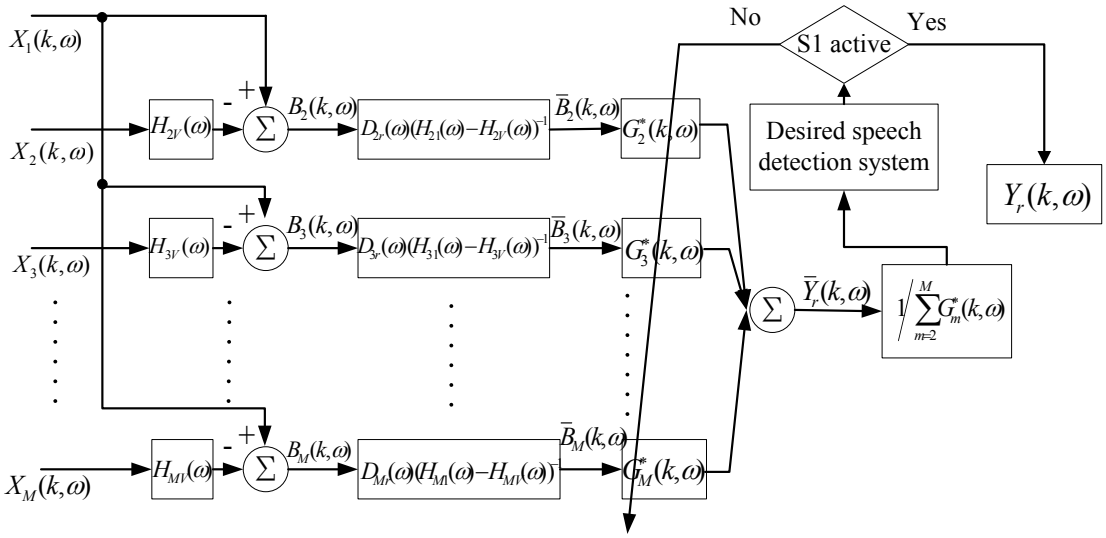

Figure 2-2 The system architecture of the TFR-based adaptive beamformer

According to Section 2.2.2, equation (2-2) can be written as

$$
\begin{aligned}
X_m(k,\omega) &= \sum_{p=1}^{P} A_{mp}(\omega) S_p(k,\omega) + N_m(k,\omega) \\
&= A_{m1}(\omega) S_1(k,\omega) + \sum_{p=2}^{P} A_{mp}(\omega) S_p(k,\omega) + N_m(k,\omega) \\
&= A_{m1}(\omega) S_1(k,\omega) + \left(A_{mV}(\omega) + \Delta_{mV}(k,\omega)\right) S_V(k,\omega) + N_m(k,\omega)
\end{aligned}
\tag{2-6}
$$

For the virtual sound source components, we consider $A_{mV}(\omega)S_V(k,\omega)$ and $\Delta_{mV}(k,\omega)S_V(k,\omega)$ to be the principal part and residual part respectively, since $\boldsymbol{A}_V(\omega)$ is the highest gain output direction of the transfer function matrix $\mathbf{A}_1(\omega)$ and $A_{mV}(\omega)S_V(k,\omega)$ is constructed by the principal interference subspace. If the number of sound sources is two, i.e., P=2, then the residual part is zero.

2.3.1 Transfer Function Ratio Beamformer

A TFR beamformer consists of two microphones. In this work, M received microphone signals are separated into M-1 microphone pairs for the subsequent signal processing. It is

supposed that the TFRs defined in (2-7) have been identified using the method introduced in Section 2.4. The TFRs for the desired speech and virtual sound source are defined as

$$H_{m1}(\omega)=\frac{A_{11}(\omega)}{A_{m1}(\omega)}\ ,\quad H_{mV}(\omega)=\frac{A_{1V}(\omega)}{A_{mV}(\omega)},\qquad m=2,3,\cdots,M \tag{2-7}$$

First, this dissertation employs the TFR of the virtual sound source to remove the principal part of the virtual sound source for each microphone pair:

$$\begin{aligned}
B_m(k,\omega) &= X_1(k,\omega)-\left(\frac{A_{1V}(\omega)}{A_{mV}(\omega)}\right)X_m(k,\omega)\\
&=\left(A_{11}(\omega)-\frac{A_{1V}(\omega)}{A_{mV}(\omega)}A_{m1}(\omega)\right)S_1(k,\omega)+N_1(k,\omega)-\frac{A_{1V}(\omega)}{A_{mV}(\omega)}N_m(k,\omega)\\
&\quad+\left(\Delta_{1V}(k,\omega)-\frac{A_{1V}(\omega)}{A_{mV}(\omega)}\Delta_{mV}(k,\omega)\right)S_V(k,\omega)\\
&=A_{m1}(\omega)\left(\frac{A_{11}(\omega)}{A_{m1}(\omega)}-\frac{A_{1V}(\omega)}{A_{mV}(\omega)}\right)S_1(k,\omega)+N_1(k,\omega)-\frac{A_{1V}(\omega)}{A_{mV}(\omega)}N_m(k,\omega)\\
&\quad+\left(\Delta_{1V}(k,\omega)-\frac{A_{1V}(\omega)}{A_{mV}(\omega)}\Delta_{mV}(k,\omega)\right)S_V(k,\omega)
\end{aligned} \tag{2-8}$$

for $m=2,3,\cdots,M$

Equation (2-8) means that the spatial null is placed toward the direction of the principal part of the virtual sound source by using two microphones. If the number of sound sources is two ($\Delta_{mV}(k,\omega)=0$), equation (2-8) means that the spatial null is placed toward the single competing speech directly. The output of TFR beamformer $B_m(k,\omega)$ consists of 3 terms: distorted desired speech signal, stationary noise and residual virtual sound source. Since the TFRs, $H_{m1}(\omega)$ and $H_{mV}(\omega)$, are known and we assume $(H_{m1}(\omega)-H_{mV}(\omega))$ is non-zero. To mitigate the distortion on the desired speech signal, equation (2-8) is multiplied by $D_{mr}(\omega)(H_{m1}(\omega)-H_{mV}(\omega))^{-1}$:

$$\begin{aligned}
&\overline{B}_m(k,\omega) = B_m(k,\omega)D_{mr}(\omega)(H_{m1}(\omega)-H_{mV}(\omega))^{-1} \\
&= A_{r1}(\omega)S_1(k,\omega) \\
&+\left(N_1(k,\omega)-\frac{A_{1V}(\omega)}{A_{mV}(\omega)}N_m(k,\omega)\right)D_{mr}(\omega)(H_{m1}(\omega)-H_{mV}(\omega))^{-1} \\
&+\left(\Delta_{1V}(k,\omega)-\frac{A_{1V}(\omega)}{A_{mV}(\omega)}\Delta_{mV}(k,\omega)\right)S_V(k,\omega)D_{mr}(\omega)(H_{m1}(\omega)-H_{mV}(\omega))^{-1}
\end{aligned} \tag{2-9}$$

where

$$D_{mr}(\omega) = \frac{A_{r1}(\omega)}{A_{m1}(\omega)} = H_{m1}(\omega)\,(H_{r1}(\omega))^{-1} \qquad r = 1,2,\cdots,M$$

$D_{mr}(\omega)$ is used to adjust the desired speech signal distortion to the same reference and r is the reference microphone number selected.

The noise components of output signal $\overline{B}_m(k,\omega)$ still contain the residual part of the virtual sound source and stationary noise (the last two terms of the right side of (2-9)), and hence the multi-channel adaptive filter is employed here to minimize the noise in $\overline{B}_m(k,\omega)$. Let us sum all the output signals $\overline{B}_m(k,\omega)$ with the weighting function $G_m(k,\omega)$:

$$\begin{aligned}
&\overline{Y}_r(k,\omega) = G_2^*(k,\omega)\overline{B}_2(k,\omega)+\cdots+G_M^*(k,\omega)\overline{B}_M(k,\omega) \\
&= A_{r1}(\omega)S_1(k,\omega)\sum_{m=2}^{M}G_m^*(k,\omega) \\
&+\sum_{m=2}^{M}G_m^*(k,\omega)\left(N_1(k,\omega)-\frac{A_{1V}(\omega)}{A_{mV}(\omega)}N_m(k,\omega)\right)D_{mr}(\omega)(H_{m1}(\omega)-H_{mV}(\omega))^{-1} \\
&+\sum_{m=2}^{M}G_m^*(k,\omega)\left(\Delta_{1V}(k,\omega)-\frac{A_{1V}(\omega)}{A_{mV}(\omega)}\Delta_{mV}(k,\omega)\right)S_V(k,\omega)D_{mr}(\omega)(H_{m1}(\omega)-H_{mV}(\omega))^{-1}
\end{aligned} \tag{2-10}$$

where * represents the complex conjugation. The noise components can be cancelled if

$$\boldsymbol{G}^{\mathrm{H}}(k,\omega)\boldsymbol{Z}(k,\omega) = -G_2(k,\omega)Z_2(k,\omega) \tag{2-11}$$

where H represents conjugation transpose;

$$G_2(k,\omega)=1$$

$$\boldsymbol{G}(k,\omega)=\left[G_3(k,\omega) \quad \cdots \quad G_M(k,\omega)\right]^{\mathrm{T}}$$

$$\boldsymbol{Z}(k,\omega)=\left[Z_3(k,\omega) \quad \cdots \quad Z_M(k,\omega)\right]^{\mathrm{T}}$$

$$Z_m(k,\omega)=\left(N_1(k,\omega)-\frac{A_{1V}(\omega)}{A_{mV}(\omega)}N_m(k,\omega)\right)D_{mr}(\omega)(H_{m1}(\omega)-H_{mV}(\omega))^{-1}$$

$$+\left(\Delta_{1V}(k,\omega)-\frac{A_{1V}(\omega)}{A_{mV}(\omega)}\Delta_{mV}(k,\omega)\right)S_V(k,\omega)D_{mr}(\omega)(H_{m1}(\omega)-H_{mV}(\omega))^{-1}$$

The solution of $\boldsymbol{G}(k,\omega)$ can be found by using adaptive algorithm suggested in Section 2.3.2 when $S_1(k,\omega)$ is silent (desired speech inactive periods). Once the weight vector $\boldsymbol{G}(k,\omega)$ is obtained, the beamformer output can be given as:

$$Y_r(k,\omega)=\frac{\overline{Y}_r(k,\omega)}{\sum_{m=2}^{M}G_m^*(k,\omega)} \tag{2-12}$$

2.3.2 Multi-channel Adaptive Filter

For the real environment, it is unlikely to remove the noise components of (2-10) completely and hence the output signal $\overline{Y}_r(k,\omega)$ can be expressed as:

$$\overline{Y}_r(k,\omega)=A_{r1}(\omega)S_1(k,\omega)\sum_{m=2}^{M}G_m^*(k,\omega)+e_n(k,\omega) \tag{2-13}$$

where $e_n(k,\omega)$ is the residual noise and it is anticipated that the desired speech signal components are dominant compared to the residual noise. Therefore, equation (2-12) can be written as:

$$Y_r(k,\omega)=A_{r1}(\omega)S_1(k,\omega)+\frac{e_n(k,\omega)}{\sum_{m=2}^{M}G_m^*(k,\omega)} \tag{2-14}$$

According to (2-11), the error signal at frequency ω and frame *k* can be defined as:

$$\varepsilon_Z(k,\omega)=-G_2(k,\omega)Z_2(k,\omega)-\boldsymbol{G}^{\mathrm{H}}(k,\omega)\boldsymbol{Z}(k,\omega) \tag{2-15}$$

To minimize the error signal $\varepsilon_Z(k,\omega)$, the optimal set of filter coefficients vectors $\boldsymbol{G}(k,\omega)$ can be found using the formula:

$$\min_{G} E\left[\varepsilon_Z(k,\omega)\varepsilon_Z^*(k,\omega)\right] \tag{2-16}$$

where $E[\cdot]$ is the expectation. Observing (2-12), the weight-and-sum output $\overline{Y}_r(k,\omega)$ is divided by $\sum_{m=2}^{M} G_m^*(k,\omega)$ to be the beamformer output $Y_r(k,\omega)$. Hence, to prevent the term $e_n(k,\omega)$ in (2-14) from being amplified by $\sum_{m=2}^{M} G_m^*(k,\omega)$ and a constraint is added into (2-16) as:

$$\begin{aligned} &\min_{Q} E\left[\varepsilon_Z(k,\omega)\varepsilon_Z^*(k,\omega)\right] \\ &\text{subject to} \quad \beta = \boldsymbol{G}^{\mathrm{H}}(k,\omega)\boldsymbol{O} \end{aligned} \tag{2-17}$$

where $\boldsymbol{O} = \begin{bmatrix} 1 & 1 & \cdots & 1 \end{bmatrix}^{\mathrm{T}} \in R^{(M-2)\times 1}$ and β is a constant larger than zero to ensure the value of $\sum_{m=2}^{M} G_m^*(k,\omega)$ not to amplify the residual noise $e_n(k,\omega)$ in (2-14). H_2-optimal estimators (i.e. least-square based), such as the Wiener filter or Kalman filter, which minimize the expected estimation error energy and yield maximum-likelihood estimates are usually used to solve the optimization problem of (2-17). However, the least-square-based filters have some assumption about the disturbances. For example, Kalman filter assumes that signal generating processes have known dynamics and that the disturbances have known statistical properties. These assumptions may limit the beamformer performance. Among the classic adaptive filters, the NLMS algorithm is one of the most popular methods and widely used since it can be implemented easily. The NLMS algorithm solution of (2-17) is given by:

$$\hat{\boldsymbol{G}}(k+1,\omega) = \hat{\boldsymbol{G}}(k,\omega) + \frac{\lambda\left(\varepsilon_Z^*(k,\omega)\boldsymbol{Z}(k,\omega) + \mu\varepsilon_N^*(k,\omega)\boldsymbol{O}\right)}{\boldsymbol{Z}^{\mathrm{H}}(k,\omega)\boldsymbol{Z}(k,\omega) + \mu\boldsymbol{O}^{\mathrm{H}}\boldsymbol{O}} \tag{2-18}$$

where λ is the small positive step size; μ is the penalty parameter and

$\varepsilon_N(k,\omega)=\beta-\boldsymbol{G}^{\mathrm{H}}(k,\omega)\boldsymbol{O}$. However, the modeling error of $\boldsymbol{G}(k,\omega)$ or the nonstationary signals in $\boldsymbol{Z}(k,\omega)$ may influence the performance and convergence rate of the NLMS algorithm. Therefore, the H_∞ filter is applied here for the optimization problem. Because the disturbances in the H_∞ estimation can be arbitrary but bounded signals and the H_∞ filter was shown to be more robust than other least-square-based methods [35], [46]-[49]. To apply the H_∞ filter, the constrained minimization problem of (2-17) is casted as a state-space model:

State equation:

$$\boldsymbol{G}(k,\omega)=\boldsymbol{G}(k-1,\omega) \tag{2-19}$$

Measurement equation:

$$\begin{bmatrix}-Z_2^*(k,\omega)\\ \beta\end{bmatrix}=\begin{bmatrix}\boldsymbol{Z}^{\mathrm{H}}(k,\omega)\\ \boldsymbol{O}^{\mathrm{H}}\end{bmatrix}\boldsymbol{G}(k,\omega)+\begin{bmatrix}v_1(k,\omega)\\ v_2(k,\omega)\end{bmatrix} \tag{2-20}$$

The measurement equation can be written as:

$$\overline{\boldsymbol{M}}(k,\omega)=\overline{\mathbf{Z}}^{\mathrm{H}}(k,\omega)\boldsymbol{G}(k,\omega)+\boldsymbol{V}(k,\omega) \tag{2-21}$$

where

$$\overline{\boldsymbol{M}}(k,\omega)=\begin{bmatrix}-Z_2^*(k,\omega)\\ \beta\end{bmatrix},\ \overline{\mathbf{Z}}^{\mathrm{H}}(k,\omega)=\begin{bmatrix}\boldsymbol{Z}^{\mathrm{H}}(k,\omega)\\ \boldsymbol{O}^{\mathrm{H}}\end{bmatrix},\ \boldsymbol{V}(k,\omega)=\begin{bmatrix}v_1(k,\omega)\\ v_2(k,\omega)\end{bmatrix} \tag{2-22}$$

$v_1(k,\omega)$ and $v_2(k,\omega)$ are the beamformer residual noise and constraint noise, respectively. The H_∞ filter makes no assumption about the statistics of the noise $v_1(k,\omega)$ and $v_2(k,\omega)$ and is interested not necessarily in the estimation of $\boldsymbol{G}(k,\omega)$ but in the estimation of some arbitrary linear combination of $\boldsymbol{G}(k,\omega)$, i.e.,

$$\boldsymbol{T}(k,\omega)=\mathbf{C}\boldsymbol{G}(k,\omega) \tag{2-23}$$

where $\mathbf{C}$ is a user-defined matrix. The estimate of $\boldsymbol{T}(k,\omega)$ is denoted by $\hat{\boldsymbol{T}}(k,\omega)$ and

the estimate of initial state $\boldsymbol{G}(0,\omega)$ is denoted by $\hat{\boldsymbol{G}}(0,\omega)$. The design criterion of the H_∞ filter is to find $\hat{\boldsymbol{T}}(k,\omega)$ that minimizes $\boldsymbol{T}(k,\omega)-\hat{\boldsymbol{T}}(k,\omega)$ for any $v_1(k,\omega)$, $v_2(k,\omega)$ and $\boldsymbol{G}(0,\omega)$. The performance index J can be defined as:

$$J=\frac{\sum_{k=0}^{N-1}\left|\boldsymbol{T}(k,\omega)-\hat{\boldsymbol{T}}(k,\omega)\right|_{\mathbf{S}(k,\omega)}^2}{\left|\boldsymbol{G}(0,\omega)-\hat{\boldsymbol{G}}(0,\omega)\right|_{\mathbf{P}^{-1}(0,\omega)}^2+\sum_{k=0}^{N-1}\left|\boldsymbol{V}(k,\omega)\right|_{\mathbf{R}^{-1}(k,\omega)}^2} \tag{2-24}$$

where the notation $\left|\boldsymbol{x}(k,\omega)\right|_{\mathbf{S}(k,\omega)}^2$ is defined as the square of the weighted (by $\mathbf{S}(k,\omega)$) L_2 norm of $\boldsymbol{x}(k,\omega)$, i.e., $\left|\boldsymbol{x}(k,\omega)\right|_{\mathbf{S}(k,\omega)}^2=\boldsymbol{x}^{\mathrm{H}}(k,\omega)\mathbf{S}(k,\omega)\boldsymbol{x}(k,\omega)$. The matrices $\mathbf{P}(0,\omega)$, $\mathbf{R}(k,\omega)$ and $\mathbf{S}(k,\omega)$ are symmetric positive definite matrices chosen by the user based on the specific problem. To simplify the analysis and clarify the notation, we assume the weighting matrices, $\mathbf{R}(k,\omega)$ and $\mathbf{S}(k,\omega)$, are the same at each frame and each frequency, i.e., they are independent of frame and frequency. Hence, equation (2-24) can be reformulated as

$$J=\frac{\sum_{k=0}^{N-1}\left|\boldsymbol{T}(k,\omega)-\hat{\boldsymbol{T}}(k,\omega)\right|_{\mathbf{S}}^2}{\left|\boldsymbol{G}(0,\omega)-\hat{\boldsymbol{G}}(0,\omega)\right|_{\mathbf{P}^{-1}(0,\omega)}^2+\sum_{k=0}^{N-1}\left|\boldsymbol{V}(k,\omega)\right|_{\mathbf{R}^{-1}}^2} \tag{2-25}$$

The direct minimization of J is not tractable, so instead, a performance bound γ is selected and $\hat{\boldsymbol{T}}(k,\omega)$ is computed to satisfy

$$\sup J<\gamma \tag{2-26}$$

where sup represents supremum. The formulation of (2-26) shows that the H_∞ optimal estimators guarantee the smallest estimation error energy over all possible disturbances ($\boldsymbol{G}(0,\omega)-\hat{\boldsymbol{G}}(0,\omega)$ and $\boldsymbol{V}(k,\omega)$) of finite energy. They are over-conservative but have a better robust behavior to the disturbance variations. The H_∞ optimal strategy is to find

$\hat{\boldsymbol{T}}(k,\omega)$ that minimizes the supremum of the cost function J. Hence, the H_∞ filter can be interpreted as a *minmax* problem where the estimator strategy $\hat{\boldsymbol{T}}(k,\omega)$ plays against the exogenous inputs $\boldsymbol{V}(k,\omega)$ and the uncertainty of the initial state $\boldsymbol{G}(0,\omega)$.Therefore, the performance criterion is equivalent to

$$\begin{aligned}\min_{\hat{\boldsymbol{T}}}\max_{\boldsymbol{V},\boldsymbol{G}(0,\omega)} J = &-\gamma\left|\boldsymbol{G}(0,\omega)-\hat{\boldsymbol{G}}(0,\omega)\right|^2_{\mathbf{P}^{-1}(0,\omega)} \\ &+\sum_{k=0}^{N-1}\left[\left|\boldsymbol{T}(k,\omega)-\hat{\boldsymbol{T}}(k,\omega)\right|^2_{\mathbf{S}}-\gamma\left(\left|\boldsymbol{V}(k,\omega)\right|^2_{\mathbf{R}^{-1}}\right)\right]\end{aligned} \tag{2-27}$$

Since $\boldsymbol{V}(k,\omega)=\overline{\boldsymbol{M}}(k,\omega)-\overline{\mathbf{Z}}^{\mathrm{H}}(k,\omega)\boldsymbol{G}(k,\omega)$, $\boldsymbol{T}(k,\omega)=\mathbf{C}\boldsymbol{G}(k,\omega)$ and $\boldsymbol{T}(k,\omega)=\mathbf{C}\boldsymbol{G}(k,\omega)$, equation (2-27) can be rewritten as:

$$\begin{aligned}\min_{\hat{\boldsymbol{G}}}\max_{\overline{\boldsymbol{M}},\boldsymbol{G}(0,\omega)} J = &-\gamma\left|\boldsymbol{G}(0,\omega)-\hat{\boldsymbol{G}}(0,\omega)\right|^2_{\mathbf{P}^{-1}(0,\omega)} \\ &+\sum_{k=0}^{N-1}\left[\left|\boldsymbol{G}(k,\omega)-\hat{\boldsymbol{G}}(k,\omega)\right|^2_{\overline{\mathbf{S}}}-\gamma\left(\left|\overline{\boldsymbol{M}}(k,\omega)-\overline{\mathbf{Z}}^{\mathrm{H}}(k,\omega)\boldsymbol{G}(k,\omega)\right|^2_{\mathbf{R}^{-1}}\right)\right]\end{aligned} \tag{2-28}$$

where $\overline{\mathbf{S}}=\mathbf{C}^{\mathrm{H}}\mathbf{S}\mathbf{C}$.

According to [48], the H_∞ solution can be given as:

$$\mathbf{K}(k,\omega)=\mathbf{P}(k,\omega)\left[\mathbf{I}-\gamma^{-1}\overline{\mathbf{S}}\mathbf{P}(k,\omega)+\overline{\mathbf{Z}}(k,\omega)\mathbf{R}^{-1}\overline{\mathbf{Z}}^{\mathrm{H}}(k,\omega)\mathbf{P}(k,\omega)\right]^{-1}\overline{\mathbf{Z}}(k,\omega)\mathbf{R}^{-1} \tag{2-29}$$

$$\hat{\boldsymbol{G}}(k+1,\omega)=\hat{\boldsymbol{G}}(k,\omega)+\mathbf{K}(k,\omega)\left[\overline{\boldsymbol{M}}(k,\omega)-\overline{\mathbf{Z}}^{\mathrm{H}}(k,\omega)\hat{\boldsymbol{G}}(k,\omega)\right] \tag{2-30}$$

$$\mathbf{P}(k+1,\omega)=\mathbf{P}(k,\omega)\left[\mathbf{I}-\gamma^{-1}\overline{\mathbf{S}}\mathbf{P}(k,\omega)+\overline{\mathbf{Z}}(k,\omega)\mathbf{R}^{-1}\overline{\mathbf{Z}}^{\mathrm{H}}(k,\omega)\right]^{-1} \tag{2-31}$$

where $\mathbf{I}$ is the identity matrix. The H_∞ solution above can also be used to solve the unconstrained minimization problem of (2-16) by setting:

$$\overline{\boldsymbol{M}}(k,\omega)=\left[-Z_2^*(k,\omega)\right],\ \overline{\mathbf{Z}}^{\mathrm{H}}(k,\omega)=\left[\boldsymbol{Z}^{\mathrm{H}}(k,\omega)\right] \tag{2-32}$$

For the proposed multi-channel adaptive filter, $\overline{\boldsymbol{M}}(k,\omega)$ and $\overline{\mathbf{Z}}^{\mathrm{H}}(k,\omega)$ are set as (2-32) at the beginning of the adaptation procedure of $\hat{\boldsymbol{G}}(k,\omega)$. If the absolute value of

Table 2-1 Four experimental conditions

Condition Number	Desired Speech Location	White Noise Location	Interference Speech Location(s)
M1	90°	20°	60°
M2	90°	20°	60° and 120°
M3	90°	20°	60°, 120° and 150°
M4	90°	20°	30°, 60°, 120° and 150°

$\sum_{m=2}^{M} G_m^*(k,\omega)$ is less than one after $\tilde{k}$ times of adaptation, $\overline{\boldsymbol{M}}(k,\omega)$ and $\overline{\mathbf{Z}}^{\mathrm{H}}(k,\omega)$ will be set as (2-22). Theoretically, if $\sum_{m=2}^{M} G_m^*(k,\omega)$ is less than one, the value of β should be set as a constant close to zero to prevent the constrained value from being far away from the optimal solution. However, there is no such restriction of β in the proposed architecture, since the residual noise $e_n(k,\omega)$ is divided by $\sum_{m=2}^{M} G_m^*(k,\omega)$ to be the beamformer output.

2.3.3 The Analysis of TFR Beamformer and Multi-channel Adaptive Filter

In this section, the performances of the individual noise cancellation block ($B_m(k,\omega)$ and $Y_r(k,\omega)$) are analyzed. To analyze the performances, the image method [50] is used here to simulate the room impulse responses. The simulated room size is 4.5 m × 3.3 m × 4.2 m and the reverberation time is 0.14 second simulated by 532-taps FIR filter. A uniform linear microphone array with eight microphones placed at a distance of 0.7 m from the wall is used for the simulation. The distance between adjacent microphones is 6 cm and the sampling rate is 8 kHz. The directional sources are placed in front of the array from angle 0° to 180° with a distance of 1.5 m from the midpoint of the array. Four different conditions listed in Table 2-1 are considered to demonstrate the performances of each noise cancellation block. To compare the performances of the NLMS algorithm and

the H_∞ filter, the multi-channel adaptive filter is implemented by both methods. The STFT size is 256 with 80 shift samples and 16 zero padding samples. The parameters of λ, μ, β and γ are in (2-18), (2-18), (2-20) and (2-26) set to 0.3, 1, 2 and 10. The adaptation number $\tilde{k}$ is set to 20. In this simulation, the length of the impulse responses (532) is longer than 256. Therefore, the modeling error exists in this simulation. Fig. 2-3 shows the received signal and the outputs of each noise cancellation block ($B_2(k,\omega)$ and $Y_1(k,\omega)$) at four different conditions when the desired speech signal is inactive and Table 2-2 shows the average root mean square (RMS) power at different stage. The average RMS power is defined as:

$$\text{avg.RMS} = \frac{1}{N}\sum_{k=1}^{N} 20\log 10\left(\sqrt{\frac{1}{L}\sum_{l=1}^{L} y^2(l+kL)}\right) \tag{2-33}$$

where L denotes the length of the frame; k is the frame number and y is the input signal.

Observing the TFR beamformer output ($B_2(k,\omega)$) in Fig. 2-3, we can find that the TFR beamformer can reduce certain interference parts especially when the interference speech number (P) is small. However, the residual virtual sound source defined in (2-8) may not be relatively small when the number of interference sources becomes large. This is because the TFR beamformer only consists of two microphones and it can only place one null space toward one direction which limits the performance. As can be seen from Fig. 2-3, the H_∞ filter can reduce more noise signals than the NLMS algorithm. Since the H_∞ filter minimizes the worst possible effects of the disturbances on the estimation error of $\boldsymbol{G}(k,\omega)$. Characterizing uncertainty under the complexity of acoustic dynamics is difficult, so the best strategy may be just to assume that the disturbance is bounded. In addition, the residual virtual sound source may influence the convergence rate of the NLMS algorithm since it is nonstationary signal. Therefore, this work adopts the H_∞ filter as the multi-channel adaptive filter to cancel the residual noise from TFR beamformer

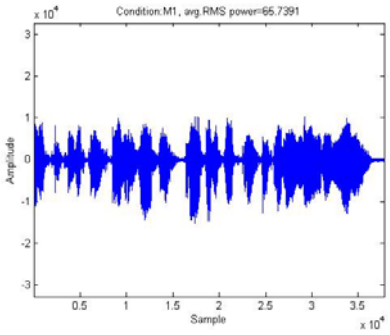
Condition:M1, avg.RMS power=65.7391
Amplitude
Sample

(a)

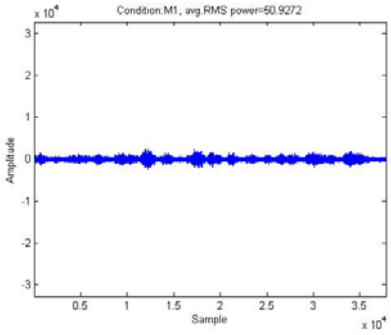
Condition:M1, avg.RMS power=50.9272
Amplitude
Sample

(b)

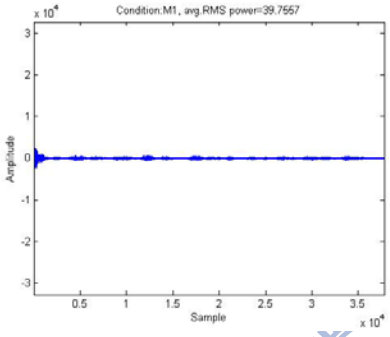
Condition:M1, avg.RMS power=39.7557
Amplitude
Sample

(c)

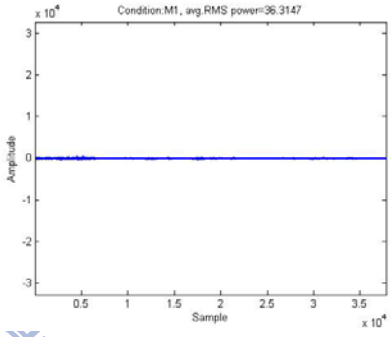
Condition:M1, avg.RMS power=36.3147
Amplitude
Sample

(d)

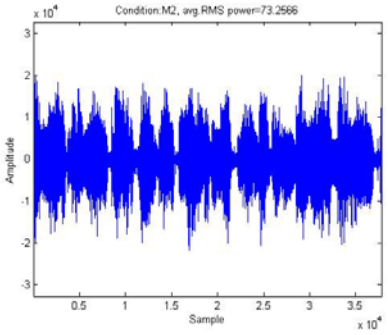
Condition:M2, avg.RMS power=73.2586
Amplitude
Sample

(e)

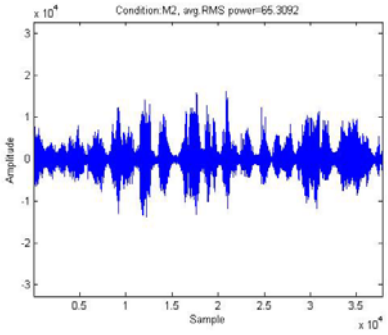
Condition:M2, avg.RMS power=65.3092
Amplitude
Sample

(f)

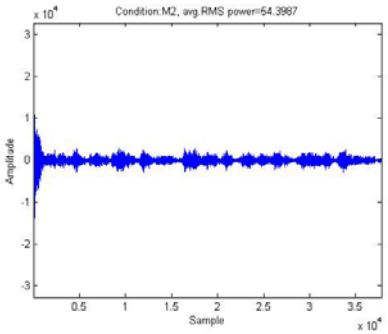
Condition:M2, avg.RMS power=54.3987
Amplitude
Sample

(g)

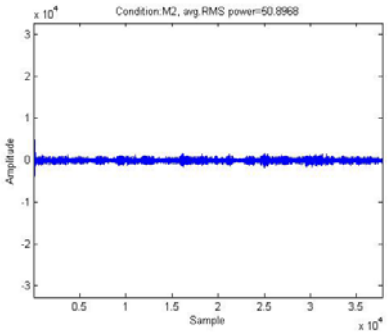
Condition:M2, avg.RMS power=50.8968
Amplitude
Sample

(h)

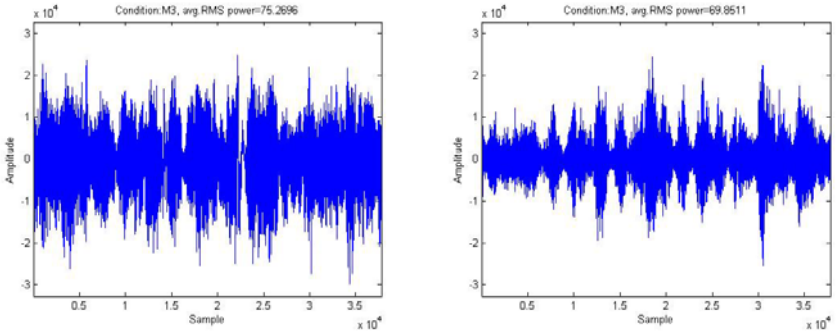

(i) (j)

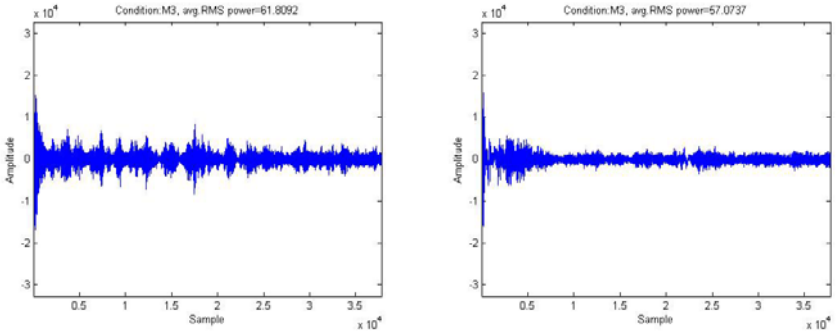

(k) (l)

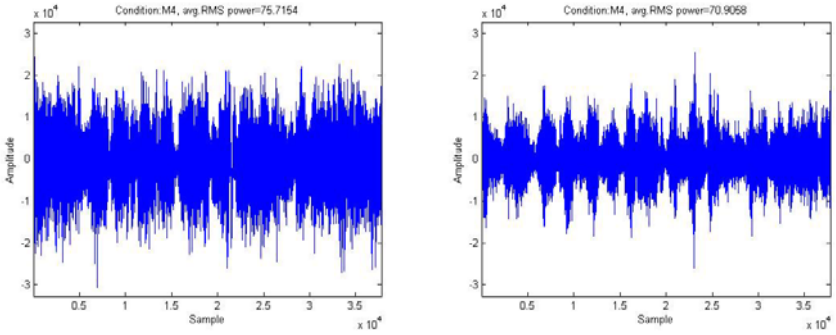

(m) (n)

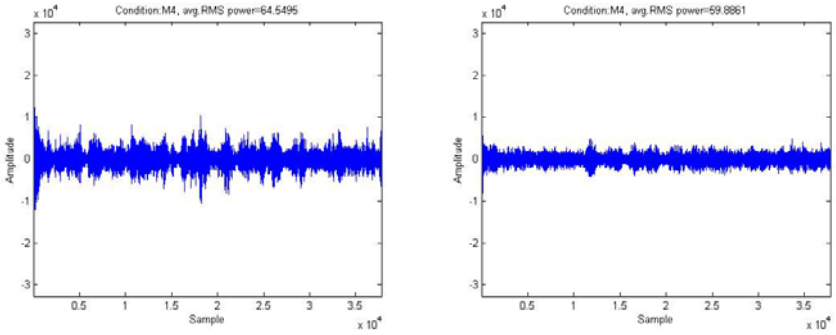

(o) (p)

Figure 2-3 Waveforms of the simulation results

(a), (e), (i), (m): received Mic#1 signal at four conditions ;

(b), (f), (j), (n): $B_2(k,\omega)$ at four conditions;

(c), (g), (k), (o): $Y_1(k,\omega)$ using NLMS algorithm at four conditions;

(d), (h), (l), (p): $Y_1(k,\omega)$ using H_∞ filter at four conditions;

Table 2-2 Average RMS power (dB) for different conditions

Condition Number	Mic #1 signal	$B_2(k,\omega)$	$Y_1(k,\omega)$ using NLMS	$Y_1(k,\omega)$ using H_∞
M1	65.74	50.93	39.76	36.31
M2	73.26	65.31	54.4	50.9
M3	75.27	69.85	61.81	57.07
M4	75.72	70.91	64.55	59.89

outputs. More comparisons between the H_∞ filter and least-square-based filters can be referred to [35], [46]-[49]. Except the advantage of the H_∞ filter, there is also an advantage of the proposed beamformer architecture. Unlike the standard weight-and-sum beamformer architecture where the beamformer output is obtained by weighting and summing signals fromdifferent microphones, the proposed architecture makes the weight-and-sum output $\overline{Y}_1(k,\omega)$ divide by $\sum_{m=2}^{M} G_m^*(k,\omega)$ to be the beamformer output and it is different from the standard weight-and-sum beamformer architecture. Hence, if $\left|\sum_{m=2}^{M} G_m^*(k,\omega)\right|$ is larger than one, the noise components in (2-10) can be attenuated again using (2-12).

To test the performance of the proposed structure, one more simulation is performed. Consider the M3 condition and the goal of this simulation is to find the weight $\hat{\boldsymbol{G}}(k,\omega)$ that minimizes $\varepsilon_Z(k,\omega)$ during noise-only-periods. Two beamformer structures shown in Table 2-3 are used for comparison. The first one is the standard weight-and-sum structure and the second one is the proposed beamformer structure. Fig. 2-4 shows the simulation results of both beamformers with NLMS algorithm and the H_∞ filter. The initial condition of $\hat{\boldsymbol{G}}(k,\omega)$ for the NLMS algorithm and the H_∞ filter are the same. The parameters of λ, μ, β and γ are in (2-18), (2-18), (2-20) and (2-26) set to 0.3, 1, 2 and 10. The weighting matrices $\mathbf{P}(0,\omega)$ and $\overline{\mathbf{S}}$ are both identically set to be identity

Table 2-3 Two beamformer structures for comparison

	Beamformer output	Minimization criterion
The first beamformer	$\sum_{m=2}^{M} G_m^*(k,\omega)\overline{B}_m(k,\omega)$	$\min_G \varepsilon_Z(k,\omega)\varepsilon_Z^*(k,\omega)$
The second beamformer	$\sum_{m=2}^{M} G_m^*(k,\omega)\overline{B}_m(k,\omega) \Big/ \sum_{m=2}^{M} G_m^*(k,\omega)$	if $\left\|\sum_{m=2}^{M} G_m^*(k,\omega)\right\| \geq 1$ $\min_G \varepsilon_Z(k,\omega)\varepsilon_Z^*(k,\omega)$ if $\left\|\sum_{m=2}^{M} G_m^*(k,\omega)\right\| < 1$ $\min_Q \varepsilon_Z(k,\omega)\varepsilon_Z^*(k,\omega)$ subject to $\beta = \boldsymbol{G}^{\mathrm{H}}(k,\omega)\boldsymbol{O}$

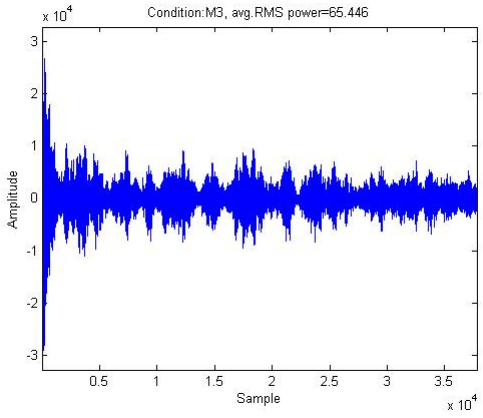

(a) avg.RMS=65.45 (dB)

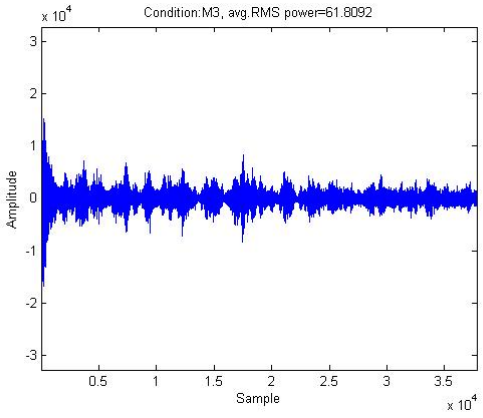

(b) avg.RMS=61.81 (dB)

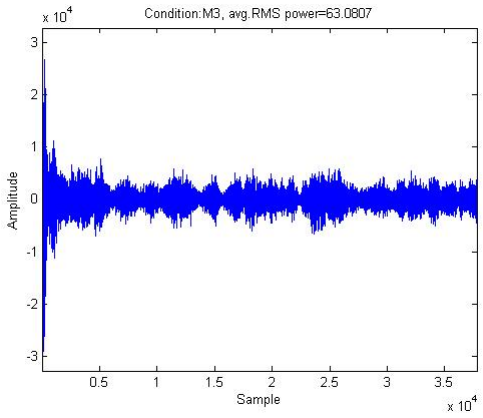

(c) avg.RMS=63.08 (dB)

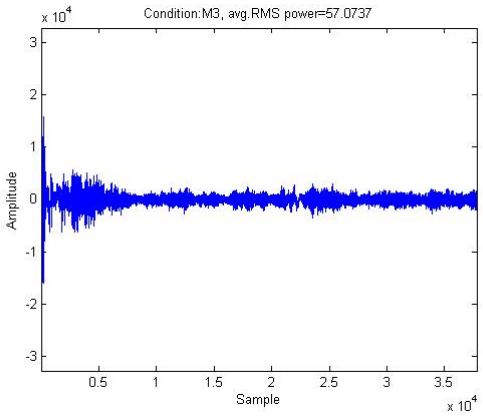

(d) avg.RMS=57.07 (dB)

Figure 2-4 Waveforms. (a): The first beamformer using NLMS; (b): The second beamformer using NLMS; (c): The first beamformer using H_∞ filter; (d): The second beamformer using H_∞ filter;

matrices and the weighting matrix $\mathbf{R}$ is set to be diag(1,10-9). (diag represents diagonal matrix) As can be seen, for both filters, the proposed system architecture can reduce more noise than the standard weight-and-sum architecture.

2.4 Transfer Function Ratio Estimation

In this work, the TFRs, $H_{m1}(\omega)$ and $H_{mV}(\omega)$, are estimated separately using the system identification method described in [51]. The TFR of the desired speech $H_{m1}(\omega)$ is estimated when only $S_1(k,\omega)$ and $N_m(k,\omega)$ are active and the TFR of the virtual sound source $H_{mV}(\omega)$ is estimated when only $S_2(k,\omega) \sim S_P(k,\omega)$ and $N_m(k,\omega)$ are active.

The method to estimate the time-invariant TFR of the virtual sound source $H_{mV}(\omega)$ is presented first. When no desired signal is in present, the received microphone signal becomes:

$$\begin{aligned} X_m(k,\omega) &= \sum_{p=2}^{P} A_{mp}(\omega) S_p(k,\omega) + N_m(k,\omega) \\ &= \left(A_{mV}(\omega) + \Delta_{mV}(k,\omega)\right) S_V(k,\omega) + N_m(k,\omega) \end{aligned} \tag{2-34}$$

Let the residual signal $R_m(k,\omega)$ during noise-only periods represent as:

$$\begin{aligned} R_m(k,\omega) &= X_m(k,\omega) - \frac{A_{mV}(\omega)}{A_{1V}(\omega)} X_1(k,\omega) \\ &= N_m(k,\omega) - \frac{A_{mV}(\omega)}{A_{1V}(\omega)} N_1(k,\omega) + \left(\Delta_{mV}(k,\omega) - \frac{A_{mV}(\omega)}{A_{1V}(\omega)} \Delta_{1V}(k,\omega) \right) S_V(k,\omega) \\ &= R_{1m}(k,\omega) + R_{2m}(k,\omega) \\ m &= 2,3,\cdots,M \end{aligned} \tag{2-35}$$

where

$$R_{1m}(k,\omega) = N_m(k,\omega) - \frac{A_{mV}(\omega)}{A_{1V}(\omega)} N_1(k,\omega)$$

$$R_{2m}(k,\omega) = \left(\Delta_{mV}(k,\omega) - \frac{A_{mV}(\omega)}{A_{1V}(\omega)} \Delta_{1V}(k,\omega) \right) S_V(k,\omega)$$

Rearrange (2-35) and we can obtain:

$$\begin{aligned} X_m(k,\omega) &= \frac{A_{mV}(\omega)}{A_{1V}(\omega)} X_1(k,\omega) + R_m(k,\omega) \\ &= H_{mV}^{-1}(\omega) X_1(k,\omega) + R_{1m}(k,\omega) + R_{2m}(k,\omega) \end{aligned} \tag{2-36}$$

Applying the cross power spectrum density (PSD) operation to (2-36), we have:

$$\Phi_{x_m x_1}(k,\omega) = H_{mV}^{-1}(\omega) \Phi_{x_1 x_1}(k,\omega) + \Phi_{r_{1m} x_1}(\omega) + \Phi_{r_{2m} x_1}(k,\omega) \tag{2-37}$$

where $\Phi_{x_i x_j}(k,\omega)$ is the cross PSD between x_i and x_j. Since $N_m(k,\omega)$ is stationary and $S_m(k,\omega)$ is independent of $N_m(k,\omega)$, hence $\Phi_{r_{1m} x_1}(\omega)$ is independent of frame *k*. Rewrite the equation above as matrix form:

$$\begin{bmatrix} \Phi_{x_m x_1}(1,\omega) \\ \Phi_{x_m x_1}(2,\omega) \\ \vdots \\ \Phi_{x_m x_1}(K,\omega) \end{bmatrix} = \begin{bmatrix} \Phi_{x_1 x_1}(1,\omega) & 1 \\ \Phi_{x_1 x_1}(2,\omega) & 1 \\ \vdots & 1 \\ \Phi_{x_1 x_1}(K,\omega) & 1 \end{bmatrix} \boldsymbol{\theta}(\omega) + \begin{bmatrix} \Phi_{r_{2m} x_1}(1,\omega) \\ \Phi_{r_{2m} x_1}(2,\omega) \\ \vdots \\ \Phi_{r_{2m} x_1}(K,\omega) \end{bmatrix} \tag{2-38}$$

where

$$\boldsymbol{\theta}(\omega) = \begin{bmatrix} H_{mV}^{-1}(\omega) \\ \Phi_{r_{1m} x_1}(\omega) \end{bmatrix}$$

To reduce the computational complexity, the recursive least-square method is applied to estimate $H_{mV}^{-1}(\omega)$:

$$\hat{\boldsymbol{\theta}}(k+1,\omega)=\hat{\boldsymbol{\theta}}(k,\omega)+\boldsymbol{K}_r(k,\omega)(\Phi_{x_m x_1}(k,\omega)-\boldsymbol{F}(k,\omega)\hat{\boldsymbol{\theta}}(k,\omega))$$
$$\hat{H}_{mV}^{-1}(k+1,\omega)=\begin{bmatrix}1 & 0\end{bmatrix}\hat{\boldsymbol{\theta}}(k+1,\omega) \quad (2\text{-}39)$$

where

$$\boldsymbol{K}_r(k,\omega)=\frac{\mathbf{P}_r(k,\omega)\boldsymbol{F}_r(k,\omega)^{\mathrm{T}}}{1+\boldsymbol{F}_r(k,\omega)\mathbf{P}_r(k,\omega)\boldsymbol{F}_r(k,\omega)^{\mathrm{T}}}$$
$$\mathbf{P}_r(1,\omega)=(\boldsymbol{F}_r(1,\omega)^{\mathrm{T}}\boldsymbol{F}_r(1,\omega))^{-1}$$
$$\mathbf{P}_r(k,\omega)=\mathbf{P}_r(k-1,\omega)-\boldsymbol{K}_r(k-1,\omega)\boldsymbol{F}_r(k-1,\omega)\mathbf{P}_r(k-1,\omega) \quad k\geq 2$$
$$\boldsymbol{F}_r(k,\omega)=\begin{bmatrix}\Phi_{x_1 x_1}(k,\omega) & 1\end{bmatrix}$$

Note that the TFR of the desired speech $H_{m1}(\omega)$ can be estimated in a similar manner when only $S_1(k,\omega)$ and $N_m(k,\omega)$ are active.

2.5 Summary

This chapter proposes a two-stage procedure beamformer to perform multiple competing speeches and stationary noise signals suppression as well as desired speech extraction based on the TFR information and the H_∞ filter. The virtual sound source concept which transforms the multiple competing speeches from MIMO to SIMO acoustic system is presented to simplify the complicated acoustic system. The performances of the individual noise cancellation block are analyzed and the advantages of the H_∞ filter and the proposed system architecture are also demonstrated.

Chapter 3

Robust Adaptive Beamformer Using the Second-Order Extended H_∞ Filter

3.1 Introduction

Most of the early methods of robust adaptive beamformers are rather *ad hoc* in that the choice of parameters or the structural modifications is not directly related to the uncertainty of the steering vector [11]. Recently, more rigorous approaches were proposed to cope with unknown mismatches via worst-case optimization [38], [39]. Unlike the earlier methods, they make explicit use of the uncertainty set of the steering vector. The work in [38] obtains the beamformer weight by minimizing the output interference-plus-noise power while maintaining a distortionless response for the worst-case steering vector mismatch. The robust MVDR problem in [38] was formulated as a second-order cone program and solved in polynomial time via the interior point method. A number of extensions of the robust MVDR beamformer of [38] have been considered [40]-[43]. However, the main shortcoming of these extensions is that they do not have a computationally efficient online implementation. To overcome this problem,

El-Keyi *et al*. [44] developed a new algorithm for the robust MVDR beamformer of [38] which was based on the constrained SOE Kalman filter that can be implemented online.

The SOE Kalman filter assumes that the dynamics of the signal generating processes are known, so are the statistical properties of noise signals (i.e., uncorrelated and zero-mean Gaussian with known covariance) [48]. However, these assumptions limit the performance since the complex acoustic dynamics is difficult to model and the uncorrelated zero-mean Gaussian noise assumption is quite stringent considering the variety of environmental interferences. To relax these assumptions, this paper proposes the SOE H_∞ filter for the MVDR beamformer of [38] that requires no prior knowledge of the noise statistics but bounded energy. Several studies on the linear and nonlinear H_∞ filter or mixed Kalman/H_∞ filter have been presented [45]-[49] and [52]-[69]. Despite these efforts to expand the use of H_∞ filter to different domains for robustness, there is still no work which considers the second-order extended case similar to that of the SOE Kalman filter presented to the adaptive beamformer.

In this chapter, the SOE H_∞ filter under the robust MVDR beamformer setting [38] is derived based on the game theory approach [69]. In the SOE H_∞ filter, the state estimator and the disturbance signals (initial condition error, process noise and measurement noise) have conflicting objectives, i.e., to minimize and maximize the estimation error, respectively. The estimation criterion in the SOE H_∞ filter design is to minimize the worst possible effects of the disturbance signals on the signal estimation errors without priori knowledge. This estimation criterion makes the SOE H_∞ filter more suitable for speech enhancement in the cases of unknown noise statistics, steering vector uncertainty and modeling error of beamformer weight. To derive the SOE H_∞ filter, the second-order Taylor series expansion is used to approximate the nonlinear function. However, the quadratic terms appear in the series expansion are too complex to make the solution tractable. In this work, they are approximated by the estimation error sample covariance

matrix which effectively simplifies the problem.

The remainder of this chapter is organized as follows. The speech enhancement problem and some necessary background on MVDR beamformer and robust MVDR beamformer of [38] are presented in Section 3.2. In Section 3.3, the SOE Kalman filter for the implementation of the robust MVDR beamformer of [38] is briefly reviewed and the proposed robust MVDR beamformer based on the SOE H_∞ filter is introduced in Section 3.4. Section 3.5 presents the SOE H_∞ filter solution of a general nonlinear discrete-time system and the detail derivation is given in the Appendix I-IV. Finally, summary is drawn in Section 3.6.

3.2 Problem Formulation

Consider an acoustic environment the same with Section 2.2.1 and the received signal of the m-th microphone in frequency domain can be written as:

$$X_m(k,\omega) = \sum_{p=1}^{P} A_{mp}(\omega) S_p(k,\omega) + N_m(k,\omega) \tag{3-1}$$

The MVDR beamformer output at frame k and frequency ω is given by

$$Y_{MV}(k,\omega) = \boldsymbol{w}_{MV}^{\mathrm{H}}(\omega)\boldsymbol{X}(k,\omega) \tag{3-2}$$

where $\boldsymbol{X}(k,\omega) = [X_1(k,\omega) \quad \cdots \quad X_M(k,\omega)]^{\mathrm{T}}$ and $\boldsymbol{w}_{MV}(\omega) \in C^{M\times 1}$ is the MVDR beamformer weights. The well-known MVDR beamformer minimizes the output power of interference-signals-plus-stationary-noise while maintaining a distortionless response to the desired signal. The frequency domain MVDR problem is given by

$$\min_{\boldsymbol{w}_{MV}} \boldsymbol{w}_{MV}^{\mathrm{H}}(\omega)\mathbf{R}_{xx}(\omega)\boldsymbol{w}_{MV}(\omega) \qquad \text{subject to} \qquad \boldsymbol{w}_{MV}^{\mathrm{H}}(\omega)\widetilde{\boldsymbol{A}}(\omega) = 1 \tag{3-3}$$

where

$$\mathbf{R}_{xx}(\omega) = E\left\{\boldsymbol{X}(k,\omega)\boldsymbol{X}^{\mathrm{H}}(k,\omega)\right\} \tag{3-4}$$

$\mathbf{R}_{xx}(\omega)$ is the $M \times M$ correlation matrix and $\widetilde{\boldsymbol{A}}(\omega) \in C^{M\times 1}$ is the presumed steering vector. The solution of the MVDR problem is given by [70],

$$\boldsymbol{w}_{MV}(\omega) = \frac{\mathbf{R}_{xx}^{-1}(\omega)\widetilde{\boldsymbol{A}}(\omega)}{\widetilde{\boldsymbol{A}}^{\mathrm{H}}(\omega)\mathbf{R}_{xx}^{-1}(\omega)\widetilde{\boldsymbol{A}}(\omega)} \tag{3-5}$$

In practice, the correlation matrix is unavailable and is usually approximated by

$$\hat{\mathbf{R}}_{xx}(\omega) = \frac{1}{K}\sum_{k=1}^{K}\boldsymbol{X}(k,\omega)\boldsymbol{X}^{\mathrm{H}}(k,\omega) \tag{3-6}$$

where K is the frame number available. The sample correlation matrix is used in (3-5) to replace the true correlation matrix and the resulting solution is commonly referred to as the sample matrix inversion (SMI) algorithm [70]. If the desired signal is present in the training procedure, the SMI algorithm degrades dramatically [38].The other disadvantage of the SMI algorithm is that it does not provide the sufficient robustness against a mismatch between presumed steering vector $\widetilde{\boldsymbol{A}}(\omega)$ and the actual steering vector $\boldsymbol{A}(\omega) = \left[A_{11}(\omega) \quad \cdots \quad A_{M1}(\omega)\right]^{\mathrm{T}}$.

In practical environment, there may exist unknown mismatches between $\widetilde{\boldsymbol{A}}(\omega)$ and $\boldsymbol{A}(\omega)$ due to the reverberation, microphone mismatch, array configuration mismatch, etc. The norm of the steering vector distortion can be bounded by some known constant $\varepsilon > 0$. Therefore, the actual steering vector belongs to the set

$$\Lambda(\omega) \equiv \left\{\boldsymbol{C}(\omega) \,\middle|\, \boldsymbol{C}(\omega) = \widetilde{\boldsymbol{A}}(\omega) + \boldsymbol{e}(\omega), \left\|\boldsymbol{e}(\omega)\right\| \le \varepsilon\right\} \tag{3-7}$$

The robust MVDR beamformer in [38] minimizes the output of the beamformer while

maintaining a distortion response, not only toward the steering vector $\widetilde{\boldsymbol{A}}(\omega)$ but also toward all the vectors that belong to $\Lambda(\omega)$. Based on this uncertainty description, Vorobyov *et al.* [38] formulated the robust MVDR beamformer problem as,

$$\min_{\boldsymbol{w}_{MV}} \boldsymbol{w}_{MV}^{\mathrm{H}}(\omega)\hat{\mathbf{R}}_{xx}(\omega)\boldsymbol{w}_{MV}(\omega) \quad \text{subject to} \quad \left|\boldsymbol{w}_{MV}^{\mathrm{H}}(\omega)\boldsymbol{C}(\omega)\right| \geq 1 \quad \text{for all} \quad \boldsymbol{C}(\omega) \in \Lambda(\omega) \tag{3-8}$$

The semi-infinite nonconvex constraint in (3-8) was reformulated as a single constraint that corresponds to the worst-case constraint [38]

$$\min_{\boldsymbol{w}_{MV}} \boldsymbol{w}_{MV}^{\mathrm{H}}(\omega)\hat{\mathbf{R}}_{xx}(\omega)\boldsymbol{w}_{MV}(\omega) \quad \text{subject to} \quad \min_{\boldsymbol{C}(\omega)\in\Lambda(\omega)} \left|\boldsymbol{w}_{MV}^{\mathrm{H}}(\omega)\boldsymbol{C}(\omega)\right| \geq 1 \tag{3-9}$$

It can be proven that the inequality constraint in (3-9) is equal to the equality constraint [38]. Therefore, the problem in (3-9) can be rewritten as

$$\begin{aligned} &\min_{\boldsymbol{w}_{MV}} \boldsymbol{w}_{MV}^{\mathrm{H}}(\omega)\hat{\mathbf{R}}_{xx}(\omega)\boldsymbol{w}_{MV}(\omega) \\ &\text{subject to } \left|\boldsymbol{w}_{MV}^{\mathrm{H}}(\omega)\widetilde{\boldsymbol{A}}(\omega) - 1\right|^2 = \varepsilon^2 \boldsymbol{w}_{MV}^{\mathrm{H}}(\omega)\boldsymbol{w}_{MV}(\omega) \end{aligned} \tag{3-10}$$

The problem in (3-10) has been solved in [38] using SOC programming. Moreover, several extensions of the robust MVDR beamformer have been considered. For example, a Newton-type iterative method was proposed for this problem and its modification [39], [40]. Re-formulating (3-10) into a state-space observer form facilitates the application of the SOE Kalman filter [44]. In the following, we briefly review the SOE Kalman filter solution and present a new approach based on the SOE H_∞ filter.

3.3 Robust MVDR beamformer based on the Second-Order Extended Klaman Filter

For the convenience of analysis, the mean square error (MSE) between the zero signal and the beamformer is introduced as,

$$E\left[\left|0-\boldsymbol{X}^{\mathrm{H}}(k,\omega)\boldsymbol{w}_{MV}(k,\omega)\right|^2\right]=\boldsymbol{w}_{MV}^{\mathrm{H}}(\omega)\mathbf{R}_{xx}(\omega)\boldsymbol{w}_{MV}(\omega) \tag{3-11}$$

where $E(\cdot)$ denotes the expectation operation. The constraint in (3-10) can be rewritten as

$$g_2(\boldsymbol{w}_{MV}(k,\omega))=1 \tag{3-12}$$

where

$$\begin{aligned} g_2(\boldsymbol{w}_{MV}(k,\omega)) &= \varepsilon^2\boldsymbol{w}_{MV}^{\mathrm{H}}(k,\omega)\boldsymbol{w}_{MV}(k,\omega)-\boldsymbol{w}_{MV}^{\mathrm{H}}(k,\omega)\widetilde{\boldsymbol{A}}(\omega)\widetilde{\boldsymbol{A}}^{\mathrm{H}}(\omega)\boldsymbol{w}_{MV}(k,\omega) \\ &\quad +\boldsymbol{w}_{MV}^{\mathrm{H}}(k,\omega)\widetilde{\boldsymbol{A}}(\omega)+\widetilde{\boldsymbol{A}}^{\mathrm{H}}(\omega)\boldsymbol{w}_{MV}(k,\omega) \end{aligned} \tag{3-13}$$

Therefore, the robust MVDR beamformer problem can be formulated as

$$\min_{\boldsymbol{w}_{MV}} E\left[\left|0-\boldsymbol{X}^{\mathrm{H}}(k,\omega)\boldsymbol{w}_{MV}(k,\omega)\right|^2\right] \quad \text{subject to} \quad g_2(\boldsymbol{w}_{MV}(k,\omega))=1 \tag{3-14}$$

The constraint minimization problem of (3-14) is written in the state space model below

State equation:

$$\boldsymbol{w}_{MV}(k+1,\omega)=\boldsymbol{w}_{MV}(k,\omega)+\boldsymbol{v}_s(k,\omega) \tag{3-15}$$

Measurement equation:

$$\begin{bmatrix}0\\1\end{bmatrix}=\begin{bmatrix}\boldsymbol{X}^{\mathrm{H}}(k,\omega)\boldsymbol{w}_{MV}(k,\omega)\\ g_2(\boldsymbol{w}_{MV}(k,\omega))\end{bmatrix}+\boldsymbol{v}_m(k,\omega)=\boldsymbol{g}(\boldsymbol{w}_{MV}(k,\omega))+\boldsymbol{v}_m(k,\omega) \tag{3-16}$$

where $\boldsymbol{v}_s(k,\omega)$ and $\boldsymbol{v}_m(k,\omega)$ are the process and measurement noise respectively. The measurement equation is then,

$$\bar{\boldsymbol{y}}=\boldsymbol{g}(\boldsymbol{w}_{MV}(k,\omega))+\boldsymbol{v}_m(k,\omega) \tag{3-17}$$

where $\bar{\boldsymbol{y}}=\begin{bmatrix}0 & 1\end{bmatrix}^{\mathrm{T}}$.

To apply the SOE Kalman filter, the noise processes $\boldsymbol{v}_s(k,\omega)$ and $\boldsymbol{v}_m(k,\omega)$ are assumed to be white, zero mean, uncorrelated, and have known covariance matrices $\widetilde{\mathbf{Q}}$

and $\widetilde{\mathbf{R}}$ respectively.

$$\begin{aligned} E\left[\boldsymbol{v}_s(k,\omega)\boldsymbol{v}_s^{\mathrm{H}}(k,\omega)\right] &= \widetilde{\mathbf{Q}} \\ E\left[\boldsymbol{v}_m(k,\omega)\boldsymbol{v}_m^{\mathrm{H}}(k,\omega)\right] &= \widetilde{\mathbf{R}} \\ E\left[\boldsymbol{v}_s(k,\omega)\boldsymbol{v}_m^{\mathrm{H}}(k,\omega)\right] &= 0 \end{aligned} \tag{3-18}$$

The SOE Kalman filter expands the nonlinear function by using the second-order Taylor series and finds the optimal estimate $\hat{\boldsymbol{w}}_{MV}(k,\omega)$ to minimize the estimation error defined below

$$E\left[\boldsymbol{w}_{MV}(k,\omega)-\hat{\boldsymbol{w}}_{MV}(k,\omega)\right]=0 \tag{3-19}$$

To present the SOE Kalman filter solution, we start by evaluating the Jacobian $\mathbf{G}_w(k,\omega)$ of $g(\boldsymbol{w}_{MV}(k,\omega))$ and Hessian matrices $\mathbf{G}_{ww}^{(1)}(\omega)$ and $\mathbf{G}_{ww}^{(2)}(\omega)$ of its components as

$$\begin{aligned} \mathbf{G}_w(k,\omega) &= \left\{\nabla_{w_{MV}} g^{\mathrm{T}}(\boldsymbol{w}_{MV}(k,\omega))\right\}^{\mathrm{T}} \\ &= \begin{bmatrix} \boldsymbol{X}^{\mathrm{H}}(k,\omega) \\ \varepsilon^2 \boldsymbol{w}_{MV}^{\mathrm{H}}(k,\omega) - \left(\widetilde{\boldsymbol{A}}(\omega)\widetilde{\boldsymbol{A}}^{\mathrm{H}}(\omega)\boldsymbol{w}_{MV}(k,\omega)\right)^{\mathrm{H}} + \widetilde{\boldsymbol{A}}^{\mathrm{H}}(\omega) \end{bmatrix} \end{aligned} \tag{3-20}$$

$$\mathbf{G}_{ww}^{(1)}(\omega) = \nabla_{w_{MV}} \nabla_{w_{MV}}^{\mathrm{H}} \left\{\boldsymbol{X}^{\mathrm{H}}(k,\omega)\boldsymbol{w}_{MV}(k,\omega)\right\} = 0 \tag{3-21}$$

$$\mathbf{G}_{ww}^{(2)}(\omega) = \nabla_{w_{MV}} \nabla_{w_{MV}}^{\mathrm{H}} \left\{g_2(\boldsymbol{w}_{MV}(k,\omega))\right\} = \varepsilon^2 \mathbf{I} - \widetilde{\boldsymbol{A}}(\omega)\widetilde{\boldsymbol{A}}^{\mathrm{H}}(\omega) \tag{3-22}$$

where $\mathbf{I}$ is the identity matrix. For the state space model (3-15) and (3-16), the SOE Kalman filter solution is given by [48]

$$\hat{\boldsymbol{w}}_{MV}(k+1,\omega) = \hat{\boldsymbol{w}}_{MV}(k,\omega) + \widetilde{\mathbf{K}}(k,\omega)\left[\bar{\boldsymbol{y}} - \hat{\boldsymbol{y}}_{km}(k,\omega)\right] \tag{3-23}$$

where the predicted measurement is obtained by

$$\hat{\boldsymbol{y}}_{km}(k,\omega) = \begin{bmatrix} \boldsymbol{X}^{\mathrm{H}}(k,\omega)\hat{\boldsymbol{w}}_{MV}(k,\omega) \\ g_2(\hat{\boldsymbol{w}}_{MV}(k,\omega)) + 0.5 \cdot tr\left\{\mathbf{G}_{ww}^{(2)}(\omega)\widetilde{\mathbf{P}}^{-}(k,\omega)\right\} \end{bmatrix} \tag{3-24}$$

and the filter gain and predicted weight error covariance matrix are given by

$$\widetilde{\mathbf{K}}(k,\omega)=\widetilde{\mathbf{P}}^{-}(k,\omega)\mathbf{G}_{w}^{\mathrm{H}}(k,\omega)\left(\mathbf{G}_{w}(k,\omega)\widetilde{\mathbf{P}}^{-}(k,\omega)\mathbf{G}_{w}^{\mathrm{H}}(k,\omega)+\widetilde{\mathbf{R}}\right)^{-1} \tag{3-25}$$

$$\widetilde{\mathbf{P}}^{-}(k,\omega)=\widetilde{\mathbf{P}}^{+}(k-1,\omega)+\widetilde{\mathbf{Q}} \tag{3-26}$$

$$\widetilde{\mathbf{P}}^{+}(k,\omega)=\left(\mathbf{I}-\widetilde{\mathbf{K}}(k,\omega)\mathbf{G}_{w}(k,\omega)\right)\widetilde{\mathbf{P}}^{-}(k,\omega) \tag{3-27}$$

where $\widetilde{\mathbf{K}}(k,\omega)$ is the Kalman gain; $\widetilde{\mathbf{P}}^{-}(k,\omega)$ is the priori error covariance matrix and $\widetilde{\mathbf{P}}^{+}(k,\omega)$ is the posteriori error covariance matrix. After some algebra operations [48], the Kalman gain can be rewritten as (3-28) and covariance matrices $\widetilde{\mathbf{P}}^{-}(k,\omega)$ and $\widetilde{\mathbf{P}}^{+}(k,\omega)$ can be integrated as (3-29)

$$\widetilde{\mathbf{K}}(k,\omega)=\widetilde{\mathbf{P}}^{-}(k,\omega)\left(\mathbf{I}+\mathbf{G}_{w}^{\mathrm{H}}(k,\omega)\widetilde{\mathbf{R}}^{-1}\mathbf{G}_{w}(k,\omega)\widetilde{\mathbf{P}}^{-}(k,\omega)\right)^{-1}\mathbf{G}_{w}^{\mathrm{H}}(k,\omega)\widetilde{\mathbf{R}}^{-1} \tag{3-28}$$

$$\widetilde{\mathbf{P}}^{-}(k+1,\omega)=\widetilde{\mathbf{P}}^{-}(k,\omega)(\mathbf{I}+\mathbf{G}_{w}^{\mathrm{H}}(k,\omega)\widetilde{\mathbf{R}}^{-1}\mathbf{G}_{w}(k,\omega)\widetilde{\mathbf{P}}^{-}(k,\omega))^{-1}+\widetilde{\mathbf{Q}} \tag{3-29}$$

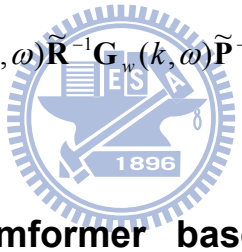

3.4 Robust MVDR beamformer based on the Second-Order Extended H_∞ Filter

In contrast to minimizing the expected value of the estimation error variance like the SOE Kalman filter, another strategy is to minimize the worst possible effects of the disturbances on the signal estimation errors. This is essentially to minimize the infinity norm of the input-output relation. In this case, no assumptions on the noise statistics are necessary (such as (3-18)) but the boundedness of the noise energy. Considering the state space model (3-15) and (3-16), and the estimation of some arbitrary linear combination of $\boldsymbol{w}_{MV}(k,\omega)$, i.e.,

$$\boldsymbol{z}(k,\omega)=\mathbf{C}\boldsymbol{w}_{MV}(k,\omega) \tag{3-30}$$

where $\mathbf{C}$ is a user-defined matrix. The estimate of $\boldsymbol{z}(k,\omega)$ is denoted by $\hat{\boldsymbol{z}}(k,\omega)$ and the estimate of initial state $\boldsymbol{w}_{MV}(0,\omega)$ is denoted by $\hat{\boldsymbol{w}}_{MV}(0,\omega)$. The design criterion of the SOE H_∞ filter is to find $\hat{\boldsymbol{z}}(k,\omega)$ that minimizes J for any $\boldsymbol{v}_s(k,\omega)$, $\boldsymbol{v}_m(k,\omega)$ and $\boldsymbol{w}_{MV}(0,\omega)$. The performance index J can be defined as:

$$J=\frac{\sum_{k=0}^{N-1}\left|\boldsymbol{z}(k,\omega)-\hat{\boldsymbol{z}}(k,\omega)\right|^2_{\mathbf{S}(k,\omega)}}{\left|\boldsymbol{w}_{MV}(0,\omega)-\hat{\boldsymbol{w}}_{MV}(0,\omega)\right|^2_{\mathbf{P}^{-1}(0,\omega)}+\sum_{k=0}^{N-1}\left(\left|\boldsymbol{v}_s(k,\omega)\right|^2_{\mathbf{Q}^{-1}(k,\omega)}+\left|\boldsymbol{v}_m(k,\omega)\right|^2_{\mathbf{R}^{-1}(k,\omega)}\right)} \tag{3-31}$$

The notation $\left|\boldsymbol{x}(k,\omega)\right|^2_{\mathbf{S}(k,\omega)}$ is defined as the square of the weighted (by $\mathbf{S}(k,\omega)$) L_2 norm of $\boldsymbol{x}(k,\omega)$, i.e., $\left|\boldsymbol{x}(k,\omega)\right|^2_{\mathbf{S}(k,\omega)}=\boldsymbol{x}^{\mathrm{H}}(k,\omega)\mathbf{S}(k,\omega)\boldsymbol{x}(k,\omega)$. The matrices $\mathbf{P}(0,\omega),\mathbf{Q}(k,\omega),\mathbf{R}(k,\omega)$ and $\mathbf{S}(k,\omega)$ are symmetric positive definite matrices chosen by the user based on the specific problem. To simplify the analysis, we assume the weighting matrices $\mathbf{Q}(k,\omega)$, $\mathbf{R}(k,\omega)$ and $\mathbf{S}(k,\omega)$ are independent of frame and frequency. Hence, equation (3-31) can be reformulated as

$$J=\frac{\sum_{k=0}^{N-1}\left|\boldsymbol{z}(k,\omega)-\hat{\boldsymbol{z}}(k,\omega)\right|^2_{\mathbf{S}}}{\left|\boldsymbol{w}_{MV}(0,\omega)-\hat{\boldsymbol{w}}_{MV}(0,\omega)\right|^2_{\mathbf{P}^{-1}(0,\omega)}+\sum_{k=0}^{N-1}\left(\left|\boldsymbol{v}_s(k,\omega)\right|^2_{\mathbf{Q}^{-1}}+\left|\boldsymbol{v}_m(k,\omega)\right|^2_{\mathbf{R}^{-1}}\right)} \tag{3-32}$$

To solve the problem, a performance bound γ is selected and $\hat{\boldsymbol{z}}(k,\omega)$ is computed to satisfy

$$\sup J<\gamma \tag{3-33}$$

where sup represents supremum. The formulation of (3-33) shows that the SOE H_∞ optimal estimators guarantee the smallest estimation error energy over all possible disturbances ($\boldsymbol{w}_{MV}(0,\omega)-\hat{\boldsymbol{w}}_{MV}(0,\omega),\boldsymbol{v}_s(k,\omega)$ and $\boldsymbol{v}_m(k,\omega)$) of finite energy. They are over-conservative but have a better robust behavior to the disturbance variations. The SOE H_∞ filter can be interpreted as a *minmax* problem where the estimator strategy

$\hat{\boldsymbol{z}}(k,\omega)$ plays against the exogenous inputs $\boldsymbol{v}_s(k,\omega)$, $\boldsymbol{v}_m(k,\omega)$ and the uncertainty of the initial state $\boldsymbol{w}_{MV}(0,\omega)$, so the performance criterion is equivalent to

$$\begin{aligned}\min_{\hat{\boldsymbol{z}}} \max_{\boldsymbol{v}_s,\boldsymbol{v}_m,\boldsymbol{w}_{MV}(0,\omega)} J = &-\gamma\left|\boldsymbol{w}_{MV}(0,\omega)-\hat{\boldsymbol{w}}_{MV}(0,\omega)\right|^2_{\mathbf{P}^{-1}(0,\omega)} \\ &+\sum_{k=0}^{N-1}\left[\left|\boldsymbol{z}(k,\omega)-\hat{\boldsymbol{z}}(k,\omega)\right|^2_{\mathbf{S}}-\gamma\left(\left|\boldsymbol{v}_s(k,\omega)\right|^2_{\mathbf{Q}^{-1}}+\left|\boldsymbol{v}_m(k,\omega)\right|^2_{\mathbf{R}^{-1}}\right)\right]\end{aligned} \tag{3-34}$$

Since $\boldsymbol{v}_m(k,\omega)=\bar{\boldsymbol{y}}-\boldsymbol{g}(\boldsymbol{w}_{MV}(k,\omega))$, $\boldsymbol{z}(k,\omega)=\mathbf{C}\boldsymbol{w}_{MV}(k,\omega)$ and $\hat{\boldsymbol{z}}(k,\omega)=\mathbf{C}\hat{\boldsymbol{w}}_{MV}(k,\omega)$, equation (3-34) can be rewritten as:

$$\begin{aligned}\min_{\hat{\boldsymbol{w}}_{MV}} \max_{\boldsymbol{v}_s,\bar{\boldsymbol{y}},\boldsymbol{w}_{MV}(0,\omega)} J = &-\gamma\left|\boldsymbol{w}_{MV}(0,\omega)-\hat{\boldsymbol{w}}_{MV}(0,\omega)\right|^2_{\mathbf{P}^{-1}(0,\omega)} \\ &+\sum_{k=0}^{N-1}\left[\left|\boldsymbol{w}_{MV}(k,\omega)-\hat{\boldsymbol{w}}_{MV}(k,\omega)\right|^2_{\bar{\mathbf{S}}}-\gamma\left(\left|\boldsymbol{v}_s(k,\omega)\right|^2_{\mathbf{Q}^{-1}}+\left|\bar{\boldsymbol{y}}-\boldsymbol{g}(\boldsymbol{w}_{MV}(k,\omega))\right|^2_{\mathbf{R}^{-1}}\right)\right]\end{aligned} \tag{3-35}$$

where $\bar{\mathbf{S}}=\mathbf{C}^{\mathrm{H}}\mathbf{S}\mathbf{C}$.

Considering a second-order approximation of the nonlinearity in (3-35), the solution of (3-35) leads to the SOE H_∞ filter. The solution of the SOE H_∞ filter for a class of discrete-time nonlinear systems has been briefly explained in Section 3.5 and is derived in Appendix I-IV. By substituting the corresponding matrices to (3-61)-(3-65), the solution of the SOE H_∞ filter for the state space model (3-15) and (3-16) is given as,

$$\hat{\boldsymbol{w}}_{MV}(k+1,\omega)=\hat{\boldsymbol{w}}_{MV}(k,\omega)+\mathbf{K}(k,\omega)\left[\bar{\boldsymbol{y}}-\hat{\boldsymbol{y}}_h(k,\omega)\right] \tag{3-36}$$

$$\mathbf{K}(k,\omega)=\mathbf{P}(k,\omega)\left(\mathbf{I}-\frac{1}{\gamma}\bar{\mathbf{S}}\mathbf{P}(k,\omega)+\mathbf{G}_w^{\mathrm{H}}(k,\omega)\mathbf{R}^{-1}\mathbf{G}_w(k,\omega)\mathbf{P}(k,\omega)\right)^{-1}\mathbf{G}_w^{\mathrm{H}}(k,\omega)\mathbf{R}^{-1} \tag{3-37}$$

$$\mathbf{P}(k+1,\omega)=\mathbf{P}(k,\omega)(\mathbf{I}-\frac{1}{\gamma}\bar{\mathbf{S}}\mathbf{P}(k,\omega)+\mathbf{G}_w^{\mathrm{H}}(k,\omega)\mathbf{R}^{-1}\mathbf{G}_w(k,\omega)\mathbf{P}(k,\omega))^{-1}+\mathbf{Q} \tag{3-38}$$

$$\boldsymbol{\lambda}(k+1,\omega)=\left[\mathbf{I}-\frac{1}{\gamma}\bar{\mathbf{S}}\mathbf{P}(k,\omega)+\mathbf{G}_w^{\mathrm{H}}(k,\omega)\mathbf{R}^{-1}\mathbf{G}_w(k,\omega)\mathbf{P}(k,\omega)\right]\boldsymbol{\lambda}(k,\omega)-\mathbf{G}_w^{\mathrm{H}}(k,\omega)\mathbf{R}^{-1}\left(\bar{\boldsymbol{y}}-\hat{\boldsymbol{y}}_h(k,\omega)\right) \tag{3-39}$$

$$\bar{\mathbf{P}}(k+1,\omega)=\eta\bar{\mathbf{P}}(k,\omega)+(1-\eta)\mathbf{P}(k,\omega)\boldsymbol{\lambda}(k,\omega)\boldsymbol{\lambda}^{\mathrm{H}}(k,\omega)\mathbf{P}^{\mathrm{H}}(k,\omega) \tag{3-40}$$

where $0 < \eta \le 1$ and the predicted measurement is obtained by

$$\hat{\boldsymbol{y}}_h(k,\omega) = \begin{bmatrix} \boldsymbol{X}^{\mathrm{H}}(k,\omega)\hat{\boldsymbol{w}}_{MV}(k,\omega) \\ g_2(\hat{\boldsymbol{w}}_{MV}(k,\omega)) + 0.5 \cdot tr\left\{\mathbf{G}_{ww}^{(2)}(\omega)\overline{\mathbf{P}}(k,\omega)\right\} \end{bmatrix} \tag{3-41}$$

Comparing with the SOE Kalman filter solution, we can observe the following.

1. The structures of the matrices $\widetilde{\mathbf{K}}(k,\omega)$ and $\widetilde{\mathbf{P}}^{-}(k+1,\omega)$ ((3-28) and (3-29)) in the SOE Kalman filter are similar to the structures of $\mathbf{K}(k,\omega)$ and $\mathbf{P}(k+1,\omega)$ ((3-37) and (3-38)) in the SOE H_∞ filter. If the weighting matrices $\widetilde{\mathbf{P}}(0,\omega)$, $\widetilde{\mathbf{Q}}$ and $\widetilde{\mathbf{R}}$ are the same with the covariance matrices $\mathbf{P}(0,\omega)$, $\mathbf{Q}$ and $\mathbf{R}$, $\widetilde{\mathbf{K}}(k,\omega)$ and $\widetilde{\mathbf{P}}^{-}(k+1,\omega)$ have the same structures with $\mathbf{K}(k,\omega)$ and $\mathbf{P}(k+1,\omega)$ respectively when $\gamma \to \infty$.

2. The second-order terms of Taylor series in the SOE H_∞ filter and the SOE Kalman filter are both approximated by the state estimation error sample covariance matrix. However, unlike the error covariance matrix $\widetilde{\mathbf{P}}^{-}(k,\omega)$ or $\widetilde{\mathbf{P}}^{+}(k,\omega)$ in the SOE Kalman filter, the matrix $\mathbf{P}(k,\omega)$ in the SOE H_∞ filter does not represent the estimation error covariance matrix. Therefore, equations (3-39) and (3-40) are utilized to approximate the estimation error covariance matrix.

3.5 The Second-Order Extended H_∞ Filter

This section provides the SOE H_∞ filter solution of a general nonlinear discrete-time system shown in (3.42). Although, the state space model (3-15) and (3-16) are not exactly the same with (A-1). However, like the SOE Kalman filter solution [48], the SOE H_∞ filter solution of (3.42) can be easily applied to (3-15) and (3-16).

Consider a nonlinear discrete-time system

$$\begin{aligned} \boldsymbol{x}_a(t+1) &= f(\boldsymbol{x}_a(t)) + \boldsymbol{w}_a(t) \\ \boldsymbol{y}_a(t) &= h(\boldsymbol{x}_a(t)) + \boldsymbol{v}_a(t) \end{aligned} \tag{3-42}$$

where $\boldsymbol{x}_a(t)$ and $\boldsymbol{y}_a(t)$ are the state and measurement vectors with the dimensions of d_s and d_m respectively; $\boldsymbol{w}_a(t)$ and $\boldsymbol{v}_a(t)$ are the process and measurement noise. $f(\cdot)$ and $h(\cdot)$ are vectors of smooth nonlinear functions that are second-order differentiable with respect to $\boldsymbol{x}_a(t)$. The second-order Taylor series expansion of $f(\boldsymbol{x}_a(t))$ and $h(\boldsymbol{x}_a(t))$ around the nominal point $\hat{\boldsymbol{x}}_a(t)$ (the estimated state) are

$$\begin{aligned} f(\boldsymbol{x}_a(t)) &= f(\hat{\boldsymbol{x}}_a(t)) + \left.\frac{\partial f}{\partial x_a(t)}\right|_{\hat{\boldsymbol{x}}_a(t)} (\boldsymbol{x}_a(t) - \hat{\boldsymbol{x}}_a(t)) \\ &\quad + \frac{1}{2}\sum_{i=1}^{d_s} \phi_i^f (\boldsymbol{x}_a(t) - \hat{\boldsymbol{x}}_a(t))^{\mathrm{T}} \left.\frac{\partial^2 f_i}{\partial x_a^2(t)}\right|_{\hat{\boldsymbol{x}}_a(t)} (\boldsymbol{x}_a(t) - \hat{\boldsymbol{x}}_a(t)) \\ h(\boldsymbol{x}_a(t)) &= h(\hat{\boldsymbol{x}}_a(t)) + \left.\frac{\partial h}{\partial x_a(t)}\right|_{\hat{\boldsymbol{x}}_a(t)} (\boldsymbol{x}_a(t) - \hat{\boldsymbol{x}}_a(t)) \\ &\quad + \frac{1}{2}\sum_{i=1}^{d_m} \phi_i^h (\boldsymbol{x}_a(t) - \hat{\boldsymbol{x}}_a(t))^{\mathrm{T}} \left.\frac{\partial^2 h_i}{\partial x_a^2(t)}\right|_{\hat{\boldsymbol{x}}_a(t)} (\boldsymbol{x}_a(t) - \hat{\boldsymbol{x}}_a(t)) \end{aligned} \tag{3-43}$$

where f_i and h_i are the ith element of $f(\boldsymbol{x}_a(t))$ and $h(\boldsymbol{x}_a(t))$. ϕ_i^f and ϕ_i^h are the $d_s \times 1$ and $d_m \times 1$ vectors with all zeros expect for the one in the ith element. The quadratic term in (3-43) can be written as

$$\begin{aligned} (\boldsymbol{x}_a(t) - \hat{\boldsymbol{x}}_a(t))^{\mathrm{T}} \left.\frac{\partial^2 f_i}{\partial x_a^2(t)}\right|_{\hat{\boldsymbol{x}}_a(t)} (\boldsymbol{x}_a(t) - \hat{\boldsymbol{x}}_a(t)) &= tr\left[\left.\frac{\partial^2 f_i}{\partial x_a^2(t)}\right|_{\hat{\boldsymbol{x}}_a(t)} (\boldsymbol{x}_a(t) - \hat{\boldsymbol{x}}_a(t))(\boldsymbol{x}_a(t) - \hat{\boldsymbol{x}}_a(t))^{\mathrm{T}} \right] \\ (\boldsymbol{x}_a(t) - \hat{\boldsymbol{x}}_a(t))^{\mathrm{T}} \left.\frac{\partial^2 h_i}{\partial x_a^2(t)}\right|_{\hat{\boldsymbol{x}}_a(t)} (\boldsymbol{x}_a(t) - \hat{\boldsymbol{x}}_a(t)) &= tr\left[\left.\frac{\partial^2 h_i}{\partial x_a^2(t)}\right|_{\hat{\boldsymbol{x}}_a(t)} (\boldsymbol{x}_a(t) - \hat{\boldsymbol{x}}_a(t))(\boldsymbol{x}_a(t) - \hat{\boldsymbol{x}}_a(t))^{\mathrm{T}} \right] \end{aligned} \tag{3-44}$$

where $tr[\cdot]$ is the trace operation. Assume that the matrix $(\boldsymbol{x}_a(t)-\hat{\boldsymbol{x}}_a(t))(\boldsymbol{x}_a(t)-\hat{\boldsymbol{x}}_a(t))^{\mathrm{T}}$ can be obtained by the expected values of the past data, i.e., it becomes independent of the current state $\boldsymbol{x}_a(t)$. Denote the matrix as $\overline{\mathbf{P}}_a$, and we assume that the value of this matrix can be estimated. Hence, we have

$$\begin{aligned} tr\left[\left.\frac{\partial^2 f_i}{\partial x_a^2(t)}\right|_{\hat{\boldsymbol{x}}_a(t)}(\boldsymbol{x}_a(t)-\hat{\boldsymbol{x}}_a(t))(\boldsymbol{x}_a(t)-\hat{\boldsymbol{x}}_a(t))^{\mathrm{T}}\right] &\approx tr\left[\left.\frac{\partial^2 f_i}{\partial x_a^2(t)}\right|_{\hat{\boldsymbol{x}}_a(t)}\overline{\mathbf{P}}_a\right] \\ tr\left[\left.\frac{\partial^2 h_i}{\partial x_a^2(t)}\right|_{\hat{\boldsymbol{x}}_a(t)}(\boldsymbol{x}_a(t)-\hat{\boldsymbol{x}}_a(t))(\boldsymbol{x}_a(t)-\hat{\boldsymbol{x}}_a(t))^{\mathrm{T}}\right] &\approx tr\left[\left.\frac{\partial^2 h_i}{\partial x_a^2(t)}\right|_{\hat{\boldsymbol{x}}_a(t)}\overline{\mathbf{P}}_a\right] \end{aligned} \tag{3-45}$$

Later $\overline{\mathbf{P}}_a$ is approximated by the sample covariance matrix of the estimation error. The goal is to estimate a linear combination of $\boldsymbol{x}_a(t)$ using the observation, i.e.,

$$\boldsymbol{z}_a(t)=\mathbf{C}_a\boldsymbol{x}_a(t) \tag{3-46}$$

where $\mathbf{C}_a$ is a user-defined matrix. The estimate of $\boldsymbol{z}_a(t)$ is denoted by $\hat{\boldsymbol{z}}_a(t)$ and the estimate of initial state $\boldsymbol{x}_a(0)$ is denoted by $\hat{\boldsymbol{x}}_a(0)$. The design criterion of the SOE H_∞ filter is to find $\hat{\boldsymbol{z}}_a(t)$ that minimizes J for any $\boldsymbol{w}_a(t)$, $\boldsymbol{v}_a(t)$ and $\boldsymbol{x}_a(0)$. The cost function can be defined as:

$$J=\frac{\sum_{t=0}^{N-1}\left|\boldsymbol{z}_a(t)-\hat{\boldsymbol{z}}_a(t)\right|^2_{\mathbf{S}_a(t)}}{\left|\boldsymbol{x}_a(0)-\hat{\boldsymbol{x}}_a(0)\right|^2_{\mathbf{P}_a^{-1}(0)}+\sum_{t=0}^{N-1}\left(\left|\boldsymbol{w}_a(t)\right|^2_{\mathbf{Q}_a^{-1}(t)}+\left|\boldsymbol{v}_a(t)\right|^2_{\mathbf{R}_a^{-1}(t)}\right)} \tag{3-47}$$

The term $\left|\boldsymbol{x}(t)\right|^2_{\mathbf{S}(t)}$ is defined as the square of the weighted (by $\mathbf{S}(t)$) L_2 norm of $\boldsymbol{x}(t)$, i.e., $\left|\boldsymbol{x}(t)\right|^2_{\mathbf{S}(t)}=\boldsymbol{x}^{\mathrm{T}}(t)\mathbf{S}(t)\boldsymbol{x}(t)$. The matrices $\mathbf{P}_a(0),\mathbf{Q}_a(t),\mathbf{R}_a(t)$ and $\mathbf{S}_a(t)$ are symmetric positive definite matrices chosen by the user based on the specific problem. For the SOE

H_∞ filter, a performance bound γ is selected and $\hat{z}_a(t)$ is computed to satisfy

$$\sup J < \gamma \tag{3-48}$$

where sup represents supremum. The SOE H_∞ filter can be interpreted as a *minmax* problem where the estimator strategy $\hat{z}_a(t)$ plays against the exogenous inputs $\boldsymbol{w}_a(t)$, $\boldsymbol{v}_a(t)$ and the initial state $\boldsymbol{x}_a(0)$. The performance criterion is equivalent to

$$\min_{\hat{z}_a(t)} \max_{\boldsymbol{w}_a(t),\boldsymbol{v}_a(t),\boldsymbol{x}_a(0)} J = -\gamma\left|\boldsymbol{x}_a(0)-\hat{\boldsymbol{x}}_a(0)\right|^2_{\mathbf{P}_a^{-1}(0)} + \sum_{t=0}^{N-1}\left[\left|\boldsymbol{z}_a(t)-\hat{\boldsymbol{z}}_a(t)\right|^2_{\mathbf{S}_a(t)} - \gamma\left(\left|\boldsymbol{w}_a(t)\right|^2_{\mathbf{Q}_a^{-1}(t)} + \left|\boldsymbol{v}_a(t)\right|^2_{\mathbf{R}_a^{-1}(t)}\right)\right] \tag{3-49}$$

Since $\boldsymbol{v}_a(t) = \boldsymbol{y}_a(t) - h(\boldsymbol{x}_a(t))$, $\boldsymbol{z}_a(t) = \mathbf{C}_a\boldsymbol{x}_a(t)$ and $\hat{\boldsymbol{z}}_a(t) = \mathbf{C}_a\hat{\boldsymbol{x}}_a(t)$, equation (3-49) can be rewritten as:

$$\begin{aligned}\min_{\hat{\boldsymbol{x}}_a(t)} \max_{\boldsymbol{w}_a(t),\boldsymbol{y}_a(t),\boldsymbol{x}_a(0)} J = {} & -\gamma\left|\boldsymbol{x}_a(0)-\hat{\boldsymbol{x}}_a(0)\right|^2_{\mathbf{P}_a^{-1}(0)} \\ & + \sum_{t=0}^{N-1}\left[\left|\boldsymbol{x}_a(t)-\hat{\boldsymbol{x}}_a(t)\right|^2_{\overline{\mathbf{S}}_a(t)} - \gamma\left(\left|\boldsymbol{w}_a(t)\right|^2_{\mathbf{Q}_a^{-1}(t)} + \left|\boldsymbol{y}_a(t)-h(\boldsymbol{x}_a(t))\right|^2_{\mathbf{R}_a^{-1}(t)}\right)\right]\end{aligned} \tag{3-50}$$

where $\overline{\mathbf{S}}_a(t) = \mathbf{C}_a^{\mathrm{H}}\mathbf{S}_a(t)\mathbf{C}_a$. Let's define $\psi\left(\boldsymbol{x}_a(0)\right) = -\gamma\left|\boldsymbol{x}_a(0)-\hat{\boldsymbol{x}}_a(0)\right|^2_{\mathbf{P}_a^{-1}(0)}$ and

$$L(t) = \left|\boldsymbol{x}_a(t)-\hat{\boldsymbol{x}}_a(t)\right|^2_{\overline{\mathbf{S}}_a(t)} - \gamma\left(\left|\boldsymbol{w}_a(t)\right|^2_{\mathbf{Q}_a^{-1}(t)} + \left|\boldsymbol{y}_a(t)-h(\boldsymbol{x}_a(t))\right|^2_{\mathbf{R}_a^{-1}(t)}\right)$$

Therefore, J in (3.50) is written as

$$J = \psi\left(\boldsymbol{x}_a(0)\right) + \sum_{t=0}^{N-1} L(t) \tag{3-51}$$

Because $\boldsymbol{x}_a(0)$, $\boldsymbol{w}_a(t)$ and $\boldsymbol{y}_a(t)$ influences J independently, the stationary point of J with respect to $\boldsymbol{x}_a(0)$, $\boldsymbol{w}_a(t)$ and $\boldsymbol{y}_a(t)$ can be found sequentially. To solve the minmax problem, a stationary point of J with respect to $\boldsymbol{x}_a(0)$ and $\boldsymbol{w}_a(t)$ is found first, and then a stationary point of J with respect to $\hat{\boldsymbol{x}}_a(t)$ and $\boldsymbol{y}_a(t)$ is found. The steps of this derivation can be separated into three steps. First, a stationary point of J with respect to $\boldsymbol{x}_a(0)$ and $\boldsymbol{w}_a(t)$ is found in Appendix I. Secondly, a stationary point of J with

respect to $\hat{\boldsymbol{x}}_a(t)$ and $\boldsymbol{y}_a(t)$ is found in Appendix II based on the results from Appendix I. Finally, according to Appendix I and Appendix II, the SOE H_∞ filter solution of the nonlinear discrete-time system in (3.42) is given in Appendix III.

3.5.1. The Second-Order Extended H_∞ Filter Solution

Theorem 1: Consider the minmax problem in (3-50) and use the second-order Taylor series described in (3-43)-(3-45) to approximate the nonlinear function in (3-42). The stationary point of J with respect to $\boldsymbol{x}_a(0)$ and $\boldsymbol{w}_a(t)$ is given by:

$$\boldsymbol{x}_a(0) = \hat{\boldsymbol{x}}_a(0) + \mathbf{P}_a(0)\boldsymbol{\lambda}(0) \tag{3-52}$$

$$\boldsymbol{w}_a(t) = \mathbf{Q}_a(t)\boldsymbol{\lambda}(t+1) \tag{3-53}$$

$$\boldsymbol{\lambda}(N) = 0 \tag{3-54}$$

$$\boldsymbol{\lambda}(t) = \left[\mathbf{I} - \frac{1}{\gamma}\overline{\mathbf{S}}_a(t)\mathbf{P}_a(t) + H^{\mathrm{T}}(t)\mathbf{R}_a^{-1}(t)H(t)\mathbf{P}_a(t)\right]^{-1} \times \left[F^{\mathrm{T}}(t)\boldsymbol{\lambda}(t+1) + \frac{1}{\gamma}\overline{\mathbf{S}}_a(t)\left(\mu(t) - \hat{\boldsymbol{x}}_a(t)\right)\right.$$
$$\left. + H^{\mathrm{T}}(t)\mathbf{R}_a^{-1}(t)\left(\boldsymbol{y}_a(t) - h(\hat{\boldsymbol{x}}_a(t)) - H(t)(\mu(t) - \hat{\boldsymbol{x}}_a(t)) - \frac{1}{2}\sum_{i=1}^{d_m}\phi_i^h tr\left[\left.\frac{\partial^2 h_i}{\partial x_a^2(t)}\right|_{\hat{\boldsymbol{x}}_a(t)}\overline{\mathbf{P}}_a\right]\right)\right] \tag{3-55}$$

$$\mathbf{P}_a(t+1) = F(t)\mathbf{P}_a(t)\left[\mathbf{I} - \frac{1}{\gamma}\overline{\mathbf{S}}_a(t)\mathbf{P}_a(t) + H^{\mathrm{T}}(t)\mathbf{R}_a^{-1}(t)H(t)\mathbf{P}_a(t)\right]^{-1}F^{\mathrm{T}}(t) + \mathbf{Q}_a(t) \tag{3-56}$$

$$\mu(0) = \hat{\boldsymbol{x}}_a(0) \tag{3-57}$$

$$\mu(t+1) = f(\hat{\boldsymbol{x}}_a(t)) + F(t)(\mu(t) - \hat{\boldsymbol{x}}_a(t)) + \frac{1}{2}\sum_{i=1}^{d_s}\phi_i^f tr\left[\left.\frac{\partial^2 f_i}{\partial x_a^2(t)}\right|_{\hat{\boldsymbol{x}}_a(t)}\overline{\mathbf{P}}_a\right]$$
$$+ F(t)\mathbf{P}_a(t)\left[\mathbf{I} - \frac{1}{\gamma}\overline{\mathbf{S}}_a(t)\mathbf{P}_a(t) + H^{\mathrm{T}}(t)\mathbf{R}_a^{-1}(t)H(t)\mathbf{P}_a(t)\right]^{-1}$$
$$\times\left[\frac{1}{\gamma}\overline{\mathbf{S}}_a(t)\left(\mu(t) - \hat{\boldsymbol{x}}_a(t)\right) + H^{\mathrm{T}}(t)\mathbf{R}_a^{-1}(t)\left(\boldsymbol{y}_a(t) - h(\hat{\boldsymbol{x}}_a(t)) - H(t)(\mu(t) - \hat{\boldsymbol{x}}_a(t)) - \frac{1}{2}\sum_{i=1}^{d_m}\phi_i^h tr\left[\left.\frac{\partial^2 h_i}{\partial x_a^2(t)}\right|_{\hat{\boldsymbol{x}}_a(t)}\overline{\mathbf{P}}_a\right]\right)\right] \tag{3-58}$$

where $F_k = \left.\frac{\partial f}{\partial x_k}\right|_{\hat{x}_k}$ and $H_k = \left.\frac{\partial h}{\partial x_k}\right|_{\hat{x}_k}$.

[Proof]: Please see Appendix I.

Theorem 2: Given the values of $\boldsymbol{x}_a(0)$ and $\boldsymbol{w}_a(t)$ described in Theorem 1, the stationary point of J with respect to $\hat{\boldsymbol{x}}_a(t)$ and $\boldsymbol{y}_a(t)$ is given by:

$$\hat{\boldsymbol{x}}_a(t) = \mu(t) \tag{3-59}$$

$$\boldsymbol{y}_a(t) = h(\hat{\boldsymbol{x}}_a(t)) + \frac{1}{2}\sum_{i=1}^{d_m} \phi_i^h tr\left[\left.\frac{\partial^2 h_i}{\partial x_a^2(t)}\right|_{\hat{x}_a(t)} \overline{\mathbf{P}}_a \right] \tag{3-60}$$

[Proof]: Please see Appendix II.

Theorem 3: According to Theorem 1 and Theorem 2, the SOE H_∞ filter solution for the state space model (3-42) can be given by

$$\begin{aligned}\hat{\boldsymbol{x}}_a(t+1) = f(\hat{\boldsymbol{x}}_a(t)) &+ \frac{1}{2}\sum_{i=1}^{d_s} \phi_i^f tr\left[\left.\frac{\partial^2 f_i}{\partial x_a^2(t)}\right|_{\hat{x}_a(t)} \overline{\mathbf{P}}_a(t) \right] \\ &+ \mathbf{K}_a(t)\left(\boldsymbol{y}_a(t) - h(\hat{\boldsymbol{x}}_a(t)) - \frac{1}{2}\sum_{i=1}^{d_m} \phi_i^h tr\left[\left.\frac{\partial^2 h_i}{\partial x_a^2(t)}\right|_{\hat{x}_a(t)} \overline{\mathbf{P}}_a(t) \right] \right)\end{aligned} \tag{3-61}$$

$$\mathbf{K}_a(t) = F(t)\mathbf{P}_a(t)\left[\mathbf{I} - \frac{1}{\gamma}\overline{\mathbf{S}}_a(t)\mathbf{P}_a(t) + H^{\mathrm{T}}(t)\mathbf{R}_a^{-1}(t)H(t)\mathbf{P}_a(t) \right]^{-1} H^{\mathrm{T}}(t)\mathbf{R}_a^{-1}(t) \tag{3-62}$$

$$\mathbf{P}_a(t+1) = F(t)\mathbf{P}_a(t)\left[\mathbf{I} - \frac{1}{\gamma}\overline{\mathbf{S}}_a(t)\mathbf{P}_a(t) + H^{\mathrm{T}}(t)\mathbf{R}_a^{-1}(t)H(t)\mathbf{P}_a(t) \right]^{-1} F^{\mathrm{T}}(t) + \mathbf{Q}_a(t) \tag{3-63}$$

$$\begin{aligned}\boldsymbol{\lambda}(t+1) = \left(F(t)F^{\mathrm{T}}(t) + \varepsilon I\right)^{-1} F(t)\Bigg\{ &\left[\mathbf{I} - \frac{1}{\gamma}\overline{\mathbf{S}}_a(t)\mathbf{P}_a(t) + H^{\mathrm{T}}(t)\mathbf{R}_a^{-1}(t)H(t)\mathbf{P}_a(t) \right]\boldsymbol{\lambda}(t) \\ &- H^{\mathrm{T}}(t)\mathbf{R}_a^{-1}(t)\left(\boldsymbol{y}_a(t) - h(\hat{\boldsymbol{x}}_a(t)) - \frac{1}{2}\sum_{i=1}^{d_m} \phi_i^h tr\left[\left.\frac{\partial^2 h_i}{\partial x_a^2(t)}\right|_{\hat{x}_a(t)} \overline{\mathbf{P}}_a(t) \right] \right)\Bigg\}\end{aligned} \tag{3-64}$$

$$\overline{\mathbf{P}}_a(t+1) = \eta\overline{\mathbf{P}}_a(t) + (1-\eta)\mathbf{P}_a(t)\boldsymbol{\lambda}(t)\boldsymbol{\lambda}^{\mathrm{T}}(t)\mathbf{P}_a^{\mathrm{T}}(t) \tag{3-65}$$

where $\overline{\mathbf{S}}_a(t) = \mathbf{C}_a^{\mathrm{T}}\mathbf{S}_a(t)\mathbf{C}_a$, $F(t) = \left.\frac{\partial f}{\partial x_a(t)}\right|_{\hat{x}_a(t)}$ and $H(t) = \left.\frac{\partial h}{\partial \boldsymbol{x}_a(t)}\right|_{\hat{x}_a(t)}$; ε is a positive scalar to prevent the term $F(t)F^{\mathrm{T}}(t)$ from being singular and $0 < \eta \le 1$. The value of γ must satisfy (A-46) to ensure the optimized value of $\hat{\boldsymbol{x}}_a(t)$ yields a local minimum of J.

[Proof]: Please see Appendix III.

3.6 Summary

The SOE H_∞ filter-based robust MVDR beamformer for the acoustic environment has been proposed and the detail derivation of the SOE H_∞ filter filter has also been given in this chapter. The comparisons between the proposed beamformer and the SOE Klaman filter-based robust MVDR beamformer are described. For the derivation of the SOE H_∞ filter, the second-order Taylor series expansion is used to approximate the nonlinear function and the second-order term is approximated by the estimation error sample covariance matrix. The SOE H_∞ filter provides a rigorous method for dealing with systems that have model uncertainty.

Chapter 4

Experimental Results

This chapter presents the experimental results of the simulated and practical environment to access the capability of the proposed TFR-based adaptive beamformer, the SOE H_∞ filter and the robust MVDR beamformer based on the SOE H_∞ filter. The experimental results about the TFR-based adaptive beamformer are shown in Section 4.1 and those about the SOE H_∞ filter and the SOE H_∞ filter-based robust MVDR beamformer are shown in Section 4.2 and Section 4.3, respectively.

4.1. Experimental Results of the Proposed Transfer Function Ratio-based Adaptive Beamformer

This section provides the experimental results of the proposed TFR-based adaptive beamformer. The proposed beamformer was tested both in a real room environment and in a car environment. In addition, the proposed beamformer was also tested by an automatic speech recognition system (ASR) for the application consideration.

Three speech enhancement algorithms, DSB [1], reference-signal-based adaptive

beamformer (RAB) implemented in frequency domain [34] and dual-source transfer-function generalized sidelobe canceller (DTF-GSC) [32] are adopted to compare with the proposed algorithm. The performance criterion of the RAB algorithm can be written as

$$\min_{G}\left[D(k,\omega)-\boldsymbol{G}^{\mathrm{H}}(k,\omega)\hat{\boldsymbol{X}}(k,\omega)\right]\left[D(k,\omega)-\boldsymbol{G}^{\mathrm{H}}(k,\omega)\hat{\boldsymbol{X}}(k,\omega)\right]^{*} \tag{4-1}$$

where $\hat{\boldsymbol{X}}(k,\omega)$ is the vector containing the linear combination of present microphone received signal and pre-recorded signal $A_{m1}(\omega)\widetilde{S}_1(k,\omega)$. $\widetilde{S}_1(k,\omega)$ is the representative speech signal at the position of the desired speech and $A_{m1}(\omega)\widetilde{S}_1(k,\omega)$ are the pre-recorded speech signals which can be recorded when the environment is quiet. $D(k,\omega)$ is the reference signal set to be $A_{11}(\omega)\widetilde{S}_1(k,\omega)$ and the adaptive weight $\boldsymbol{G}(k,\omega)$ can be trained using NLMS algorithm when the desired speech signal is inactive.

The DTF-GSC algorithm is comprised of three building blocks. The first is the FB designed to block one competing speech while maintaining the desired speech signal. The second is the BM which can block both the desired speech and one competing speech. The FB and BM are designed with the TFRs of the desired speech and the competing speech. Finally, the residual noise from the BM is cancelled by the adaptive filter using the NLMS algorithm. Notably, in this experiment, the TFRs for the desired speech of the DTF-GSC algorithm are the same with those of the proposed algorithm.

In the RAB, DTF-GSC and proposed algorithms, we assume a perfect desired speech detection system exists, allowing the adaptive noise cancellation system to adapt weight during inactive periods of desired speech. The STFT size is 1024 with 320 shift samples and 64 zero padding samples. In the RAB and DTF-GSC algorithms, the step size of the NLMS algorithm is set to be 0.1 and the initial values of the adaptive weight of the RAB,

DTF-GSC and proposed algorithms are identically set to be 0.1+0.1i. The TFRs for the DTF-GSC and proposed algorithms are estimated using 20 frames. For the proposed beamformer, the parameters of r, β and γ in (2-12), (2-20) and (2-26) are set to be 1, 10 and 2, respectively. The adaptation number $\tilde{k}$ is set to 10. The weighting matrices $\mathbf{P}(0,\omega)$ and $\overline{\mathbf{S}}$ in (2-29) are identically set to be identity matrices and $\mathbf{R}$ in (2-29) is set to be diag(1,10^{-9}).

Four objective performance indices are used to measure the waveform property directly. The first is segmental signal-to-interference-plus-noise ratio (segSINR) defined as

$$\text{segSINR(dB)} = 10\frac{1}{K_s}\sum_{k=0}^{K_s-1}\log 10\left(\frac{\sum_{t=L_s\cdot k}^{L_s\cdot k+L_s-1}x_{1,s}^2(t)}{\sum_{t=L_s\cdot k}^{L_s\cdot k+L_s-1}(x_{1,s}(t)-g_y\cdot y(t))^2}\right) \tag{4-2}$$

where L_s is the frame length and k is the frame number when the desired speech signal is active. Note that $x_{1,s}(t)$ is the desired signal component recorded by the first microphone, g_y is the gain factor and $y(t)$ is the output of the algorithm. The second is the average SINR (avgSINR) defined as

$$\text{avgSINR} = \frac{\sum_{t\in T_s}x^2(t)-\sum_{t\in T_n}x^2(t)}{\sum_{t\in T_n}x^2(t)} \tag{4-3}$$

where T_s and T_n denote periods in time where only the desired speech is active and only the interference-plus-noise signals are active respectively. The first quality measure stresses on the speech distortion more than the second quality measure. The third quality measure is segmental noise level (segNL)

$$\text{segNL(dB)} = \frac{1}{K}\sum_{k=1}^{K}\left(10\cdot\log_{10}(\sum_{i=1}^{I}g_y^2\cdot y^2(i+kI))\right) \tag{4-4}$$

where $y(t)$ is the algorithm output when only $s_2(t) \sim s_P(t)$ and $n_m(t)$ are all active. I is the length of the frame and k is the frame number. A lower segNL represents a better ability of noise suppression. The fourth quality measure is log spectral distortion (LSD) defined as

$$\mathrm{LSD} = \frac{1}{K}\sum_{k=1}^{K}\sqrt{\frac{1}{W}\sum_{\omega=1}^{W}\left(20\cdot\log_{10}\left|A_{11}(\omega)S_1(k,\omega)\right| - 20\cdot\log_{10}\left|Y(k,\omega)\right|\right)^2} \tag{4-5}$$

where $Y(k,\omega)$ is the STFT of the algorithm output. LSD means the speech distortion in frequency domain. Note that a lower LSD level corresponds to a better performance.

4.1.1. Real Room Environment

For the real room environment, the dimension is 10 m × 6 m × 3.6 m and the reverberation time at 1000 Hz is 0.52 second. A uniform linear microphone array of eight un-calibrated microphones separated by 0.05 m was constructed for this experiment. The amplified microphone signals were sampled at 8 kHz and 16 bits. The microphone array was placed on a table at a distance of 2 m from the wall and the picture of microphone array in real room is shown in Fig. 4-1. The arrangement of microphone array and sound sources is shown in Fig. 4-2. The desired speech signal at 0° consists of sentences from TCC-300 database [71] spoken by 150 males and 150 females. The interference signals 2, 3 and 4 are speech signals spoken by 3 females and interference signal 1 is the speech signal spoken by a male. Five conditions denoted from C1 to C5 for the experiments are listed in Table 4-1.

The experimental results are shown in Fig. 4-3 and Mic#1 represents the contaminated speech recorded by the first microphone. The range of average input SINR is from 0 dB to -7 dB. As can be seen, the best performance is obtained by the proposed algorithm and the

Figure 4-1 Microphone array in real room

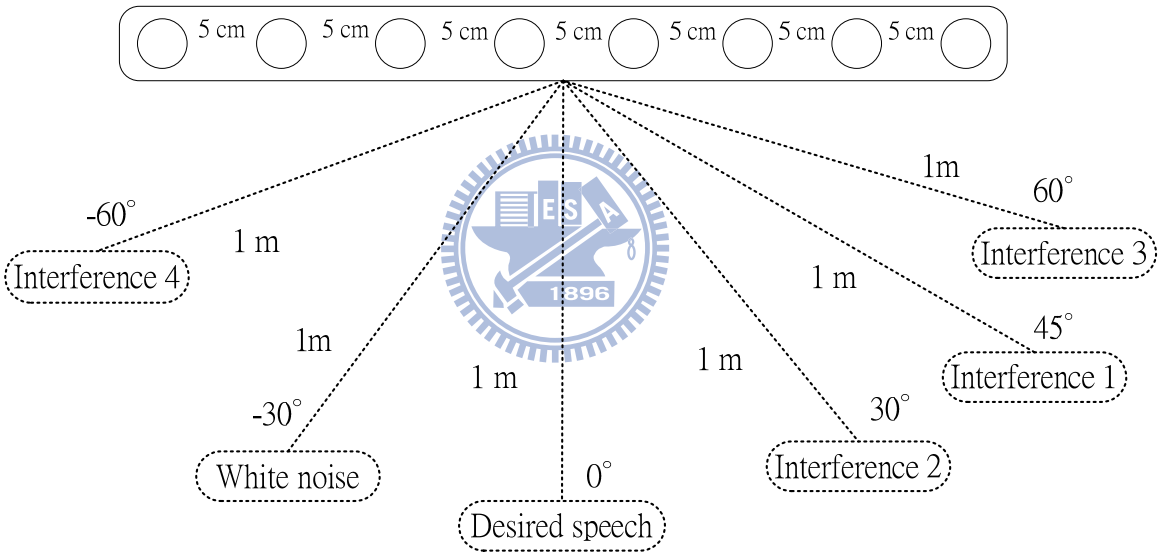

Figure 4-2 Configuration of microphones, desired speech, white noise and interference signals

Table 4-1 Five experimental conditions

Condition Number	Desired Speech Location	Stationary Noise Location	Interference Speech Location(s)
C1	0°	-30°	none
C2	0°	-30°	one of (30°, 45°, 60°, -60°)
C3	0°	-30°	two of (30°, 45°, 60°, -60°)
C4	0°	-30°	three of (30°, 45°, 60°, -60°)
C5	0°	-30°	30°, 45°, 60° and -60°

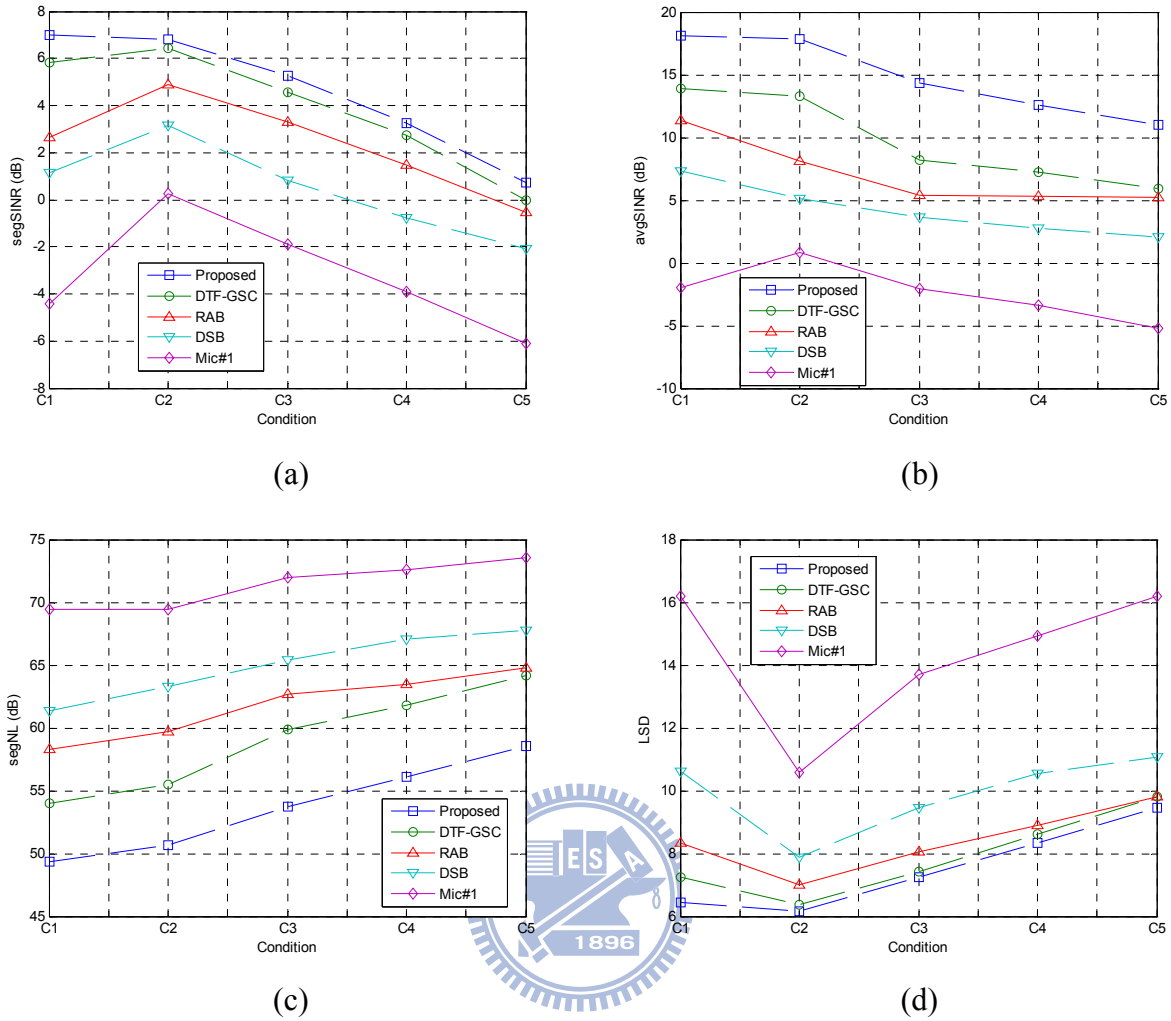

Figure 4-3 Experimental results in real room environment (a) segSINR results (b) avgSINR results (c) segNL results (d) LSD results

DSB performs worst. Since the DSB aligns only the direct path signal, it does not take reflections into account and no nulls are placed directly in interference signal directions.

For the RAB algorithm, the finite impulse response coefficients $\boldsymbol{G}(k,\omega)$ are trained to achieve two objectives simultaneously during the desired speech inactive periods: to suppress the interference and stationary noise signals, and to adjust the distorted desired speech of each microphone $A_{m1}(\omega)\widetilde{S}_1(k,\omega)$ to the same channel effect $A_{11}(\omega)\widetilde{S}_1(k,\omega)$. However, the finite number of taps and NLMS adaptive algorithm are unlikely to achieve these two objectives fully at the same time especially for complex channel dynamics. (e.g.,

competing speeches are present). It is unlike the DTF-GSC algorithm or the proposed algorithm which separates these two objectives. The DTF-GSC algorithm or the proposed algorithm suppresses competing speech and adjusts desired speech channel effect first using TFR techniques and then minimizes the residual noise with multi-channel adaptive filter. This is the reason why the RAB performs better than the DSB but worse than the DTF-GSC algorithm and the proposed algorithm.

The concept of the noise suppression method of the proposed algorithm is similar to that of the DTF-GSC algorithm with the desired speech detection system. The major difference between the algorithms lies in the system structure and adaptive filter algorithm. In addition, this dissertation proposes the virtual sound source concept to explain the components been removed from the TFR beamformer. The proposed system architecture is somewhat like the integration of the FB and BM of the DTF-GSC algorithm and the architecture of beamformer output is different from the standard weight-and-sum architecture. The advantage of the proposed system architecture is explained in Section 2.3.3. Besides, the proposed beamformer employs the H_∞ filter algorithm to be the adaptive filter, rather than NLMS algorithm. In the DTF-GSC algorithm, if the BM outputs contain the nonstationary signals or the modeling errors exist in the adaptive filter, these factors will influence the performance of the NLMS algorithm. However, the H_∞ filter can be more robust to the nonstationary signals and the modeling errors than the NLMS algorithm [35]. Therefore, the proposed algorithm has a better ability to suppress interference signals and stationary noise than the DTF-GSC algorithm.

For subjective evaluations, Fig. 4-4 ~ Fig. 4-8 show the waveforms and spectrograms at different conditions of the clean speech recorded by the first microphone, the contaminated speech at the first microphone and the enhanced speech obtained by different algorithms.

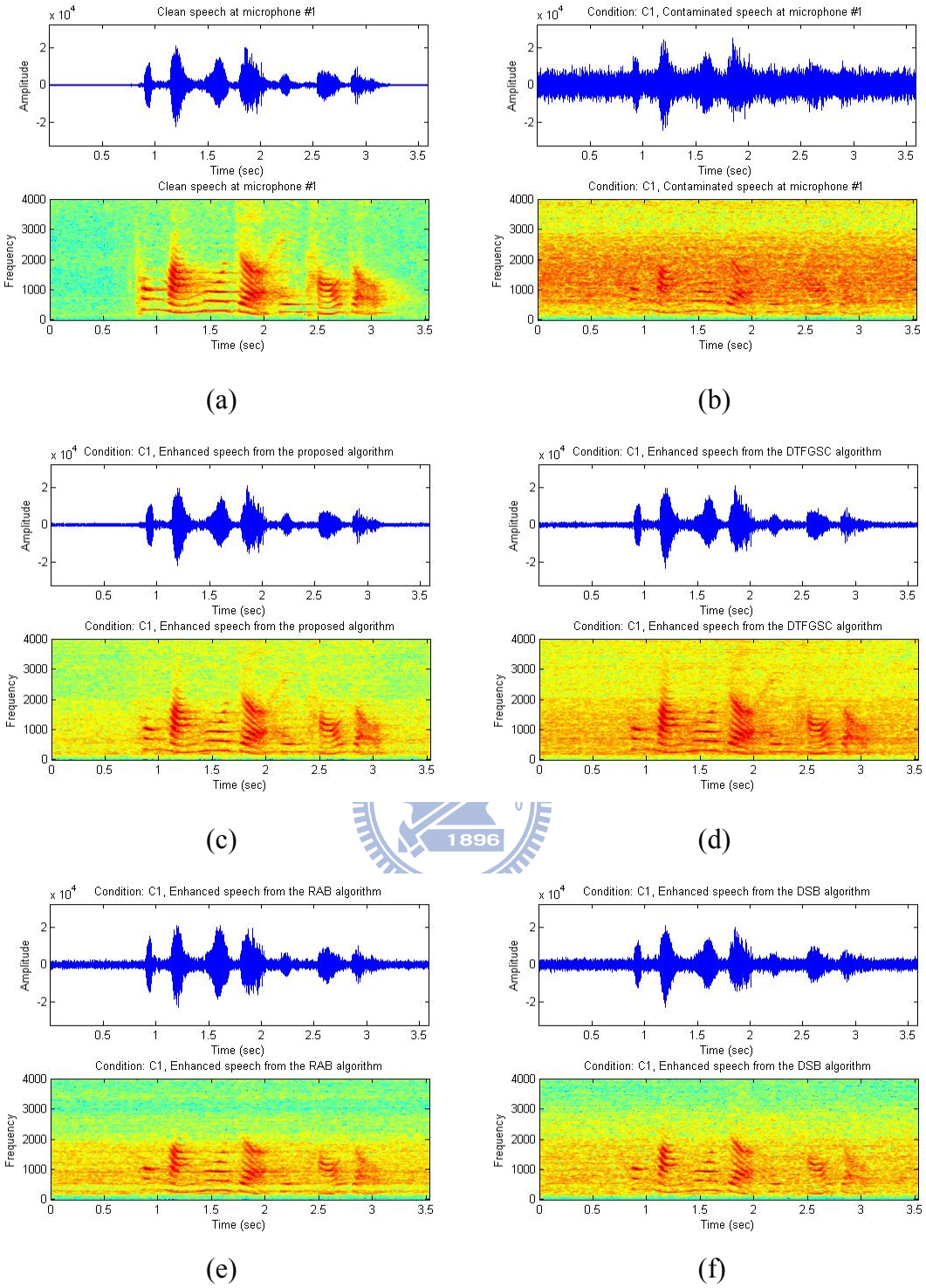

Figure 4-4 Waveforms and spectrograms at condition C1.
(a) Clean speech at Mic#1 (b) Contaminated speech at Mic#1
(c) Enhanced speech from the proposed algorithm (d) Enhanced speech from DTF-GSC
(e) Enhanced speech from RAB (f) Enhanced speech from DSB

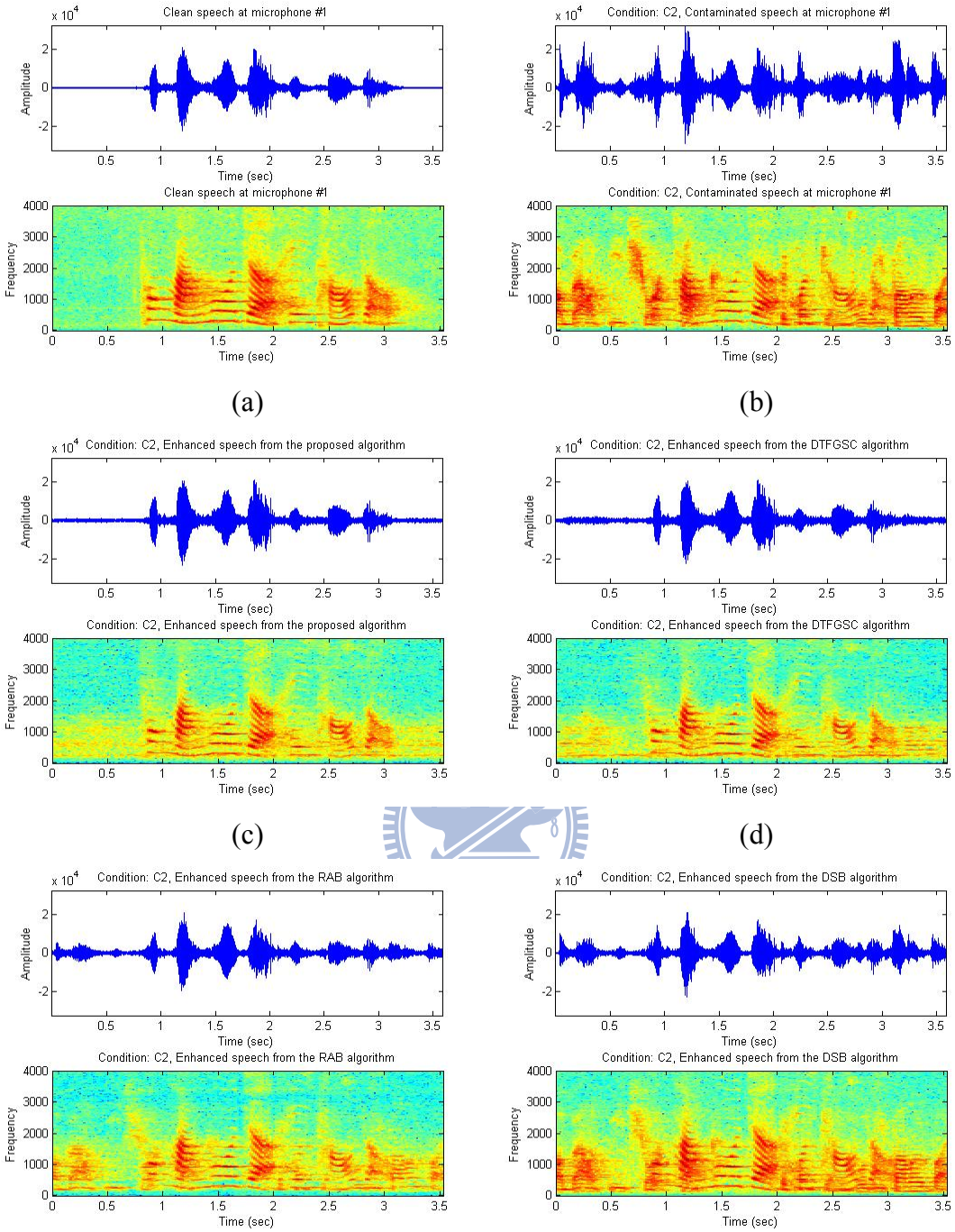

Figure 4-5 Waveforms and spectrograms at condition C2.

(a) Clean speech at Mic#1 (b) Contaminated speech at Mic#1

(c) Enhanced speech from the proposed algorithm (d) Enhanced speech from DTF-GSC

(e) Enhanced speech from RAB (f) Enhanced speech from DSB

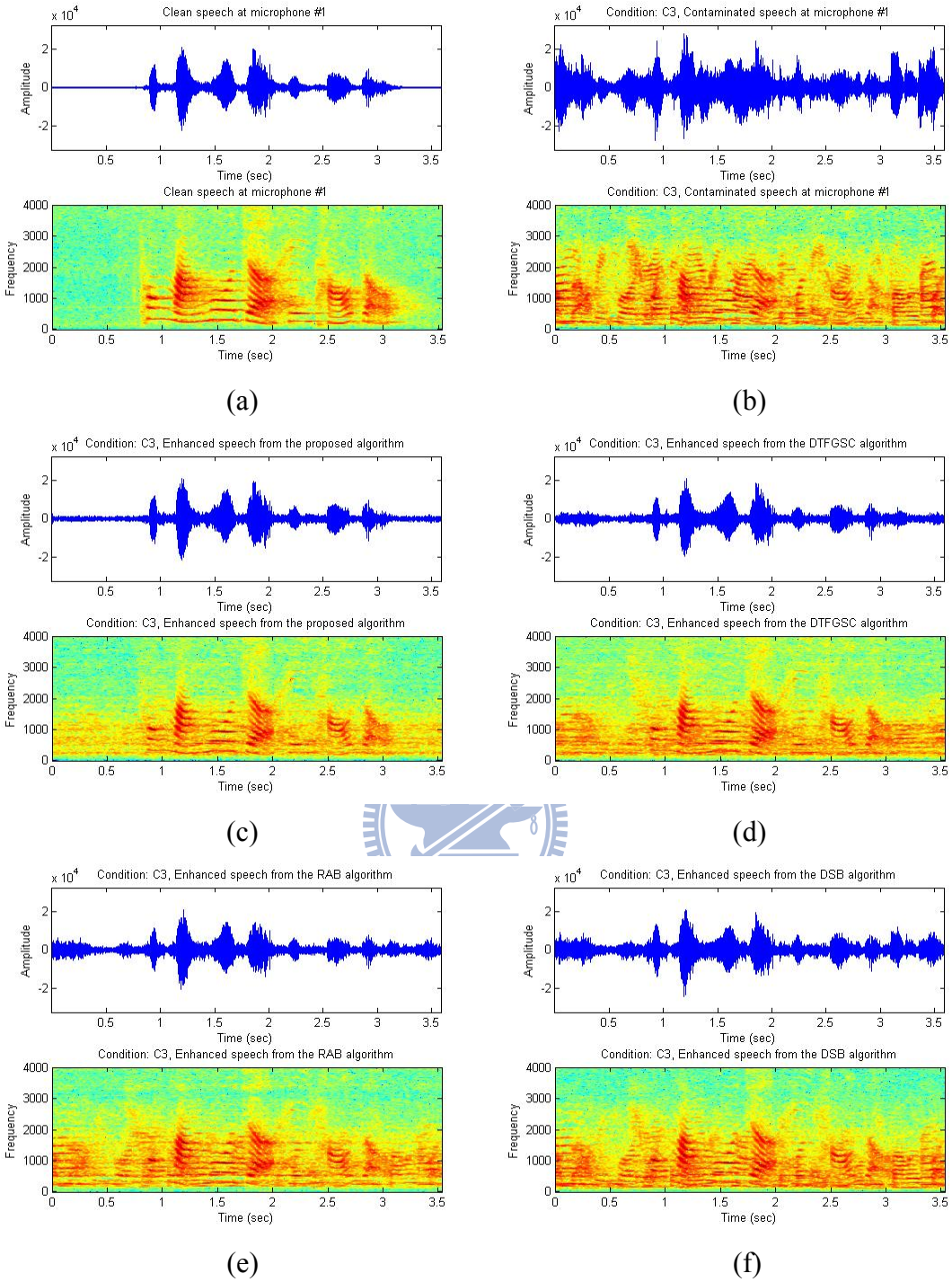

Figure 4-6 Waveforms and spectrograms at condition C3.
(a) Clean speech at Mic#1 (b) Contaminated speech at Mic#1
(c) Enhanced speech from the proposed algorithm (d) Enhanced speech from DTF-GSC
(e) Enhanced speech from RAB (f) Enhanced speech from DSB

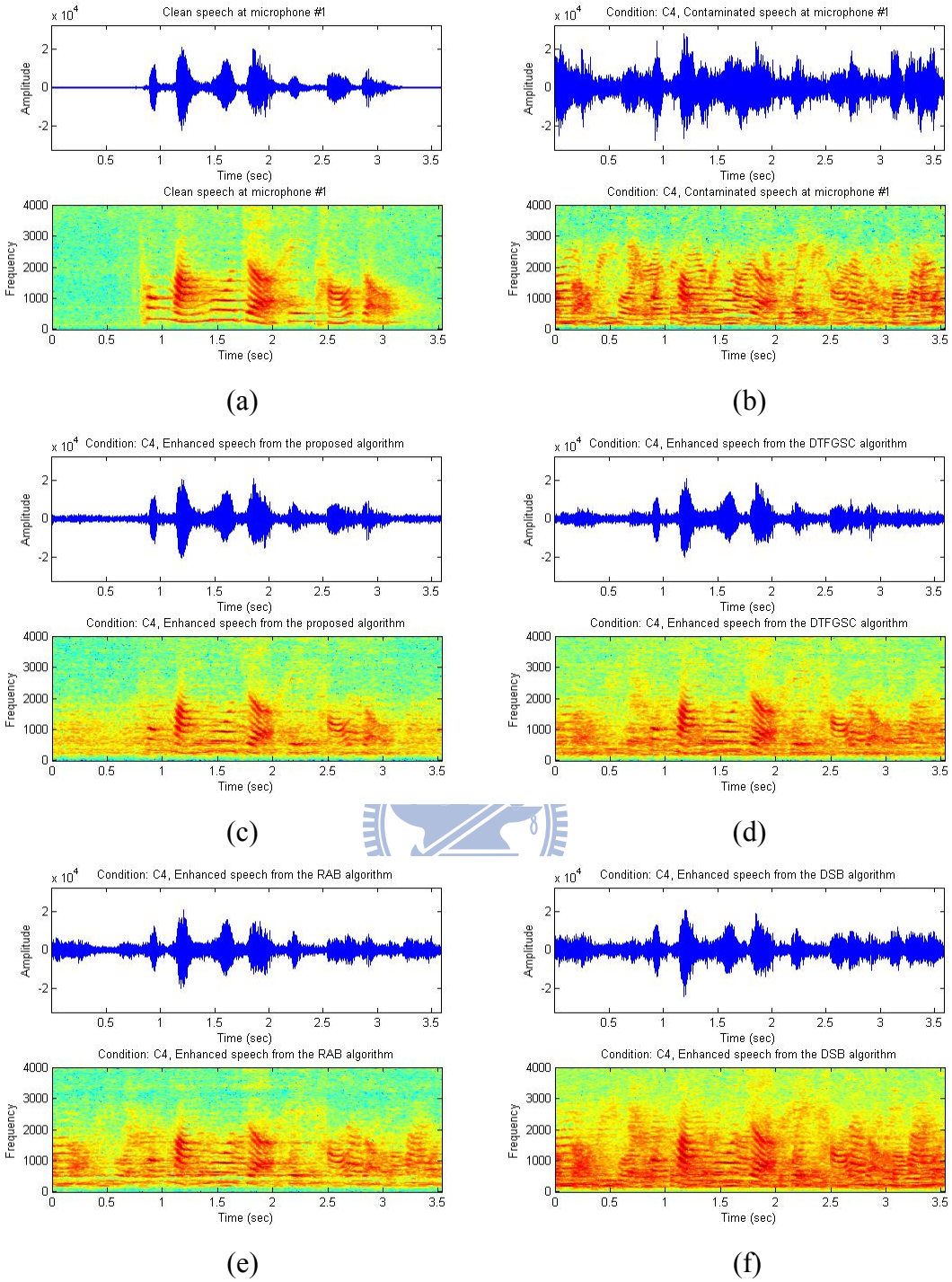

Figure 4-7 Waveforms and spectrograms at condition C4.
(a) Clean speech at Mic#1 (b) Contaminated speech at Mic#1
(c) Enhanced speech from the proposed algorithm (d) Enhanced speech from DTF-GSC
(e) Enhanced speech from RAB (f) Enhanced speech from DSB

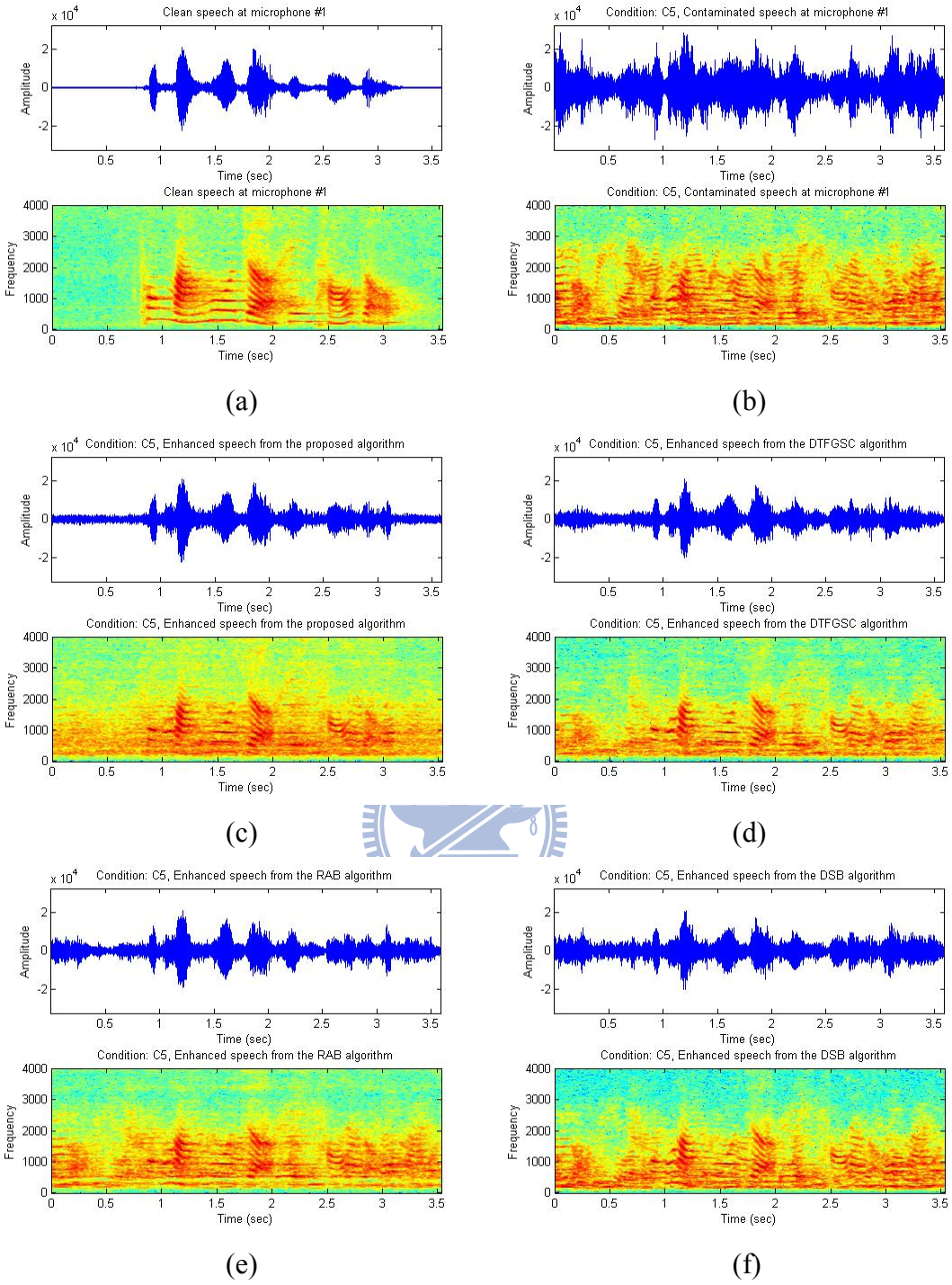

Figure 4-8 Waveforms and spectrograms at condition C5.
(a) Clean speech at Mic#1 (b) Contaminated speech at Mic#1
(c) Enhanced speech from the proposed algorithm (d) Enhanced speech from DTF-GSC
(e) Enhanced speech from RAB (f) Enhanced speech from DSB

4.1.2. Car Environment

The experiment was also performed in a Ford FOCUS car. The picture of microphone array in car is shown in Fig. 4-9. Fig. 4-10 shows the locations of the four in-car loudspeakers and the locations of the desired and interference speech signals. The desired speech is at location L2 and the interference signals are at location L1 and L3. The distance from the desired speech to the microphone array is about 0.52 m and the desired speech source is from TCC 300 database. A uniform array of eight microphones with 0.05 m spacing is mounted in front of L2. The sampling rate is 8 kHz, and the A/D resolution is 16 bits. All windows were closed during the experiment to protect the microphones from saturation. Four conditions denoted from K1 to K4 listed in Table 4-2 are considered for the car environment tests. The CD player played a song from a Taiwanese female singer.

The experimental results are shown in Fig. 4-11 and Mic#1 represents the contaminated speech recorded by the first microphone. As can be seen, the experimental results in car environment are consistent with those in real room environment. It is notable that the performance of the DTF-GSC and the proposed algorithm is comparable under the K1 condition. This may be because that the space of the car environment is smaller than that of the real room environment. It is easier to model the TFR in the car environment than in the real room environment and there is less desired speech leakage in the car environment. However, when the competing speech increases, the superiority of the proposed algorithm over other algorithms is evident.

Table 4-2 Four experimental conditions

Condition Number	Car Engine Speed	Desired Speech Location	Interference Speech Location(s)	In-car CD Player
K1	80 km/h	L2	L1	Off
K2	80 km/h	L2	L1 and L3	Off
K3	80 km/h	L2	L1	On
K4	80 km/h	L2	L1 and L3	On

Figure 4-9　Microphone array in car

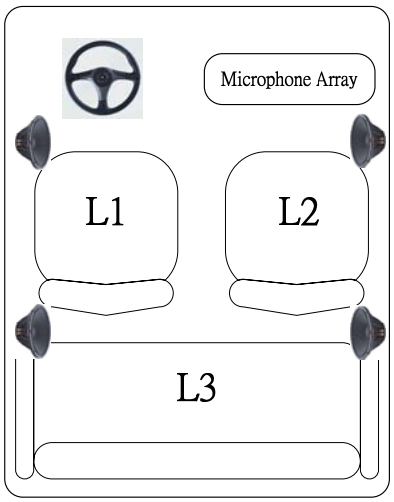

Figure 4-10　Car environment

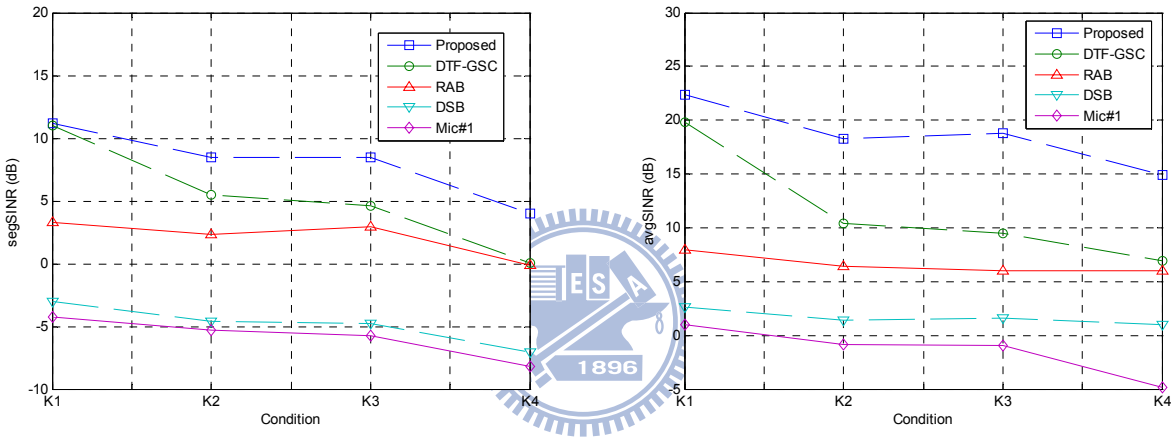

(a)　(b)

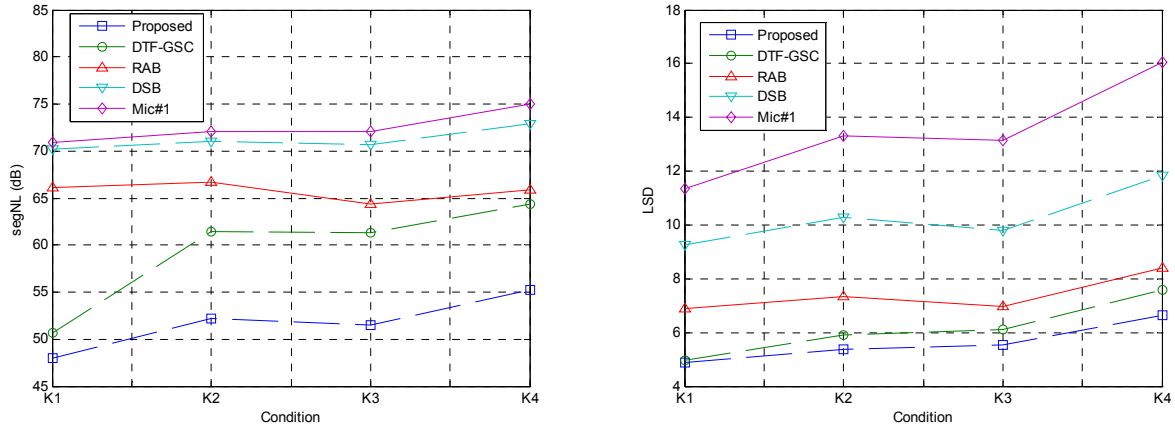

(c)　(d)

Figure 4-11　Experimental results in car environment (a) segSINR results (b) avgSINR results (c) segNL results (d) LSD results

4.1.3. Automatic Speech Recognition Test

ASR systems are sensitive to additive noise and speech distortion, especially for the competing speech. Therefore, this section utilizes the ASR rates to measure the performance of the proposed algorithm. The ASR system [72] that we use is the hidden markov model (HMM) based Mandarin speech recognition system. The feature vector is 26-dimensional mel frequency cepstral coefficients (MFCC) and the TCC-300 database is used for training. The testing database is speaker independent 3332 words spoken by 11 female and 18 male and each word is one Chinese name. The testing environment is the same with Section 4.1.1. and the testing words are played at the desired speech position in Fig. 4.2. The time domain speech enhancement output is sent directly to the ASR system for further processing. The recognition result is considered correct when the output of the ASR system is completely the same with the known input. The correct rates, when tested on the clean 3332 words ($s_1(t)$), is 100 %. The recognition results for different conditions are summarized in Table 4-3 and the correct rate of each condition is obtained by using 500 words chosen randomly from the testing database. In Table 4-3, clean Mic#1 and Mic#1 represent the clean speech recorded by the first microphone and the contaminated speech recorded by the first microphone, respectively. As can be seen, the proposed algorithm has the optimal correction rate and Table 4-3 also indicates that ASR system can be considered an application of the proposed algorithm. Notably, the improvement rates of the proposed algorithm are better than other algorithms, especially in C2~C5 conditions and it indicates that the proposed algorithm is more robust to the complicated acoustic environments than other algorithms.

Table 4-3 ASR Correction Rates (%)

Input SINR	Conditions	Algorithms					
		Proposed	DTF-GSC	RAB	DSB	Mic#1	Clean Mic#1
-7 ~ 0 (dB)	C1	90.8	80	48.8	41.8	5.6	91.2
	C2	86	74	43	39	12.4	86.6
	C3	79.5	55.2	27.4	20.4	4.8	84.4
	C4	71.4	48.2	31.4	23.6	2	87.4
	C5	72.4	51.6	37.8	36.8	4.4	84.4

4.2. Simulation Results of the Second-Order Extended H_∞ Filter

This section provides the simulation results of the SOE H_∞ filter. The performance of the SOE H_∞ filter is analyzed and a numerical example of a vehicle tracking problem is given in Section 4.2.1 to compare the SOE H_∞ filter with the SOE Kalman filter and the extended H_∞ filter.

4.2.1 Numerical Example for the Second-Order Extended H_∞ Filter

This section compares the performance of the SOE H_∞ filter proposed in Section 3.5 with those of the SOE Kalman filter [48] and the extended H_∞ filter [52] for a tracking problem in [48]. Consider the problem of tracking a moving vehicle in two dimensional space (north and east). The vehicle's velocity in the north and east directions consists of independent white noise. Two tracking stations, located at north-east coordinates $(\overline{N}_1, \overline{E}_1)$ and $(\overline{N}_2, \overline{E}_2)$, measure the distance to the vehicle. The system model can therefore be written as

$$\begin{bmatrix} n(t+1) \\ e(t+1) \\ \dot{n}(t+1) \\ \dot{e}(t+1) \end{bmatrix} = \begin{bmatrix} 1 & 0 & T & 0 \\ 0 & 1 & 0 & T \\ 0 & 0 & 1 & 0 \\ 0 & 0 & 0 & 1 \end{bmatrix} \begin{bmatrix} n(t) \\ e(t) \\ \dot{n}(t) \\ \dot{e}(t) \end{bmatrix} + \boldsymbol{w}(t)$$
$$\boldsymbol{y}(t) = \begin{bmatrix} \sqrt{\left(n(t)-\overline{N}_1\right)^2 + \left(e(t)-\overline{E}_1\right)^2} \\ \sqrt{\left(n(t)-\overline{N}_2\right)^2 + \left(e(t)-\overline{E}_2\right)^2} \end{bmatrix} + \boldsymbol{v}(t) \tag{4-6}$$

where $n(t)$ and $e(t)$ are the vehicle's north and east coordinates at time step t; T is the time step of the system, $\boldsymbol{w}(t) = \begin{bmatrix} w_1(t) & w_2(t) & w_3(t) & w_4(t) \end{bmatrix}^{\mathrm{T}}$ is the process noise, and $\boldsymbol{v}(t) = \begin{bmatrix} v_1(t) & v_2(t) \end{bmatrix}^{\mathrm{T}}$ is the measurement noise. The process noise $w_1(t) = w_2(t) = 0$, $w_3(t)$ and $w_4(t)$ are normally distributed white noise sequences whose means are 20 and whose variances are 4. The measurement noise is also a normally distributed white noise sequence with mean=10 and variance=1. Suppose that the time step T = 0.1s and the execution time is one minute. The SOE H_∞ filter solution of the nonlinear discrete system (3.42) is given in Section 3.5 and the SOE Kalman filter solution of the nonlinear discrete system (3.42) is given as follows

Time update equations:

$$\hat{\boldsymbol{x}}_a^-(t) = f(\hat{\boldsymbol{x}}_a^+(t-1)) + \frac{1}{2}\sum_{i=1}^{d_n} \phi_i^f tr\left[\left. \frac{\partial^2 f_i}{\partial x_a^2(t)} \right|_{\hat{x}_a^+(t-1)} \widetilde{\mathbf{P}}_a^+(t) \right] \tag{4-7}$$

$$\widetilde{\mathbf{P}}_a^-(t) = \widetilde{F}(t-1)\widetilde{\mathbf{P}}_a^+(t-1)\widetilde{F}^{\mathrm{T}}(t-1) + \widetilde{\mathbf{Q}}_a(t-1) \tag{4-8}$$

Measurement update equations:

$$\hat{\boldsymbol{x}}_a^+(t) = \hat{\boldsymbol{x}}_a^-(t) + \widetilde{\mathbf{K}}_a(t)\left(\boldsymbol{y}_a(t) - h(\hat{\boldsymbol{x}}_a^-(t)) - \frac{1}{2}\sum_{i=1}^{d_m} \phi_i^h tr\left[\left. \frac{\partial^2 h_i}{\partial x_a^2(t)} \right|_{\hat{x}_a^-(t)} \widetilde{\mathbf{P}}_a^-(t) \right] \right) \tag{4-9}$$

$$\widetilde{\mathbf{K}}_a(t) = \widetilde{\mathbf{P}}_a^-(t)\widetilde{H}_k^{\mathrm{T}}\left(\widetilde{H}(t)\widetilde{\mathbf{P}}_a^-(t)\widetilde{H}^{\mathrm{T}}(t) + \widetilde{\mathbf{R}}_a(t)\right)^{-1} \tag{4-10}$$

$$\widetilde{\mathbf{P}}_a^+(t) = \left(\mathbf{I} - \widetilde{\mathbf{K}}(t)\widetilde{H}(t)\right)\widetilde{\mathbf{P}}_a^-(t) \tag{4-11}$$

where $\widetilde{F}(t)=\left.\frac{\partial f}{\partial x_a(t)}\right|_{\hat{x}_a^+(t)}$ and $\widetilde{H}(t)=\left.\frac{\partial h}{\partial \boldsymbol{x}_a(t)}\right|_{\hat{x}_a^-(t)}$. After some linear algebra operations [48], the Kalman gain $\widetilde{\mathbf{K}}_a(t)$ can be rewritten as (4-12) and the estimation error covariance matrix $\widetilde{\mathbf{P}}_a^-(t)$ and $\widetilde{\mathbf{P}}_a^+(t)$ can be integrated as (4-13)

$$\widetilde{\mathbf{K}}_a(t)=\widetilde{\mathbf{P}}_a^-(t)\widetilde{H}^{\mathrm{T}}(t)\left(\mathbf{I}+\widetilde{H}^{\mathrm{T}}(t)\widetilde{\mathbf{R}}_a^{-1}(t)\widetilde{H}(t)\widetilde{\mathbf{P}}_a^-(t)\right)^{-1}\widetilde{H}^{\mathrm{T}}(t)\widetilde{\mathbf{R}}_a^{-1}(t) \tag{4-12}$$

$$\widetilde{\mathbf{P}}_a^-(t+1)=\widetilde{F}(t)\widetilde{\mathbf{P}}_a^-(t)\left(\mathbf{I}+\widetilde{H}^{\mathrm{T}}(t)\widetilde{\mathbf{R}}_a^{-1}(t)\widetilde{H}(t)\widetilde{\mathbf{P}}_a^-(t)\right)^{-1}\widetilde{F}^{\mathrm{T}}(t)+\widetilde{\mathbf{Q}}_a(t) \tag{4-13}$$

For the SOE Kalman filter, the process noise covariance matrix $\widetilde{\mathbf{Q}}_a(t)$ in (4-8) is set to diag(0,0,4,4), and the measurement noise covariance matrix and $\widetilde{\mathbf{R}}_a(t)$ in (4-10) is diag(1,l). The tracking stations are located at $(\overline{N}_1,\overline{E}_1)=(20,0)$ and $(\overline{N}_2,\overline{E}_2)=(0,20)$. The initial state of the vehicle $\boldsymbol{x}(0)=[0\quad 0\quad 50\quad 50]^{\mathrm{T}}$ and is perfectly known. For the extended and SOE H_∞ filter, the weighting matrices $\mathbf{Q}_a(t)$ and $\mathbf{R}_a(t)$ in (3-63) and (3-62) are selected to be identical to matrices $\widetilde{\mathbf{Q}}_a(t)$ and $\widetilde{\mathbf{R}}_a(t)$ respectively. The parameters γ, ε and η in (3-48), (3-64) and (3-65) are set to 100, 0.5 and 0.9, respectively. The matrices $\mathbf{C}_a$ and $\mathbf{S}_a(t)$ in (3-62) are both set to be identity matrices and the matrices $\widetilde{\mathbf{P}}_a^+(0)$ and $\mathbf{P}_a(0)$ in (4-8) and (3-62) are both set to be zero.

Fig. 4-12 shows the true states and the estimated states of all filters. Table 4-4 represents the mean of absolute state estimation error. As can be seen, the SOE H_∞ filter performs better than all of the other filters. The SOE H_∞ filter performs better than the extended H_∞ filter since the SOE H_∞ filter has a smaller linearization error than the extended H_∞ filter. Next, the SOE Kalman filter is compared with the SOE H_∞ filter. The SOE Kalman filter assumes that the process noise and the measurement noise are zero-mean Gaussian noises. However, this assumption is not satisfied with this example

since the noises in this example are non-zero mean. As seen in the preceding section, the SOE Kalman filter and the SOE H_∞ filter have similar observer structures and the difference between them is that the SOE H_∞ filter has the $\frac{1}{\gamma}\overline{\mathbf{S}}_a(t)\mathbf{P}_a(t)$ item in $\mathbf{K}_a(t)$ and $\mathbf{P}_a(t+1)$, which is absent in the $\widetilde{\mathbf{K}}_a(t)$ and $\widetilde{\mathbf{P}}_a^-(t+1)$ matrices of the SOE Kalman filter. In (3.62) and (3.63), we can find that subtracting $\frac{1}{\gamma}\overline{\mathbf{S}}_a(t)\mathbf{P}_a(t)$ on the right side of $\mathbf{K}_a(t)$ and $\mathbf{P}_a(t+1)$ tends to increase $\mathbf{K}_a(t)$ and $\mathbf{P}_a(t+1)$. Studies [48] have shown that the Kalman filter can be made more robust to unmodeled noise and unmodeled dynamics by artificially increasing the process noise covariance matrix $\widetilde{\mathbf{Q}}_a(t)$ which results in a larger $\widetilde{\mathbf{K}}_a(t)$ and $\widetilde{\mathbf{P}}_a^-(t+1)$. Increasing the process noise covariance matrix $\widetilde{\mathbf{Q}}_a(t)$ of the SOE Kalman filter is conceptually the same as increasing $\mathbf{K}_a(t)$ and $\mathbf{P}_a(t+1)$ in the SOE H_∞ filter. Therefore, in this example, the SOE H_∞ filterer performs better than the SOE Kalman filter owing to the effect of the element $-\frac{1}{\gamma}\overline{\mathbf{S}}_a(t)\mathbf{P}_a(t)$ in $\mathbf{K}_a(t)$ and $\mathbf{P}_a(t+1)$.

Theoretically, the noise covariance matrices $\widetilde{\mathbf{Q}}_a(t)$ and $\widetilde{\mathbf{R}}_a(t)$ in the SOE Kalman filter should be set to be diagonal matrices. However, the weighting matrices $\mathbf{Q}_a(t), \mathbf{R}_a(t)$ and $\mathbf{S}_a(t)$ in the SOE H_∞ filter are symmetric positive definite matrices which can be designed by the user without requiring them to be diagonal. Different weighting matrices result in different performance and this example just reveals that the SOE H_∞ filter can be more robust to the unmodeled noise than the SOE Kalman filter when the weighting matrices $\mathbf{Q}_a(t)$ and $\mathbf{R}_a(t)$ are identical to the $\widetilde{\mathbf{Q}}_a(t)$ and $\widetilde{\mathbf{R}}_a(t)$ matrices of the SOE Kalman filter.

Table 4-4 Mean of absolute state estimation error

	$n(t)$	$e(t)$	$\dot{n}(t)$	$\dot{e}(t)$
SOE Kalman	4126.1089	4073.1391	254.30057	143.68455
Extended H_∞	1896.4524	792.98992	44.266306	122.16865
SOE H_∞	1700.782	613.90405	37.768583	112.13477

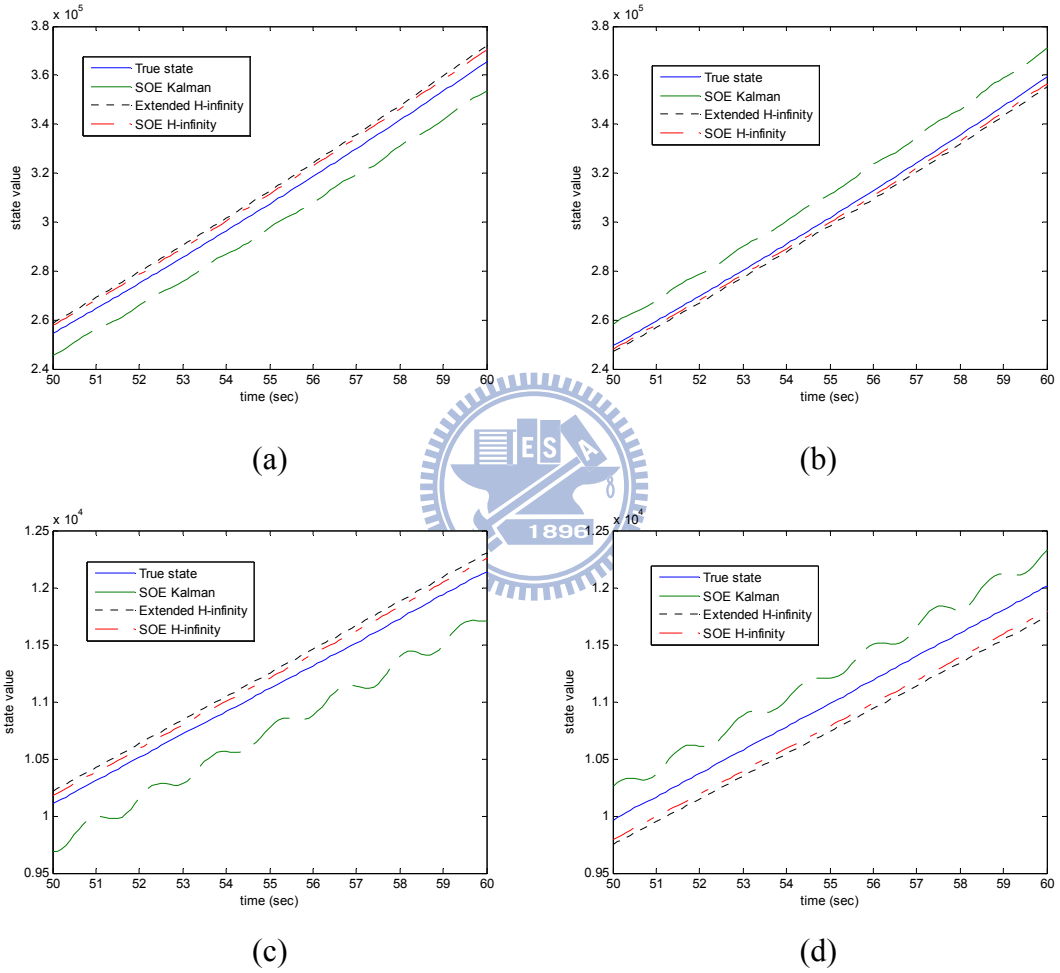

Figure 4-12 Estimation results of state values. (a) $n(t)$ (b) $e(t)$ (c) $\dot{n}(t)$ (d) $\dot{e}(t)$

4.3. Experimental Results of the Robust MVDR Beamformer Based on the Second-Order Extended H_∞ Filter

This section provides the experimental results of the robust MVDR beamformer based on the SOE H_∞ filter. The performance of the proposed SOE H_∞ filter-based robust MVDR beamformer is compared with the SOE Kalman filter-based robust MVDR beamformer for the speech enhancement problem both in a simulated room and in a real room. The experimental results in a simulated room and in a real room are provided in Section 4.3.1 and Section 4.3.2, respectively.

4.3.1. Simulation Results of the Second-Order Extended H_∞ Filter-based Robust MVDR Beamformer

The purpose of the simulation is to compare the performance of the SOE H_∞ and Kalman filters with respect to the room acoustic response and the ability to reject impulse noise. In this simulation, the image method [50] is adopted to model the room impulse response and the room impulse response is convolved with source signals to generate microphone signals. The room size is 4.5m×3.3m×4.2m and a 4-channel linear microphone array is placed at a distance of 0.7 m from the wall. The arrangement of microphone array and sound sources is shown in Fig. 4-13. The presumed steering vector $\tilde{\boldsymbol{A}}(\omega)$ is set to be $[1 \quad 1 \quad 1 \quad 1]$ for each frequency and following the guidelines of [38], the robustness parameter $\varepsilon = 3$ in (3-10) is used both in the SOE Kalman filter-based robust MVDR beamformer and the SOE H_∞ filter-based robust MVDR beamformer. The matrices $\tilde{\mathbf{Q}}$ and $\mathbf{Q}$ in (3-26) and (3-38) are both selected as zero and the matrices $\tilde{\mathbf{R}}$ and $\mathbf{R}$ in (3-25) and (3-37) are both set to be diag(10,0.1). The parameters γ and η in (3-33) and (3-40) are chosen 10 and 0.99, respectively. The

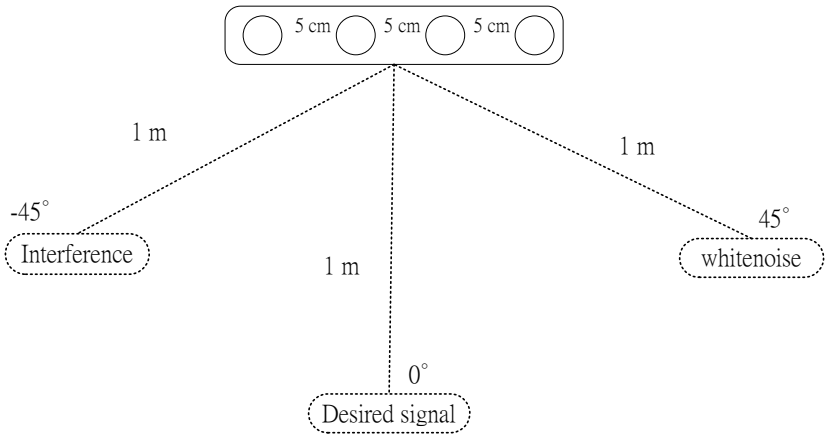

Figure 4-13 Configuration of microphones, desired speech, white noise and interference signals

matrices $\widetilde{\mathbf{P}}^{+}(0,\omega)$ in (3-26), $\mathbf{P}(0,\omega)$, $\mathbf{S}$ and $\mathbf{C}$ in (3-37) are equally set to be identity matrices. The weight vectors of both filters are trained with the same data when the desired speech is inactive.

Two reverberation times T_{60}, 0.2 second and 0.3 second, are used for this simulation. The sampling rate is 8 KHz. As a result, the corresponding impulse responses from the interference position to the first microphone position are shown in Fig. 4-14(a) and Fig. 4-14(d). The STFT size is 256 with 80 shift samples and 16 zero padding samples. As can be seen, the length of each impulse responses is longer than 256. Therefore, a single STFT frame is not able to capture the room response. This makes the channel response time-varying in practice and it can be viewed as model uncertainty. Throughout the simulation, the desired source is silent. Two scenarios are considered for the interference rejection ability:

1. The interference signal is speech signal spoken by a male.
2. The interference signal is a transient noise (drum).

Fig. 4-14 shows the simulation results of the scenario 1 for different reverberations. Fig. 4-14(b) and Fig. 4-14(f) represent the received signal of the first microphone. The segNL

defined in (4-4) is used for performance comparison. Fig. 4-14(c) and Fig. 4-14(g) show the results for SOE Kalman filter while the cases of SOE H_∞ filter are depicted in Fig. 4-14(d) and Fig. 4-14(h). From the segNL, both methods exhibit certain reduction ability but the SOE H_∞ filter performs slightly better than the SOE Kalman one.

Fig. 4-15 shows the simulation results of the scenario 2 for different reverberations. Fig. 4-15(a) and Fig. 4-15(d) are the received signal of the first microphone when only the drum and white noise are active. Comparing Fig. 4-15(b) with Fig. 4-15(c) and Fig. 4-15(e) with Fig. 4-15(f), the SOE H_∞ filter has a faster convergent speed than the SOE Kalman one. This indicates that SOE H_∞ filter is more capable of rejecting transient interferences.

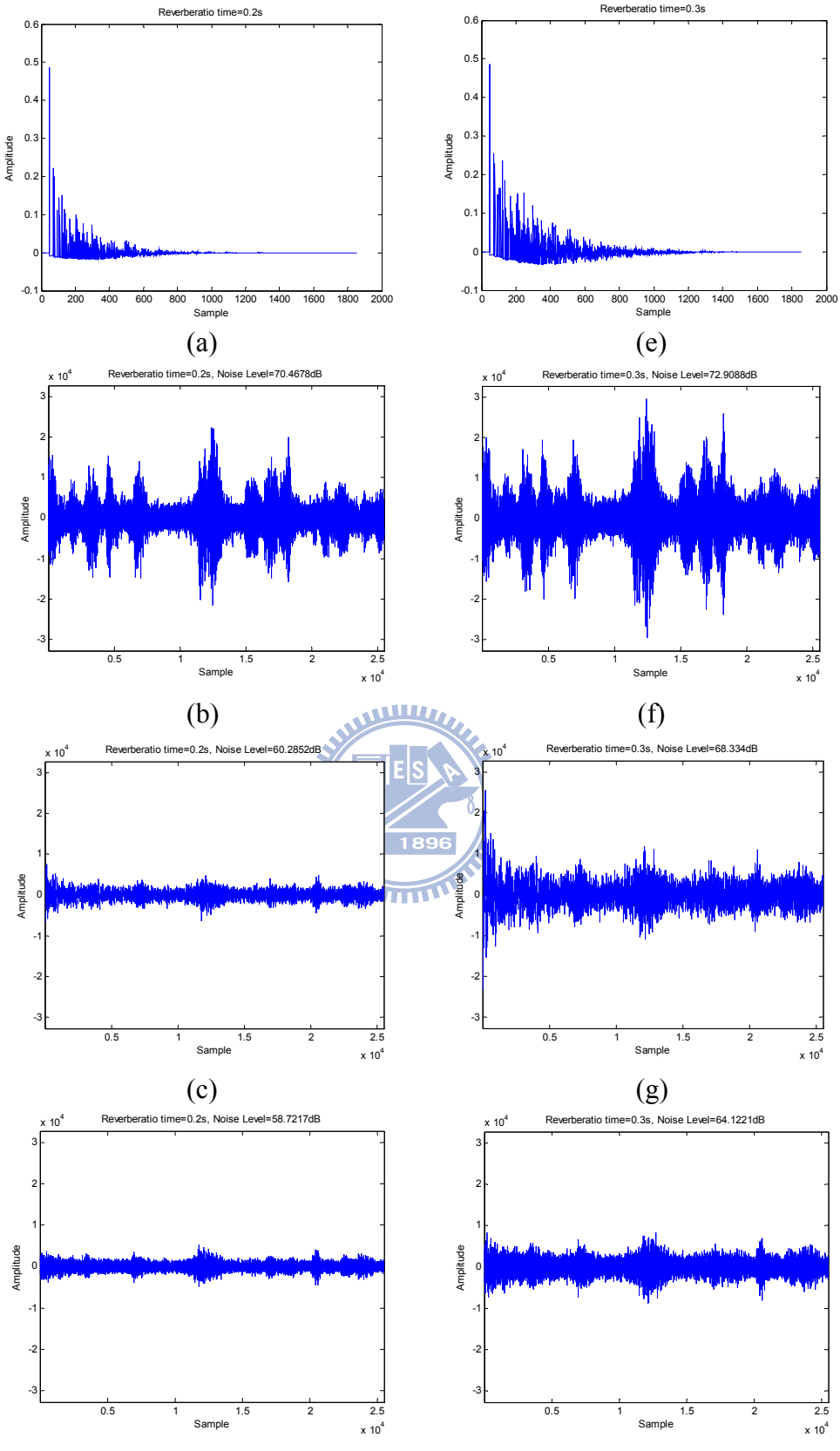

Figure 4-14 Simulation results. (a) and (e): Impulse responses, (b) and (f): Microphone #1 signals when only the interfering speech and white noise are active, (c) and (g): Enhanced signals of the SOE Kalman filter, (d) and (h): Enhanced signals of the SOE H_∞ filter

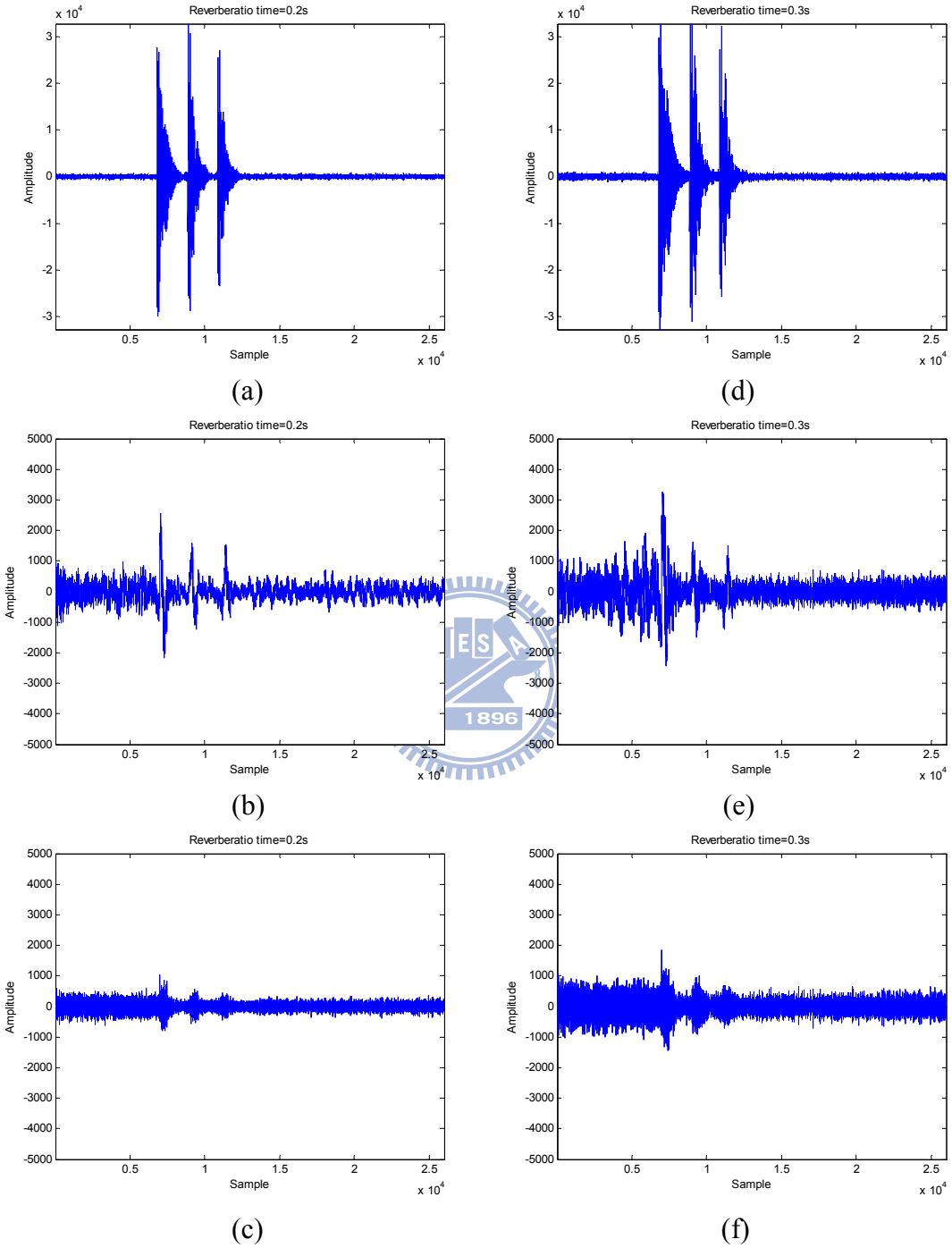

Figure 4-15 Simulation results. (a) and (d): Microphone #1 signals when only the drum and white noise are active, (b) and (e): Enhanced signals of the SOE Kalman filter, (c) and (f): Enhanced signals of the SOE H_∞ filter

4.3.2. Experimental Results of the Second-Order Extended H_∞ Filter-based Robust MVDR Beamformer in a Real Room

In this section, the performance of the proposed SOE H_∞ filter-based robust MVDR beamformer is compared with the SOE Kalman filter-based robust MVDR beamformer for the speech enhancement problem in a real room. The real room dimension is 10 m × 6 m × 3.6 m and the reverberation time at 1000 Hz is 0.52 second. The microphone array was placed on a table at a distance of 2 m from the wall. The microphone array arrangement and all other parameters setting of both filters are the same as Section 4.3.1. According to the investigation of room acoustics [73], the number of eigen-frequencies can be obtained by the following equation:

$$\overline{Q} = \frac{4\pi}{3} B(\frac{f_s}{2c})^3 \tag{4-14}$$

where B represents the geometrical volume, f_s denotes the sampling frequency, and c means the sound velocity ($c \fallingdotseq 346$m/s). This equation indicates that the number of poles is very large when the room volume is high, and that the transient response occurs in almost any processing duration. In this experimental environment, the number of poles is about 1.398×10^6 when the sampling frequency is 8 kHz and the room volume is 216 m^3. Accordingly, the STFT window length (256) in this experiment is shorter than the channel response duration and is likely to create channel modeling error.

Because the robust MVDR beamformer does not consider the de-reverberation or channel adjustment effect Three performance indices, avgSINR, segNL and LSD defined in (4-3), (4-4) and (4-5), are used to measure the waveform property directly.

The experimental results are shown in Fig. 4-16 according to different input average SINR and Mic#1 represents the contaminated speech recorded by the first microphone. As can be seen, the proposed SOE H_∞ filter performs better than the SOE Kalman filter in

robust MVDR beamformer. It is clear that the model uncertainties (room reverberation and microphone mismatch) have a greater influence to the SOE Kalman filter. As can be seen from Fig. 4-16 (a) and Fig. 4-16 (b), the SOE H_∞ filter has a higher average SINR and suppresses more interference-plus-noise. Notably, Fig. 4-16 (c) further demonstrates that the SOE H_∞ filter still has less desired signal distortion while maintaining better average SINR and segNL. For subjective evaluations, Fig. 4-17 shows the waveforms and spectrograms of the clean speech recorded by the first microphone, the contaminated speech at the first microphone and the enhanced speech obtained by the SOE Kalman filter and the SOE H_∞ filter. In Fig. 4-17, the average SINR of the contaminated speech is about 1.32 dB.

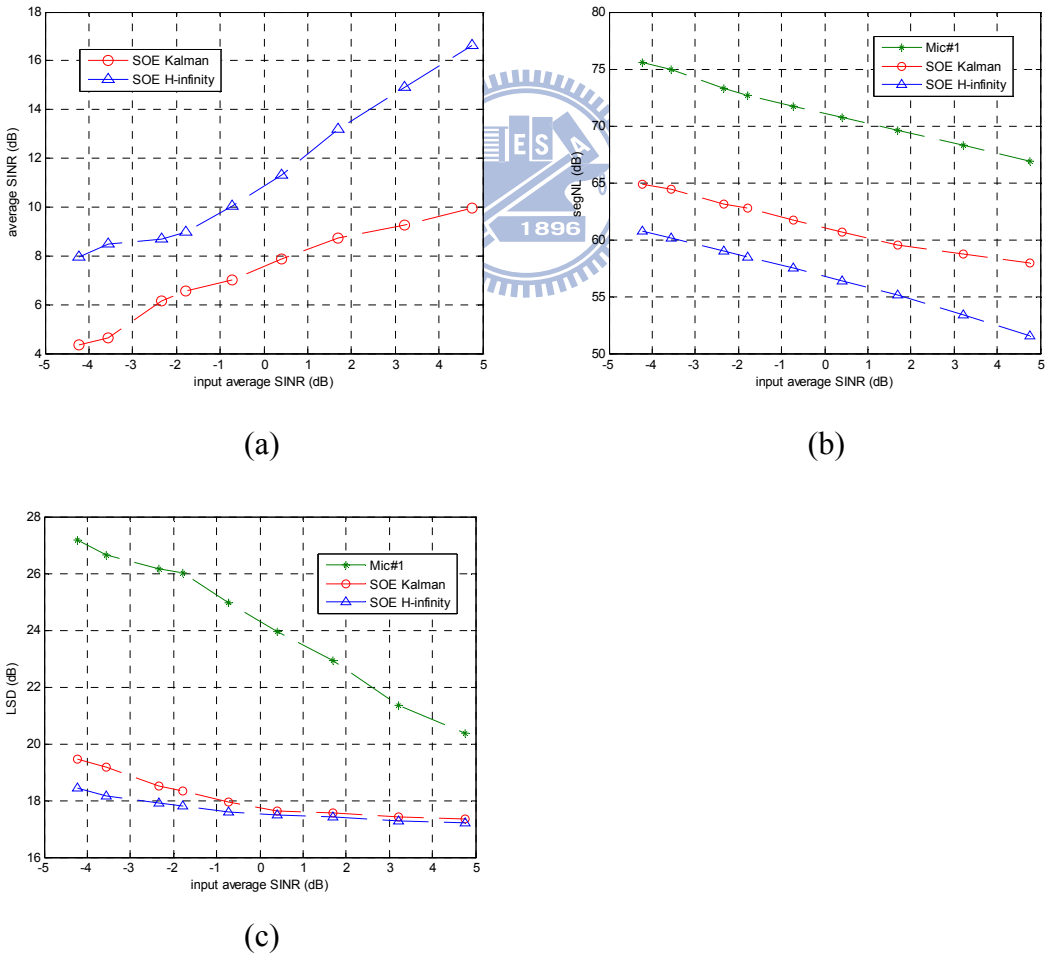

Figure 4-16 Experimental results in real room environment (a) avgSINR results (b) segNL results (c) LSD results

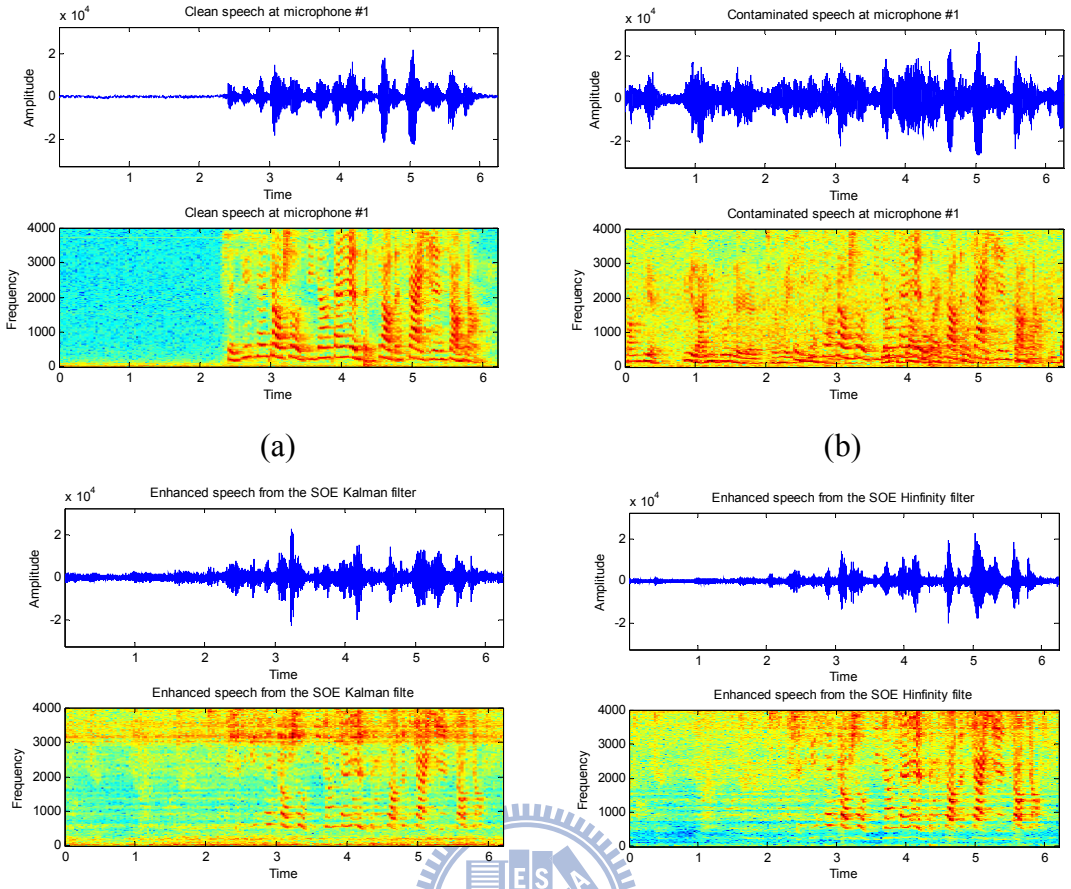

Figure 4-17 Waveforms and spectrograms: (a) the clean speech recorded by the first microphone; (b) the contaminated speech at the first microphone; (c) the enhanced speech obtained by the SOE Kalman filter; (d) the enhanced speech obtained by the SOE H_∞ filter.

4.4. Summary

This chapter evaluates the proposed TFR-based adaptive beamformer, the SOE H_∞ filter, and the SOE H_∞ filter-based robust MVDR beamformer through simulation and real experimental results. Section 4.1.1 and Section 4.1.2 show that the proposed TFR-based adaptive beamformer performs better than other famous beamformers both in a real room environment and in a car environment. Section 4.1.3 utilizes the ASR to demonstrate the advantages of the proposed TFR-based adaptive beamformer.

In Section 4.2.1, a numerical example is given to compare the SOE H_∞ filter with the first-order extended H_∞ filter, and the SOE Kalman filter. The simulation results show that the SOE H_∞ filter has the best performance among others in terms of noise model uncertainty. Section 4.3.1 simulates the reverberant environment, while performing the experiments when the interference signal is speech signal or a transient noise, to show that the proposed SOE H_∞ filter-based robust MVDR beamformer can be robust to the modeling error of beamformer weight. Section 4.3.2 demonstrates the performance of the proposed SOE H_∞ filter-based robust MVDR beamformer in a noisy and reverberant environment and shows its superiority over the robust MVDR beamformer based on the SOE Kalman filter.

Chapter 5

Conclusions and Future Researches

5.1. Conclusions

Two adaptive beamformers, namely TFR-based adaptive beamformer and robust adaptive beamformer based on the SOE H_∞ filter, are proposed in this dissertation.

In the TFR-based adaptive beamformer, a null space is placed toward the direction of the principal component of the virtual sound using the TFR beamformer and the channel effect of the desired speech is equalized by the TFR information. The residual components of the virtual sound source and stationary noise are suppressed by the H_∞ filter. The comparison between the H_∞ filter and the NLMS algorithm and the advantage of the proposed system architecture are also analyzed. In addition, the virtual sound source concept which transforms the multiple competing speeches from MIMO to SIMO acoustic system is presented to simplify the complicated acoustic system. The performance of the proposed algorithm is compared to that of DSB, RAB and DTF-GSC algorithms in a real, noisy and reverberant environment and we also show the improvement on correct rate using Mandarin ASR system.

In the robust adaptive beamformer based on the SOE H_∞ filter, the SOE H_∞ filter is

proposed for the implementation of the robust MVDR beamformer of [38] for the acoustic environment and the detail derivation of the SOE H_∞ filter filter is also given in this dissertation. For the derivation of the SOE H_∞ filter, the second-order Taylor series expansion is used to approximate the nonlinear function and the second-order term is approximated by the estimation error sample covariance matrix. The SOE H_∞ filter provides a rigorous method for dealing with systems that have model uncertainty. A numerical example of a nonlinear discrete-time system is given to proof that the SOE H_∞ filter is more robust to the noise model uncertainty than the SOE Kalman filter and the extended H_∞ filter. In addition, speech enhancement experiments show that the proposed SOE H_∞ filter-based robust MVDR beamformer outperforms the SOE Kalman filter-based robust MVDR beamformer.

5.2. Future Researches

The future researches can be summarized as follows.

1. This dissertation assumes that a perfect desired speech detection system exists. The adaptive beamformer performance is affected by the accuracy of the desired speech detection system since the presence of the desired speech in training data reduce the convergence rates of adaptive beamformer algorithms [38]. Therefore, the desired speech detection system is very important and can be the further research topic.
2. This dissertation assumes that the sound source positions are fixed in the experiment. However, the sound source may move in many practical environments. Therefore, developing an adaptive beamformer or a TFR identification method which can cope with moving sound sources is worth a further study in the further.

3. In the TFR-based adaptive beamformer, the experiments are performed using eight microphones. The sub-array technique may be incorporated to improve the performance or to decrease the microphone number requirement.
4. The effectiveness of the SOE H_∞ filter can be sensitive to the weighting functions ($\mathbf{S}_a, \mathbf{P}_a(0), \mathbf{Q}_a, \mathbf{R}_a$ and γ in (3-61) ~ (3-65)) and the choices of these weighting functions are left as a subject of future work.

Reference

[1] D.H. Johnson and D.E. Dudgeon, *Array Signal Processing*, Prentice Hall, Englewood Cliffs, NJ, 1993.

[2] C. Winter, "Using continuous apertures discretely," *IEEE Trans. on Antennas and Propagation,* vol. AP-25, pp. 695-700, Sep. 1977.

[3] G. W. Elko, T. C. Chou, R. J. Lustberg, M. M. Goodwin, "A constant-directivity beamforming microphone array," *J. Acoust. Soc. Amer.,* vol. 96, no. 5, pp.3244, Nov. 1994.

[4] J. H. Doles III and F. D. Benedict, "Broad-band array design using the asymptotic theory of unequally spaced arrays," *IEEE Trans. on on Antennas and Propagation,* vol. 36, no. 1, pp. 27-33, Jan. 1988.

[5] B. D. Van Veen and K. M. Buckley, "Beamforming: a versatile approach to spatial filtering," *IEEE Acoustic, Speech, Signal Processing Magazine*, pp. 4-24, Apr. 1988.

[6] M. Doerbecker, "Speech enhancement using small microphone array with optimized directivity," *International Workshop on Acoustic, Echo, and Noise Control*, pp. 100-103, Sep. 1997.

[7] J. Bitzer, K. U. Simmer, and K. D. Kammeyer, "An alternative implementation of the superdierective beamformer,"in Proc. *IEEE International Workshop on Application Signal Processing to Audio Acoustics*, New Paltz, NY, USA, pp. 7-10, Oct. 1997.

[8] E. E. Jan and J. Flanagan, "Sound capture from spatial volumes: Matched-filter processing of microphone arrays having randomly-distributed sensors," *in Proc. Int. Conf. Acoust., Speech, Signal Process*., Atlanta, GA, pp. 917–920, May 1996.

[9] O.L. Frost, "An Algorithm for Linear Constrained Adaptive Array Processing," *Proc. IEEE*, vol.60, no.8, pp.926-935, Aug. 1972.

[10] L.J. Griffiths and C.W. Jim, "An alternative approach to linearly constrained adaptive beamforming," *IEEE Trans. on Antennas Propagation,* vol. AP-30, pp. 27-34, Jan. 1982.

[11] J. Li, and P. Stoica, *Robust Adaptive Beamforming*. Jonh Wiley & Sons, Inc., 2006.

[12] S. A. Vorobyov, A. B. Gershman, and Z. Q. Luo, "Robust adaptive beamforming using worst-case performance optimization: A solution to the signal mismatch problem," *IEEE Trans. Signal Processing*, vol. 51, no. 2, pp. 313-324, Fed. 2003.

[13] J. W. Kim and C. K. Un, "An adaptive array robust to beam pointing error," *IEEE Trans. Signal Processing*, vol. 40, no. 6, pp. 1582-1584, Jun. 1992.

[14] N.K. Jablon, "Adaptive beamforming with the generalized sidelobe canceller in the presence of array imperfections," *IEEE Trans. Antennas Propag*., vol.AP-34, no.8, pp.996-1012, Aug. 1986.

[15] Y.J. Hong, C.C. Yeh, and D.R. Ucci, "The effect of finite-distance signal source on a far-field steering Applebaum array—Two dimensional array case," *IEEE Trans. Antennas Propag*., vol.36, no.4, pp.468-475, April 1988.

[16] J. Ringelstein, A.B. Gershman, and J.F. B¨ohme, "Direction finding in random inhomogeneous media in the presence of multiplicative noise," *IEEE Signal Process. Lett*., vol.7, no.10, pp.269-272, Oct.2000.

[17] D. Astely and B. Ottersten, "The effects of local scattering on direction of arrival estimation with MUSIC," *IEEE Trans. Signal Process*., vol.47, no.12, pp.3220-3234, Dec. 1999.

[18] A. B. Gershman, "Robustness issues in adaptive beamforming and high-resolution direction finding, in High-Resolution and Robust Signal Processing," Y. Hua, A. B. Gershman, and Q. Cheng, Eds., New York: Marcel Dekker, 2003, pp. 63-110.

[19] H. Cox, R. M. Zeskind, and M. H. Owen, "Robust adaptive beamforming," *IEEE Trans. Acoust. Speech Signal Process*., vol.ASSP-35, no.10, pp.1365-1376, Oct. 1987.

[20] O. Hoshuyama, A. Sugiyama, and A. Hirano, "A robust adaptive beamformer for microphone arrays with blocking matrix using constrained adaptive filters," *IEEE Trans. Signal Process*., vol.47, no.10, pp.2677-2684, Oct. 1999.

[21] K. L. Bell, Y. Ephraim and H. L. Van Trees, "A Bayesian approach to robust adaptive beamforming," *IEEE Trans. Signal Process*, vol. 48, pp. 386-398, Feb. 2000.

[22] A. Spriet, M. Moonen and J. Wouters, "Spatially pre-processed speech distortion weighted multi-channel Wiener filtering for noise reduction," *Signal Process*., vol.84, no.12, pp. 2367-2387, 2004.

[23] S. Doclo, A. Spriet, J. Wouters and M. Moone, "Frequency-domain criterion for the speech distortion weighted multichannel Wiener filter for robust noise reduction," *Speech Communication.,* vol.49, no.7-8, pp. 636-656, 2007

[24] B. D. Carlson, "Covariance matrix estimation errors and diagonal loading in adaptive arrays," *IEEE Trans. Aerosp. Electron. Syst*., vol. 24, pp. 397–401, July 1988.

[25] M. H. Er and T. Cantoni, "An alternative formulation for an optimum beamformer with robustness capability," *Proc. Inst. Elect. Eng. Radar, Sonar, Navig*., pp. 447–460, Oct. 1985.

[26] L. Chang and C. C. Yeh, "Performance of DMI and eigenspace-based beamformers," *IEEE Trans. Antennas Propagat*., vol. 40, pp. 1336–1347, Nov. 1992.

[27] D. D. Feldman and L. J. Griffiths, "A projection approach to robust adaptive beamforming," *IEEE Trans. Signal Process.*, vol. 42, pp. 867–876, Apr. 1994.

[28] D. Rabinkin, R. Renomeron , J. Flanagan and D. F. Macomber, "Optimal truncation time for matched filter array Processing," *in Proc. Int. Conf. Acoust., Speech, Signal Process*., Seattle, WA, May 1998, pp. 3629-3632.

[29] S. Affes and Y. Grenier, "A signal subspace tracking algorithm for microphone array processing of speech," *IEEE Trans. Speech Audio Process.*, vol.5, no.5, pp.425–437, Sep. 1997.

[30] S. Gannot, D. Burshtein, and E. Weinstein, "Signal enhancement using beamforming and nonstationarity with applications to speech," *IEEE Trans. Signal Process*., vol.49, no.8, pp. 1614-1626, Aug. 2001.

[31] S. Gannot and I. Cohen, "Speech enhancement based on the general transfer function GSC and postfiltering," *IEEE Trans. Speech and Audio Process*., vol.12, no.6, pp.561-571, Nov. 2004.

[32] G. Reuven, S. Gannot and I. Cohen, "Dual-source transfer-function generalized sidelobe canceller," *IEEE Trans. Audio, Speech and Language Process*., vol.16, no.4, pp.711-727, May 2008.

[33] S. Markovich, S. Gannot, and I. Cohen, "Multichannel eigenspace beamforming in a reverberant noisy environment with multiple interfering speech signals," *IEEE Trans. Audio, Speech, Language Process*., vol. 17, no. 6, pp. 1071–1086,Aug. 2009.

[34] M. Dahl, and I. Claesson "Acoustic noise and echo canceling with microphone array," *IEEE Trans. Vehicular Technology*, vol. 48, pp.1518 -1526, Sep. 1999.

[35] J. S. Hu, W. H. Liu, and C. C. Cheng, "Robust beamforming of microphone array using H_∞ adaptive filtering technique," *IEICE Transactions on Fundamentals of Electronics, Communications and Computer Science*, vol. E89-A, no. 3, pp. 708-715, Mar. 2006.

[36] Y. Huang, J. Benesty, and J. Chen, "A blind channel identification-based two-stage approach to separation and dereverberation of speech signals in a reverberant environment," *IEEE Trans. Speech and Audio Process*., vol. 13, no. 5, pp. 882-895, Sep. 2005.

[37] J. Benesty, J. Chen, Y. Huang, and J. Dmochowski, "On microphone-array beamforming from a MIMO acoustic signal processing perspective," *IEEE Trans. Speech and Audio Process*., vol. 15, no. 3, pp. 1053-1065, Mar. 2007.

[38] S. A. Vorobyov, A. B. Gershman, and Z. Q. Luo, "Robust adaptive beamforming using worst-case performance optimization: A solution to the signal mismatch problem," *IEEE Trans. Signal Processing*, vol. 51, no. 2, pp. 313-324, Fed. 2003.

[39] Z L Yu, W Ser, M H Er, Z Gu and Y Li, "Robust Adaptive Beamformers Based on Worst-Case Optimization and Constraints on Magnitude Response", *IEEE Trans. Signal Process*., vol. 57, no. 7, pp. 2615-2628, July 2009.

[40] J. Li, P. Stoica, and Z. Wang, "On robust Capon beamforming and diagonal loading," *IEEE Trans. Signal Process*., vol. 51, no. 7, pp. 1702–1715, Jul. 2003.

[41] R. Lorenz and S. P. Boyd, "Robust minimum variance beamforming," *IEEE Trans. Signal Process*., vol. 53, no. 5, pp. 1684–1696, May 2005.

[42] S. Vorobyov, A. B. Gershman, Z.-Q. Luo, and N. Ma, "Adaptive beamforming with joint robustness against mismatched signal steering vector and interference nonstationarity," *IEEE Signal Process. Lett*., vol. 11, no. 2, pp. 108–111, Feb. 2004.

[43] K. Zarifi, S. Shahbazpanahi, A. B. Gershman, and Z.-Q. Luo, "Robust blind multiuser detection based on theworst-case performance optimization of the MMSE receiver," *IEEE Trans. Signal Process*., vol. 53, no.1, pp. 295–305, Jan.. 2005.

[44] A. El-Keyi, T. Kirubarajan, and A. B. Gershman, "Robust adaptive beamforming based on the Kalman filter," *IEEE Trans. Signal Process*., vol. 53, pp. 3032-3041, Aug. 2005.

[45] J. S. Hu and Chieh-Cheng Cheng, "Frequency domain microphone array calibration and beamforming for automatic speech recognition,", *IEICE Trans. Fundamentals*, vol. E88-A, no. 9, pp. 2401-2411, Sep. 2005.

[46] X. Shen and L. Deng, "A dynamic system approach to speech enhancement using the H_∞ filtering algorithm," *IEEE Trans. Speech ,Audio Process.,* vol.7, no.4, pp.391–399, July 1999.

[47] B. Hassibi and T. Kailath, "H_∞ adaptive filtering**,**" *in Proc. Int. Conf. Acoust., Speech, Signal Process.,* Detroit, MI, pp. 949-952, May 1995.

[48] D. Simon, "Optimal State Estimation: Kalman, H_∞, and Nonlinear Approaches," Wiley & Sons, Incorporated, John, 2006.

[49] W. Zhuang, "Adaptive H_∞ channel equation for wireless personal communications," *IEEE Trans*. *Vehicular Technology*, vol. 48, no. 1, pp. 126-136, January 1999.

[50] J.B. Allen and D.A. Berkley, "Image method for efficiently simulating small-room acoustics," *J. Acoust. Soc. Am.,* vol. 65, pp. 943-950, Apr. 1978.

[51] O. Shalvi and E. Weinstein, "System identification using non-stationary signals," *IEEE Trans. Signal Process.,* vol. 44, no. 8, pp. 2055-2063, Aug. 1996.

[52] G.A. Einicke and L.B. White, "Robust Extended Kalman filtering," *IEEE Trans. Signal Process.,* vol. 47, no.9, pp.2596–2599, 1999.

[53] K. Reff, F. Sonnemann and R. Unbehauen, "Nonlinear state observation using H_∞-filtering Riccati design," *IEEE Trans. Automatic Control,* vol.44, no.1, pp.203-208, Jan. 1999.

[54] A. G. Kallapur, I. R. Petersen and S. G. Anavatti, "A Discrete-Time Robust Extended Kalman Filter for Uncertain Systems with Sum Quadratic Constraints," *IEEE Trans. Automatic Control*, vol. 54, no. 4, April 2009.

[55] N. Berman and U. Shaked. "H_∞ nonlinear filtering," *International Journal of Robust and Nonlinear Control*, vol. 6, pp. 281 -296, 1996.

[56] U. Shaked and N. Berman, "H_∞ Nonlinear Filtering of Discrete-Time Processes," *IEEE Trans. Signal Process.*, vol. 43, no. 9, pp. 2205-2209, Sep. 1995.

[57] W.H. Zhang, B.S. Chen and C.S. Tseng, "Robust H_∞ filtering for nonlinear stochastic systems," *IEEE Trans. Signal Process.*, vol. 53, pp. 589-598, Feb. 2005.

[58] N. Abdelkrim1 , N. Aouf, A. Tsourdos and B. White, "Robust nonlinear filtering for INS/GPS UAV localization," *16th Mediterranean Conference on Control and Automation*, Congress Centre, Ajaccio, France, June 25-27, 2008.

[59] H. Dong, Z. Wang and H. Gao, "Robust Filtering for a Class of Nonlinear Networked Systems With Multiple Stochastic Communication Delays and Packet Dropouts," *IEEE Trans. Signal Process.*, vol. 58, vo. 4, pp. 1957-2010, April 2010.

[60] H. Gao, J. Lam, L. Xie and C. Wang, "New Approach to Mixed H_2/H_∞ Filtering for Polytopic Discrete-time Systems ", *IEEE Trans. Signal Process.*, vol. 53, no. 8, pp. 3183-3192, Aug. 2005.

[61] P. Khargonekhar, M. Rotea and E. Baeyens, "Mixed H_2/H_∞ Filtering", *Int. J. of Robust and Nonlinear Control*, vol. 6, no. 4, pp. 313-330, May, 1996.

[62] R. M. Palhares and P. L. D. Peres, "LMI Approach to the Mixed H_2/H_∞ Filtering for Discrete-time Systems", *IEEE Trans. Aerospace and Electronic Systems*, vol. 37, no. 1, pp. 292-296, Jan. 2001.

[63] Y. Theodor and U. Shaked, "A Dynamic Game Approach to Mixed H_2/H_∞ Estimation", *Int. J. of Robust and Nonlinear Control*, vol. 6, no. 4, pp. 331-345, 1996.

[64] F. Yang, Z. Wang, Y. S. Hung and H. Shu, "Mixed H_2/H_∞ Filtering for Uncertain Systems with Regional Pole Assignment", *IEEE Trans. Aerospace and Electronic Systems*, vol. 41, no. 2, pp. 438-448, Feb. 2005.

[65] M. D. S. Aliyu and E. K. Boukas, "Discrete-time Mixed H_2/H_∞ Nonlinear Filtering," *2008 American Control Conference*, Seattle, Washington, USA, June 11-13, 2008.

[66] B. Shen, Z. Wang, H. Shu, and G. Wei, " On Nonlinear H_∞ Filtering for Discrete-Time Stochastic Systems With Missing Measurements," *IEEE Trans. Automatic Control*, vol. 53, no. 9, pp. 2170-2180, Oct. 2008.

[67] M. D. S. Aliyu and E. K. Boukas, "2-DOF discrete-time nonlinear H_∞-filters," *Int. J. Robust Nonlinear Control*, 2010; 20:818–833.

[68] W. Li and Y. Jia, "H_∞ filtering for a class of nonlinear discrete-time systems based on unscented transform," *Signal Process.,* vol.19, no.12, pp.3301-3307, 2010.

[69] X.M. Shen, and L. Deng, "Game theory approach to discrete H_∞ filter design," *IEEE Trans. Signal Process.,* vol.45, no.4, pp.1092-1095, Apr. 1997.

[70] R. A. Monzingo and T. W. Miller, *Introduction to Adaptive Arrays*. New York: Wiley, 1980.

[71] The Association for Computational Linguistics and Chinese Language Processing, Website: http://www.aclclp.org.tw/corp.php

[72] Prof. S.H. Chen, National Chiao-Tung University, Taiwan, Website: http://www.speech.cm.nctu.edu.tw/

[73] H. Kuttruf, *Room Acoustics*, chap. 3, p.56, Elsevier, London, 1991.

[74] J. Benesty, S. Makino, and J.E. Chen, *Speech Enhancement, chapter 12*. Berlin, Germany: Springer, 2005.

Appendix I

The problem in this appendix is to maximize $J = \psi(\boldsymbol{x}_a(0)) + \sum_{t=0}^{N-1} L(t)$ (subject to the constraint $\boldsymbol{x}_a(t+1) = f(\boldsymbol{x}_a(t)) + \boldsymbol{w}_a(t)$) with respect to $\boldsymbol{x}_a(0)$ and $\boldsymbol{w}_a(t)$. The Hamiltonian for this problem is defined as:

$$H(t) = L(t) + 2\gamma\boldsymbol{\lambda}^{\mathrm{T}}(t+1)\cdot\left(f(\boldsymbol{x}_a(t)) + \boldsymbol{w}_a(t)\right) \tag{A-1}$$

where $2\gamma\boldsymbol{\lambda}^{\mathrm{T}}(t+1)$ is the Lagrange multiplier. According to [48], the necessary conditions for the maximum value of J with respect to $\boldsymbol{x}_a(0)$ and $\boldsymbol{w}_a(t)$ are the following four equations

$$2\gamma\boldsymbol{\lambda}^{\mathrm{T}}(0) + \frac{\partial\psi(\boldsymbol{x}_a(0))}{\partial\boldsymbol{x}_a(0)} = 0 \tag{A-2}$$

$$2\gamma\boldsymbol{\lambda}^{\mathrm{T}}(N) = 0 \tag{A-3}$$

$$\frac{\partial H(t)}{\partial\boldsymbol{w}_a(t)} = 0 \tag{A-4}$$

$$2\gamma\boldsymbol{\lambda}^{\mathrm{T}}(t) = \frac{\partial H(t)}{\partial\boldsymbol{x}_a(t)} \tag{A-5}$$

From (A-2)-(A-5), the following results can be derived, respectively.

$$\boldsymbol{x}_a(0) = \hat{\boldsymbol{x}}_a(0) + \mathbf{P}_a(0)\boldsymbol{\lambda}(0) \tag{A-6}$$

$$\boldsymbol{\lambda}(N) = 0 \tag{A-7}$$

$$\boldsymbol{w}_a(t) = \mathbf{Q}_a(t)\boldsymbol{\lambda}(t+1) \tag{A-8}$$

$$\boldsymbol{\lambda}(t) = \left(\frac{\partial f}{\partial\boldsymbol{x}_a(t)}\right)^{\mathrm{T}}\boldsymbol{\lambda}(t+1) + \frac{1}{\gamma}\overline{\mathbf{S}}_a(t)\left(\boldsymbol{x}_a(t) - \hat{\boldsymbol{x}}_a(t)\right) + \left(\frac{\partial h}{\partial\boldsymbol{x}_a(t)}\right)^{\mathrm{T}}\mathbf{R}_a^{-1}(t)\left(\boldsymbol{y}_a(t) - h(\boldsymbol{x}_a(t))\right) \tag{A-9}$$

Equation (A-8) an be substituted into the process dynamics equation in (A-1) to obtain

$$\boldsymbol{x}_a(t+1) = f(\boldsymbol{x}_a(t)) + \mathbf{Q}_a(t)\boldsymbol{\lambda}(t+1) \tag{A-10}$$

By substituting (3-43) and (3-45) into (A-9), we have

$$\begin{aligned}\boldsymbol{\lambda}(t) &= F^{\mathrm{T}}(t)\boldsymbol{\lambda}(t+1) + \frac{1}{\gamma}\overline{\mathbf{S}}_a(t)\left(\boldsymbol{x}_a(t) - \hat{\boldsymbol{x}}_a(t)\right) \\ &+ H^{\mathrm{T}}(t)\mathbf{R}_a^{-1}(t)\left(\boldsymbol{y}_a(t) - h(\hat{\boldsymbol{x}}_a(t)) - H(t)(\boldsymbol{x}_a(t) - \hat{\boldsymbol{x}}_a(t)) - \frac{1}{2}\sum_{i=1}^{d_m}\phi_i^h tr\left[\left.\frac{\partial^2 h_i}{\partial x_a^2(t)}\right|_{\hat{\boldsymbol{x}}_a(t)} \overline{\mathbf{P}}_a \right] \right)\end{aligned} \tag{A-11}$$

where $F(t) = \left.\dfrac{\partial f}{\partial \boldsymbol{x}_a(t)}\right|_{\hat{\boldsymbol{x}}_a(t)}$ and $H(t) = \left.\dfrac{\partial h}{\partial \boldsymbol{x}_a(t)}\right|_{\hat{\boldsymbol{x}}_a(t)}$. Because the matrix $\overline{\mathbf{P}}_a$ is the expected value of the past data, we neglect the influence of the instantaneous value of $\boldsymbol{x}_a(t)$. Therefore, $\dfrac{\partial f}{\partial \boldsymbol{x}_a(t)}$ and $\dfrac{\partial h}{\partial \boldsymbol{x}_a(t)}$ is approximated by $F(t)$ and $H(t)$.

Since $\boldsymbol{x}_a(0) = \hat{\boldsymbol{x}}_a(0) + \mathbf{P}_a(0)\boldsymbol{\lambda}(0)$ from (A-6), we assume

$$\boldsymbol{x}_a(t) = \mu(t) + \mathbf{P}_a(t)\boldsymbol{\lambda}(t) \tag{A-12}$$

where $\mu(t)$ and $\mathbf{P}_a(t)$ are functions to be determined, with $\mathbf{P}_a(0)$ given, and the initial condition $\mu(0) = \hat{\boldsymbol{x}}_a(0)$. Substituting (3-43), (3-45) and (A-12) into (A-10), we have

$$\begin{aligned}\mu(t+1) + \mathbf{P}_a(t+1)\boldsymbol{\lambda}(t+1) &= f(\hat{\boldsymbol{x}}_a(t)) + F(t)(\mu(t) + \mathbf{P}_a(t)\boldsymbol{\lambda}(t) - \hat{\boldsymbol{x}}_a(t)) \\ &+ \frac{1}{2}\sum_{i=1}^{d_s}\phi_i^f tr\left[\left.\frac{\partial^2 f_i}{\partial x_a^2(t)}\right|_{\hat{\boldsymbol{x}}_a(t)} \overline{\mathbf{P}}_a \right] + \mathbf{Q}_a(t)\boldsymbol{\lambda}(t+1)\end{aligned} \tag{A-13}$$

Further, substituting (A-12) into (A-11), we have

$$\begin{aligned}\boldsymbol{\lambda}(t) &= F^{\mathrm{T}}(t)\boldsymbol{\lambda}(t+1) + \frac{1}{\gamma}\overline{\mathbf{S}}_a(t)\left(\mu(t) + \mathbf{P}_a(t)\boldsymbol{\lambda}(t) - \hat{\boldsymbol{x}}_a(t)\right) \\ &+ H^{\mathrm{T}}(t)\mathbf{R}_a^{-1}(t)\left(\boldsymbol{y}_a(t) - h(\hat{\boldsymbol{x}}_a(t)) - H(t)(\mu(t) + \mathbf{P}_a(t)\boldsymbol{\lambda}(t) - \hat{\boldsymbol{x}}_a(t)) - \frac{1}{2}\sum_{i=1}^{d_m}\phi_i^h tr\left[\left.\frac{\partial^2 h_i}{\partial x_a^2(t)}\right|_{\hat{\boldsymbol{x}}_a(t)} \overline{\mathbf{P}}_a \right] \right)\end{aligned} \tag{A-14}$$

From (A-14), $\boldsymbol{\lambda}(t)$ can be solved as

$$\boldsymbol{\lambda}(t)=\left[\mathbf{I}-\frac{1}{\gamma}\overline{\mathbf{S}}_a(t)\mathbf{P}_a(t)+H^{\mathrm{T}}(t)\mathbf{R}_a^{-1}(t)H(t)\mathbf{P}_a(t)\right]^{-1}\times\left[F^{\mathrm{T}}(t)\boldsymbol{\lambda}(t+1)+\frac{1}{\gamma}\overline{\mathbf{S}}_a(t)\big(\mu(t)-\hat{\boldsymbol{x}}_a(t)\big)\right.$$
$$\left.+H^{\mathrm{T}}(t)\mathbf{R}_a^{-1}(t)\left(\boldsymbol{y}_a(t)-h(\hat{\boldsymbol{x}}_a(t))-H(t)(\mu(t)-\hat{\boldsymbol{x}}_a(t))-\frac{1}{2}\sum_{i=1}^{d_m}\phi_i^h tr\left[\left.\frac{\partial^2 h_i}{\partial x_a^2(t)}\right|_{\hat{\boldsymbol{x}}_a(t)}\overline{\mathbf{P}}_a\right]\right)\right] \tag{A-15}$$

Substituting (A-15) into (A-13) gives

$$\mu(t+1)+\mathbf{P}_a(t+1)\boldsymbol{\lambda}(t+1)=f(\hat{\boldsymbol{x}}_a(t))+F(t)(\mu(t)-\hat{\boldsymbol{x}}_a(t))+\frac{1}{2}\sum_{i=1}^{d_s}\phi_i^f tr\left[\left.\frac{\partial^2 f_i}{\partial x_a^2(t)}\right|_{\hat{\boldsymbol{x}}_a(t)}\overline{\mathbf{P}}_a\right]$$
$$+\mathbf{Q}_a(t)\boldsymbol{\lambda}(t+1)+F(t)\mathbf{P}_a(t)\left[\mathbf{I}-\frac{1}{\gamma}\overline{\mathbf{S}}_a(t)\mathbf{P}_a(t)+H^{\mathrm{T}}(t)\mathbf{R}_a^{-1}(t)H(t)\mathbf{P}_a(t)\right]^{-1}$$
$$\times\left\{F^{\mathrm{T}}(t)\boldsymbol{\lambda}(t+1)+\frac{1}{\gamma}\overline{\mathbf{S}}_a(t)\big(\mu(t)-\hat{\boldsymbol{x}}_a(t)\big)\right. \tag{A-16}$$
$$\left.+H^{\mathrm{T}}(t)\mathbf{R}_a^{-1}(t)\left(\boldsymbol{y}_a(t)-h(\hat{\boldsymbol{x}}_a(n))-H(t)(\mu(t)-\hat{\boldsymbol{x}}_a(t))-\frac{1}{2}\sum_{i=1}^{d_m}\phi_i^h tr\left[\left.\frac{\partial^2 h_i}{\partial x_a^2(t)}\right|_{\hat{\boldsymbol{x}}_a(t)}\overline{\mathbf{P}}_a\right]\right)\right\}$$

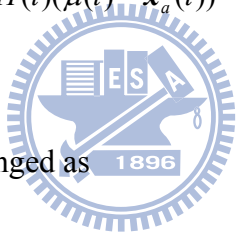

The equation above can be rearranged as

$$\mu(t+1)-f(\hat{\boldsymbol{x}}_a(t))-F(t)(\mu(t)-\hat{\boldsymbol{x}}_a(t))-\frac{1}{2}\sum_{i=1}^{d_s}\phi_i^f tr\left[\left.\frac{\partial^2 f_i}{\partial x_a^2(t)}\right|_{\hat{\boldsymbol{x}}_a(t)}\overline{\mathbf{P}}_a\right]$$
$$-F(t)\mathbf{P}_a(t)\left[\mathbf{I}-\frac{1}{\gamma}\overline{\mathbf{S}}_a(t)\mathbf{P}_a(t)+H^{\mathrm{T}}(t)\mathbf{R}_a^{-1}(t)H(t)\mathbf{P}_a(t)\right]^{-1}\times$$
$$\left[\frac{1}{\gamma}\overline{\mathbf{S}}_a(t)\big(\mu(t)-\hat{\boldsymbol{x}}_a(t)\big)+H^{\mathrm{T}}(t)\mathbf{R}_a^{-1}(t)\left(\boldsymbol{y}_a(t)-h(\hat{\boldsymbol{x}}_a(t))-H(t)(\mu(t)-\hat{\boldsymbol{x}}_a(t))-\frac{1}{2}\sum_{i=1}^{d_m}\phi_i^h tr\left[\left.\frac{\partial^2 h_i}{\partial x_a^2(t)}\right|_{\hat{\boldsymbol{x}}_a(t)}\overline{\mathbf{P}}_a\right]\right)\right]=$$
$$\left[-\mathbf{P}_a(t+1)+F(t)\mathbf{P}_a(t)\left[\mathbf{I}-\frac{1}{\gamma}\overline{\mathbf{S}}_a(t)\mathbf{P}_a(t)+H^{\mathrm{T}}(t)\mathbf{R}_a^{-1}(t)H(t)\mathbf{P}_a(t)\right]^{-1}F^{\mathrm{T}}(t)+\mathbf{Q}_a(t)\right]\boldsymbol{\lambda}(t+1)$$

(A-17)

Equation (A-17) is satisfied for any $\boldsymbol{\lambda}(t+1)$ if both sides are zero. Setting the left side of (A-17) to zero gives

$$\mu(t+1) = f(\hat{\boldsymbol{x}}_a(t)) + F(t)(\mu(t) - \hat{\boldsymbol{x}}_a(t)) + \frac{1}{2}\sum_{i=1}^{d_s}\phi_i^f tr\left[\left.\frac{\partial^2 f_i}{\partial x_a^2(t)}\right|_{\hat{\boldsymbol{x}}_a(t)} \overline{\mathbf{P}}_a\right]$$
$$+ F(t)\mathbf{P}_a(t)\left[\mathbf{I} - \frac{1}{\gamma}\overline{\mathbf{S}}_a(t)\mathbf{P}_a(t) + H^{\mathrm{T}}(t)\mathbf{R}_a^{-1}(t)H(t)\mathbf{P}_a(t)\right]^{-1}$$
$$\times\left[\frac{1}{\gamma}\overline{\mathbf{S}}_a(t)\left(\mu(t) - \hat{\boldsymbol{x}}_a(t)\right) + H^{\mathrm{T}}(t)\mathbf{R}_a^{-1}(t)\left(\boldsymbol{y}_a(t) - h(\hat{\boldsymbol{x}}_a(t)) - H(t)(\mu(t) - \hat{\boldsymbol{x}}_a(t)) - \frac{1}{2}\sum_{i=1}^{d_m}\phi_i^h tr\left[\left.\frac{\partial^2 h_i}{\partial x_a^2(t)}\right|_{\hat{\boldsymbol{x}}_a(t)} \overline{\mathbf{P}}_a\right]\right)\right] \tag{A-18}$$

Setting the right side of (A-17) to zero gives:

$$\begin{aligned}\mathbf{P}_a(t+1) &= F(t)\mathbf{P}_a(t)\left[\mathbf{I} - \frac{1}{\gamma}\overline{\mathbf{S}}_a(t)\mathbf{P}_a(t) + H^{\mathrm{T}}(t)\mathbf{R}_a^{-1}(t)H(t)\mathbf{P}_a(t)\right]^{-1} F^{\mathrm{T}}(t) + \mathbf{Q}_a(t) \\ &= F(t)\widetilde{\mathbf{P}}_a(t)F^{\mathrm{T}}(t) + \mathbf{Q}_a(t)\end{aligned} \tag{A-19}$$

where

$$\widetilde{\mathbf{P}}_a(t) = \mathbf{P}_a(t)\left[\mathbf{I} - \frac{1}{\gamma}\overline{\mathbf{S}}_a(t)\mathbf{P}_a(t) + H^{\mathrm{T}}(t)\mathbf{R}_a^{-1}(t)H(t)\mathbf{P}_a(t)\right]^{-1} = \left[\mathbf{P}_a^{-1}(t) - \frac{1}{\gamma}\overline{\mathbf{S}}_a(t) + H^{\mathrm{T}}(t)\mathbf{R}_a^{-1}(t)H(t)\right]^{-1} \tag{A-20}$$

From the derivations above, the values of $\boldsymbol{x}_a(0)$ and $\boldsymbol{w}_a(t)$ that provide a stationary point of J can be summarized as follows:

$$\boldsymbol{x}_a(0) = \hat{\boldsymbol{x}}_a(0) + \mathbf{P}_a(0)\boldsymbol{\lambda}(0) \tag{A-21}$$

$$\boldsymbol{w}_a(t) = \mathbf{Q}_a(t)\boldsymbol{\lambda}(t+1) \tag{A-22}$$

$$\boldsymbol{\lambda}(N) = 0 \tag{A-23}$$

$$\boldsymbol{\lambda}(t) = \left[\mathbf{I} - \frac{1}{\gamma}\overline{\mathbf{S}}_a(t)\mathbf{P}_a(t) + H^{\mathrm{T}}(t)\mathbf{R}_a^{-1}(t)H(t)\mathbf{P}_a(t)\right]^{-1} \times\left[F^{\mathrm{T}}(t)\boldsymbol{\lambda}(t+1) + \frac{1}{\gamma}\overline{\mathbf{S}}_a(t)\left(\mu(t) - \hat{\boldsymbol{x}}_a(t)\right)\right.$$
$$\left. + H^{\mathrm{T}}(t)\mathbf{R}_a^{-1}(t)\left(\boldsymbol{y}_a(t) - h(\hat{\boldsymbol{x}}_a(t)) - H(t)(\mu(t) - \hat{\boldsymbol{x}}_a(t)) - \frac{1}{2}\sum_{i=1}^{d_m}\phi_i^h tr\left[\left.\frac{\partial^2 h_i}{\partial x_a^2(t)}\right|_{\hat{\boldsymbol{x}}_a(t)} \overline{\mathbf{P}}_a\right]\right)\right] \tag{A-24}$$

$$\mathbf{P}_a(t+1) = F(t)\mathbf{P}_a(t)\left[\mathbf{I} - \frac{1}{\gamma}\overline{\mathbf{S}}_a(t)\mathbf{P}_a(t) + H^{\mathrm{T}}(t)\mathbf{R}_a^{-1}(t)H(t)\mathbf{P}_a(t)\right]^{-1} F^{\mathrm{T}}(t) + \mathbf{Q}_a(t) \qquad \text{(A-25)}$$

$$\mu(0) = \hat{\boldsymbol{x}}_a(0) \qquad \text{(A-26)}$$

$$\mu(t+1) = f(\hat{\boldsymbol{x}}_a(t)) + F(t)(\mu(t) - \hat{\boldsymbol{x}}_a(t)) + \frac{1}{2}\sum_{i=1}^{d_s}\phi_i^f tr\left[\left.\frac{\partial^2 f_i}{\partial x_a^2(t)}\right|_{\hat{\boldsymbol{x}}_a(t)} \overline{\mathbf{P}}_a\right]$$
$$+ F(t)\mathbf{P}_a(t)\left[\mathbf{I} - \frac{1}{\gamma}\overline{\mathbf{S}}_a(t)\mathbf{P}_a(t) + H^{\mathrm{T}}(t)\mathbf{R}_a^{-1}(t)H(t)\mathbf{P}_a(t)\right]^{-1}$$
$$\times\left[\frac{1}{\gamma}\overline{\mathbf{S}}_a(t)\left(\mu(t) - \hat{\boldsymbol{x}}_a(t)\right) + H^{\mathrm{T}}(t)\mathbf{R}_a^{-1}(t)\left(\boldsymbol{y}_a(t) - h(\hat{\boldsymbol{x}}_a(t)) - H(t)(\mu(t) - \hat{\boldsymbol{x}}_a(t)) - \frac{1}{2}\sum_{i=1}^{d_m}\phi_i^h tr\left[\left.\frac{\partial^2 h_i}{\partial x_a^2(t)}\right|_{\hat{\boldsymbol{x}}_a(t)} \overline{\mathbf{P}}_a\right]\right)\right] \qquad \text{(A-27)}$$

Appendix II

The problem in this appendix is to find a stationary point of $J = \psi(\boldsymbol{x}_a(0)) + \sum_{t=0}^{N-1} L(t)$ (subject to the constraint $\boldsymbol{x}_a(t+1) = f(\boldsymbol{x}_a(t)) + \boldsymbol{w}_a(t)$) with respect to $\hat{\boldsymbol{x}}_a(t)$ and $\boldsymbol{y}_a(t)$. It can be solved given the fact that $\boldsymbol{x}_a(0)$ and $\boldsymbol{w}_a(t)$ have already been set to their maximizing values as described in the previous section.

Since $\boldsymbol{x}_a(t) = \mu(t) + \mathbf{P}_a(t)\boldsymbol{\lambda}(t)$ and $\mu(0) = \hat{\boldsymbol{x}}_a(0)$, we have

$$\boldsymbol{\lambda}(t) = \mathbf{P}_a^{-1}(t)\left(\boldsymbol{x}_a(t) - \mu(t)\right) \quad , \quad \boldsymbol{\lambda}(0) = \mathbf{P}_a^{-1}(0)\left(\boldsymbol{x}_a(0) - \hat{\boldsymbol{x}}_a(0)\right) \tag{A-28}$$

Hence,

$$\begin{aligned} &\left|\lambda(0)\right|^2_{\mathbf{P}_a(0)} = \lambda^{\mathrm{T}}(0)\mathbf{P}_a(0)\lambda(0) \\ &= \left(\boldsymbol{x}_a(0) - \hat{\boldsymbol{x}}_a(0)\right)^{\mathrm{T}}\left(\mathbf{P}_a^{-1}(0)\right)^{\mathrm{T}}\mathbf{P}_a(0)\mathbf{P}_a^{-1}(0)\left(\boldsymbol{x}_a(0) - \hat{\boldsymbol{x}}_a(0)\right) \\ &= \left(\boldsymbol{x}_a(0) - \hat{\boldsymbol{x}}_a(0)\right)^{\mathrm{T}}\mathbf{P}_a^{-1}(0)\left(\boldsymbol{x}_a(0) - \hat{\boldsymbol{x}}_a(0)\right) = \left|\boldsymbol{x}_a(0) - \hat{\boldsymbol{x}}_a(0)\right|^2_{\mathbf{P}_a^{-1}(0)} \end{aligned} \tag{A-29}$$

Therefore, the cost function J of (3-51) can be written as

$$J = -\gamma\left|\lambda(0)\right|^2_{\mathbf{P}_a(0)} + \sum_{t=0}^{N-1}\left[\left|\boldsymbol{x}_a(t) - \hat{\boldsymbol{x}}_a(t)\right|^2_{\bar{\mathbf{S}}_a(t)} - \gamma\left(\left|\boldsymbol{w}_a(t)\right|^2_{\mathbf{Q}_a^{-1}(t)} + \left|\boldsymbol{y}_a(t) - h(\boldsymbol{x}_a(t))\right|^2_{\mathbf{R}_a^{-1}(t)}\right)\right] \tag{A-30}$$

By replacing $\boldsymbol{x}_a(t)$ and $\boldsymbol{w}_a(t)$ with the expression in (A-12) and (A-22), we have

$$\begin{aligned} &J = -\gamma\left|\lambda(0)\right|^2_{\mathbf{P}_a(0)} \\ &+ \sum_{t=0}^{N-1}\left[\left|\mu(t) + \mathbf{P}_a(t)\boldsymbol{\lambda}(t) - \hat{\boldsymbol{x}}_a(t)\right|^2_{\bar{\mathbf{S}}_a(t)} - \gamma\left(\left|\boldsymbol{y}_a(t) - h(\mu(t) + \mathbf{P}_a(t)\boldsymbol{\lambda}(t))\right|^2_{\mathbf{R}_a^{-1}(t)}\right)\right] - \gamma\sum_{t=0}^{N-1}\left[\left|\boldsymbol{\lambda}(t+1)\right|^2_{\mathbf{Q}_a(t)}\right] \\ &= -\gamma\left|\lambda(0)\right|^2_{\mathbf{P}_a(0)} + \sum_{t=0}^{N-1}\left\{\left|\mu(t) + \mathbf{P}_a(t)\boldsymbol{\lambda}(t) - \hat{\boldsymbol{x}}_a(t)\right|^2_{\bar{\mathbf{S}}_a(t)}\right. \\ &\left. - \gamma\left|\boldsymbol{y}_a(t) - h(\hat{\boldsymbol{x}}_a(t)) - H(t)(\mu(t) + \mathbf{P}_a(t)\boldsymbol{\lambda}(t) - \hat{\boldsymbol{x}}_a(t)) - \frac{1}{2}\sum_{i=1}^{d_m}\phi_i^h tr\left[\left.\frac{\partial^2 h_i}{\partial x_a^2(t)}\right|_{\hat{\boldsymbol{x}}_a(t)}\bar{\mathbf{P}}_a\right]\right|^2_{\mathbf{R}_a^{-1}(t)}\right\} - \gamma\sum_{t=0}^{N-1}\left[\left|\boldsymbol{\lambda}(t+1)\right|^2_{\mathbf{Q}_a(t)}\right] \end{aligned}$$

(A-31)

Substituting (A-55) of Appendix IV into (A-31), we obtain

$$J=\sum_{t=0}^{N-1}\Big[\left\|\mu(t)+\mathbf{P}_a(t)\boldsymbol{\lambda}(t)-\hat{\boldsymbol{x}}_a(t)\right\|^2_{\overline{\mathbf{S}}_a(t)}-\gamma\left|\boldsymbol{\lambda}(t+1)\right|^2_{\mathbf{Q}_a(t)}+\gamma\left(\boldsymbol{\lambda}^{\mathrm{T}}(t+1)\mathbf{P}_a(t+1)\boldsymbol{\lambda}(t+1)-\boldsymbol{\lambda}^{\mathrm{T}}(t)\mathbf{P}_a(t)\boldsymbol{\lambda}(t)\right)$$
$$-\gamma\left(\left\|\boldsymbol{y}_a(t)-h(\hat{\boldsymbol{x}}_a(t))-H(t)(\mu(t)+\mathbf{P}_a(t)\boldsymbol{\lambda}(t)-\hat{\boldsymbol{x}}_a(t))-\frac{1}{2}\sum_{i=1}^{d_m}\phi_i^h tr\left[\left.\frac{\partial^2 h_i}{\partial x_a^2(t)}\right|_{\hat{\boldsymbol{x}}_a(t)}\overline{\mathbf{P}}_a\right]\right\|^2_{\mathbf{R}_a^{-1}(t)}\right)\Big]$$
$$=\sum_{t=0}^{N-1}\Big[\left(\mu(t)-\hat{\boldsymbol{x}}_a(t)\right)^{\mathrm{T}}\overline{\mathbf{S}}_a(t)\left(\mu(t)-\hat{\boldsymbol{x}}_a(t)\right)+2\left(\mu(t)-\hat{\boldsymbol{x}}_a(t)\right)^{\mathrm{T}}\overline{\mathbf{S}}_a(t)\mathbf{P}_a(t)\boldsymbol{\lambda}(t)+\boldsymbol{\lambda}^{\mathrm{T}}(t)\mathbf{P}_a(t)\overline{\mathbf{S}}_a(t)\mathbf{P}_a(t)\boldsymbol{\lambda}(t)$$
$$+\gamma\boldsymbol{\lambda}^{\mathrm{T}}(t+1)\left(\mathbf{P}_a(t+1)-\mathbf{Q}_a(t)\right)\boldsymbol{\lambda}(t+1)-\gamma\boldsymbol{\lambda}^{\mathrm{T}}(t)\mathbf{P}_a(t)\boldsymbol{\lambda}(t)$$
$$-\gamma Y^{\mathrm{T}}(t)\mathbf{R}_a^{-1}(t)Y(t)+2\gamma Y^{\mathrm{T}}(t)\mathbf{R}_a^{-1}(t)H(t)\mathbf{P}_a(t)\boldsymbol{\lambda}(t)-\gamma\boldsymbol{\lambda}^{\mathrm{T}}(t)\mathbf{P}_a(t)H^{\mathrm{T}}(t)\mathbf{R}_a^{-1}(t)H(t)\mathbf{P}_a(t)\boldsymbol{\lambda}(t)\Big]$$

(A-32)

where

$$Y(t)=\left(\boldsymbol{y}_a(t)-h(\hat{\boldsymbol{x}}_a(t))-H(t)(\mu(t)-\hat{\boldsymbol{x}}_a(t))-\frac{1}{2}\sum_{i=1}^{d_m}\phi_i^h tr\left[\left.\frac{\partial^2 h_i}{\partial x_a^2(t)}\right|_{\hat{\boldsymbol{x}}_a(t)}\overline{\mathbf{P}}_a\right]\right)\qquad\text{(A-33)}$$

Now, consider the term $\boldsymbol{\lambda}^{\mathrm{T}}(t+1)\left(\mathbf{P}_a(t+1)-\mathbf{Q}(t)\right)\boldsymbol{\lambda}(t+1)$ in (A-32). Using (A-19), we have

$$\boldsymbol{\lambda}^{\mathrm{T}}(t+1)\left(\mathbf{P}_a(t+1)-\mathbf{Q}_a(t)\right)\boldsymbol{\lambda}(t+1)=\boldsymbol{\lambda}^{\mathrm{T}}(t+1)\left(F(t)\widetilde{\mathbf{P}}_a(t)F^{\mathrm{T}}(t)\right)\boldsymbol{\lambda}(t+1)\qquad\text{(A-34)}$$

From (A-14), we have

$$F^{\mathrm{T}}(t)\boldsymbol{\lambda}(t+1)=\boldsymbol{\lambda}(t)-\frac{1}{\gamma}\overline{\mathbf{S}}_a(t)\left(\mu(t)+\mathbf{P}_a(t)\boldsymbol{\lambda}(t)-\hat{\boldsymbol{x}}_a(t)\right)$$
$$-H^{\mathrm{T}}(t)\mathbf{R}_a^{-1}(t)\left(\boldsymbol{y}_a(t)-h(\hat{\boldsymbol{x}}_a(t))-H(t)(\mu(t)+\mathbf{P}_a(t)\boldsymbol{\lambda}(t)-\hat{\boldsymbol{x}}_a(t))-\frac{1}{2}\sum_{i=1}^{d_m}\phi_i^h tr\left[\left.\frac{\partial^2 h_i}{\partial x_a^2(t)}\right|_{\hat{\boldsymbol{x}}_a(t)}\overline{\mathbf{P}}_a\right]\right)$$

(A-35)

Substituting (A-35) into (A-34), we have:

$$\boldsymbol{\lambda}^{\mathrm{T}}(t+1)\left(\mathbf{P}_a(t+1)-\mathbf{Q}(t)\right)\boldsymbol{\lambda}(t+1)$$
$$=\left\{\boldsymbol{\lambda}^{\mathrm{T}}(t)\left(\mathbf{I}-\frac{1}{\gamma}\mathbf{P}_a(t)\overline{\mathbf{S}}_a(t)+\mathbf{P}_a(t)H^{\mathrm{T}}(t)\mathbf{R}_a^{-1}(t)H(t)\right)-\frac{1}{\gamma}\left(\mu(t)-\hat{\boldsymbol{x}}_a(t)\right)^{\mathrm{T}}\overline{\mathbf{S}}_a(t)-Y^{\mathrm{T}}(t)\mathbf{R}_a^{-1}(t)H(t)\right\}$$
$$\times\widetilde{\mathbf{P}}_a(t)\times\left\{\boldsymbol{\lambda}^{\mathrm{T}}(t)\left(\mathbf{I}-\frac{1}{\gamma}\mathbf{P}_a(t)\overline{\mathbf{S}}_a(t)+\mathbf{P}_a(t)H^{\mathrm{T}}(t)\mathbf{R}_a^{-1}(t)H(t)\right)-\frac{1}{\gamma}\left(\mu(t)-\hat{\boldsymbol{x}}_a(t)\right)^{\mathrm{T}}\overline{\mathbf{S}}_a(t)-Y^{\mathrm{T}}(t)\mathbf{R}_a^{-1}(t)H(t)\right\}^{\mathrm{T}}$$

(A-36)

Because $\left[\mathbf{I}-\frac{1}{\gamma}\mathbf{P}_a(t)\overline{\mathbf{S}}_a(t)+\mathbf{P}_a(t)H^{\mathrm{T}}(t)\mathbf{R}_a^{-1}(t)H(t)\right]=\mathbf{P}_a(t)\widetilde{\mathbf{P}}_a^{-1}(t)$. Equation (A-36) can be written as:

$$\boldsymbol{\lambda}^{\mathrm{T}}(t+1)\left(\mathbf{P}_a(t+1)-\mathbf{Q}_a(t)\right)\boldsymbol{\lambda}(t+1)$$
$$=\boldsymbol{\lambda}^{\mathrm{T}}(t)\mathbf{P}_a(t)\widetilde{\mathbf{P}}_a^{-1}(t)\mathbf{P}_a(t)\boldsymbol{\lambda}(t)-\frac{1}{\gamma}\left(\mu(t)-\hat{\boldsymbol{x}}_a(t)\right)^{\mathrm{T}}\overline{\mathbf{S}}_a(t)\mathbf{P}_a(t)\boldsymbol{\lambda}(t)-Y^{\mathrm{T}}(t)\mathbf{R}_a^{-1}(t)H(t)\mathbf{P}_a(t)\boldsymbol{\lambda}(t)$$
$$-\frac{1}{\gamma}\boldsymbol{\lambda}^{\mathrm{T}}(t)\mathbf{P}_a(t)\overline{\mathbf{S}}_a(t)\left(\mu(t)-\hat{\boldsymbol{x}}_a(t)\right)+\frac{1}{\gamma^2}\left(\mu(t)-\hat{\boldsymbol{x}}_a(t)\right)^{\mathrm{T}}\overline{\mathbf{S}}_a(t)\widetilde{\mathbf{P}}_a(t)\overline{\mathbf{S}}_a(t)\left(\mu(t)-\hat{\boldsymbol{x}}_a(t)\right)$$
$$+\frac{1}{\gamma}Y^{\mathrm{T}}(t)\mathbf{R}_a^{-1}(t)H(t)\widetilde{\mathbf{P}}_a(t)\overline{\mathbf{S}}_a(t)\left(\mu(t)-\hat{\boldsymbol{x}}_a(t)\right)-\boldsymbol{\lambda}^{\mathrm{T}}(t)\mathbf{P}_a(t)H^{\mathrm{T}}(t)\mathbf{R}_a^{-1}(t)Y(t)$$
$$+\frac{1}{\gamma}\left(\mu(t)-\hat{\boldsymbol{x}}_a(t)\right)^{\mathrm{T}}\overline{\mathbf{S}}_a(t)\widetilde{\mathbf{P}}_a(t)H^{\mathrm{T}}(t)\mathbf{R}_a^{-1}(t)Y(t)+Y^{\mathrm{T}}(t)\mathbf{R}_a^{-1}(t)H(t)\widetilde{\mathbf{P}}_a(t)H^{\mathrm{T}}(t)\mathbf{R}_a^{-1}(t)Y(t)$$

(A-37)

Equation (A-37) is a scalar which means that each term in (A-37) is also a scalar. Therefore, (A-37) can be rewritten as

$$\boldsymbol{\lambda}^{\mathrm{T}}(t+1)\left(\mathbf{P}_a(t+1)-\mathbf{Q}_a(t)\right)\boldsymbol{\lambda}(t+1)=\boldsymbol{\lambda}^{\mathrm{T}}(t)\mathbf{P}_a(t)\widetilde{\mathbf{P}}_a^{-1}(t)\mathbf{P}_a(t)\boldsymbol{\lambda}(t)-\frac{2}{\gamma}\left(\mu(t)-\hat{\boldsymbol{x}}_a(t)\right)^{\mathrm{T}}\overline{\mathbf{S}}_a(t)\mathbf{P}_a(t)\boldsymbol{\lambda}(t)$$
$$-2Y^{\mathrm{T}}(t)\mathbf{R}_a^{-1}(t)H(t)\mathbf{P}_a(t)\boldsymbol{\lambda}(t)+\frac{1}{\gamma^2}\left(\mu(t)-\hat{\boldsymbol{x}}_a(t)\right)^{\mathrm{T}}\overline{\mathbf{S}}_a(t)\widetilde{\mathbf{P}}_a(t)\overline{\mathbf{S}}_a(t)\left(\mu(t)-\hat{\boldsymbol{x}}_a(t)\right)$$
$$+\frac{2}{\gamma}\left(\mu(t)-\hat{\boldsymbol{x}}_a(t)\right)^{\mathrm{T}}\overline{\mathbf{S}}_a(t)\widetilde{\mathbf{P}}_a(t)H^{\mathrm{T}}(t)\mathbf{R}_a^{-1}(t)Y(t)+Y^{\mathrm{T}}(t)\mathbf{R}_a^{-1}(t)H(t)\widetilde{\mathbf{P}}_a(t)H^{\mathrm{T}}(t)\mathbf{R}_a^{-1}(t)Y(t)$$

(A-38)

Next, consider the term $\boldsymbol{\lambda}^{\mathrm{T}}(t)\mathbf{P}_a(t)\widetilde{\mathbf{P}}_a^{-1}(t)\mathbf{P}_a(t)\boldsymbol{\lambda}(t)$ in (A-38).

$$\boldsymbol{\lambda}^{\mathrm{T}}(t)\mathbf{P}_a(t)\tilde{\mathbf{P}}_a^{-1}(t)\mathbf{P}_a(t)\boldsymbol{\lambda}(t)=\boldsymbol{\lambda}^{\mathrm{T}}(t)\mathbf{P}_a(t)\left[\mathbf{I}-\frac{1}{\gamma}\bar{\mathbf{S}}_a(t)\mathbf{P}_a(t)+H^{\mathrm{T}}(t)\mathbf{R}_a^{-1}(t)H(t)\mathbf{P}_a(t)\right]\mathbf{P}_a^{-1}(t)\mathbf{P}_a(t)\boldsymbol{\lambda}(t)$$

$$=\boldsymbol{\lambda}^{\mathrm{T}}(t)\mathbf{P}_a(t)\boldsymbol{\lambda}(t)-\frac{1}{\gamma}\boldsymbol{\lambda}^{\mathrm{T}}(t)\mathbf{P}_a(t)\bar{\mathbf{S}}_a(t)\mathbf{P}_a(t)\boldsymbol{\lambda}(t)+\boldsymbol{\lambda}^{\mathrm{T}}(t)\mathbf{P}_a(t)H^{\mathrm{T}}(t)\mathbf{R}_a^{-1}(t)H(t)\mathbf{P}_a(t)\boldsymbol{\lambda}(t)$$

(A-39)

Substituting (A-39) into (A-38) we can obtain:

$$\boldsymbol{\lambda}^{\mathrm{T}}(t+1)\left(\mathbf{P}_a(t+1)-\mathbf{Q}_a(t)\right)\boldsymbol{\lambda}(t+1)=\boldsymbol{\lambda}^{\mathrm{T}}(t)\mathbf{P}_a(t)\boldsymbol{\lambda}(t)-\frac{1}{\gamma}\boldsymbol{\lambda}^{\mathrm{T}}(t)\mathbf{P}_a(t)\bar{\mathbf{S}}_a(t)\mathbf{P}_a(t)\boldsymbol{\lambda}(t)$$

$$+\boldsymbol{\lambda}^{\mathrm{T}}(t)\mathbf{P}_a(t)H^{\mathrm{T}}(t)\mathbf{R}_a^{-1}(t)H(t)\mathbf{P}_a(t)\boldsymbol{\lambda}(t)-\frac{2}{\gamma}\left(\mu(t)-\hat{\boldsymbol{x}}_a(t)\right)^{\mathrm{T}}\bar{\mathbf{S}}_a(t)\mathbf{P}_a(t)\boldsymbol{\lambda}(t)$$

$$-2Y^{\mathrm{T}}(t)\mathbf{R}_a^{-1}(t)H(t)\mathbf{P}_a(t)\boldsymbol{\lambda}(t)+\frac{1}{\gamma^2}\left(\mu(t)-\hat{\boldsymbol{x}}_a(t)\right)^{\mathrm{T}}\bar{\mathbf{S}}_a(t)\tilde{\mathbf{P}}_a(t)\bar{\mathbf{S}}_a(t)\left(\mu(t)-\hat{\boldsymbol{x}}_a(t)\right)$$

$$+\frac{2}{\gamma}\left(\mu(t)-\hat{\boldsymbol{x}}_a(t)\right)^{\mathrm{T}}\bar{\mathbf{S}}_a(t)\tilde{\mathbf{P}}(t)H^{\mathrm{T}}(t)\mathbf{R}_a^{-1}(t)Y(t)+Y^{\mathrm{T}}(t)\mathbf{R}_a^{-1}(t)H(t)\tilde{\mathbf{P}}_a(t)H^{\mathrm{T}}(t)\mathbf{R}_a^{-1}(t)Y(t)$$

(A-40)

Next, go back to the cost function J. Substituting (A-40) into (A-32) gives:

$$J=\sum_{t=0}^{N-1}\Bigg[\left(\mu(t)-\hat{\boldsymbol{x}}_a(t)\right)^{\mathrm{T}}\left(\bar{\mathbf{S}}_a(t)+\frac{1}{\gamma}\bar{\mathbf{S}}_a(t)\tilde{\mathbf{P}}_a(t)\bar{\mathbf{S}}_a(t)\right)\left(\mu(t)-\hat{\boldsymbol{x}}_a(t)\right)$$

$$+2\left(\mu(t)-\hat{\boldsymbol{x}}_a(t)\right)^{\mathrm{T}}\bar{\mathbf{S}}_a(t)\tilde{\mathbf{P}}_a(t)H^{\mathrm{T}}(t)\mathbf{R}_a^{-1}(t)\left(\boldsymbol{y}_a(t)-h(\hat{\boldsymbol{x}}_a(t))-H(t)(\mu(t)-\hat{\boldsymbol{x}}_a(t))-\frac{1}{2}\sum_{i=1}^{d_m}\phi_i^h tr\left[\left.\frac{\partial^2 h_i}{\partial x_a^2(t)}\right|_{\hat{\boldsymbol{x}}_a(t)}\bar{\mathbf{P}}_a\right]\right)$$

$$+\gamma\left(\boldsymbol{y}_a(t)-h(\hat{\boldsymbol{x}}_a(t))-H(t)(\mu(t)-\hat{\boldsymbol{x}}_a(t))-\frac{1}{2}\sum_{i=1}^{d_m}\phi_i^h tr\left[\left.\frac{\partial^2 h_i}{\partial x_a^2(t)}\right|_{\hat{\boldsymbol{x}}_a(t)}\bar{\mathbf{P}}_a\right]\right)^{\mathrm{T}}\left(\mathbf{R}_a^{-1}(t)H(t)\tilde{\mathbf{P}}_a(t)H^{\mathrm{T}}(t)\mathbf{R}_a^{-1}(t)-\mathbf{R}_a^{-1}(t)\right)$$

$$\times\left(\boldsymbol{y}_a(t)-h(\hat{\boldsymbol{x}}_a(t))-H(t)(\mu(t)-\hat{\boldsymbol{x}}_a(t))-\frac{1}{2}\sum_{i=1}^{d_m}\phi_i^h tr\left[\left.\frac{\partial^2 h_i}{\partial x_a^2(t)}\right|_{\hat{\boldsymbol{x}}_a(t)}\bar{\mathbf{P}}_a\right]\right)\Bigg]$$

(A-41)

Now, take the partial derivative of (A-41) with respect to $\hat{\boldsymbol{x}}_a(t)$ and $\boldsymbol{y}_a(t)$ and set them to zero.

$$\frac{\partial J}{\partial \hat{\boldsymbol{x}}_a(t)} = 2\left(\overline{\mathbf{S}}_a(t) + \frac{1}{\gamma}\mathbf{S}_a(t)\widetilde{\mathbf{P}}_a(t)\overline{\mathbf{S}}_a(t)\right)\left(\hat{\boldsymbol{x}}_a(t) - \mu(t)\right)$$
$$+ 2\overline{\mathbf{S}}_a(t)\widetilde{\mathbf{P}}_a(t)H^{\mathrm{T}}(t)\mathbf{R}_a^{-1}(t)\left(h(\hat{\boldsymbol{x}}_a(t)) + H(t)(\mu(t) - \hat{\boldsymbol{x}}_a(t)) + \frac{1}{2}\sum_{i=1}^{d_m}\phi_i^h tr\left[\left.\frac{\partial^2 h_i}{\partial x_a^2(t)}\right|_{\hat{\boldsymbol{x}}_a(t)}\overline{\mathbf{P}}_a\right] - \boldsymbol{y}_a(t)\right)$$
$$- 2M^{\mathrm{T}}(t)\mathbf{R}_a^{-1}(t)H(t)\widetilde{\mathbf{P}}_a(t)\overline{\mathbf{S}}_a(t)\left(\hat{\boldsymbol{x}}_a(t) - \mu(t)\right)$$
$$- 2\gamma M^{\mathrm{T}}(t)\left(\mathbf{R}_a^{-1}(t)H(t)\widetilde{\mathbf{P}}_a(t)H^{\mathrm{T}}(t)\mathbf{R}_a^{-1}(t) - \mathbf{R}_a^{-1}(t)\right)\left(h(\hat{\boldsymbol{x}}_a(t)) + H(t)(\mu(t) - \hat{\boldsymbol{x}}_a(t)) + \frac{1}{2}\sum_{i=1}^{d_m}\phi_i^h tr\left[\left.\frac{\partial^2 h_i}{\partial x_a^2(t)}\right|_{\hat{\boldsymbol{x}}_a(t)}\overline{\mathbf{P}}_a\right] - \boldsymbol{y}_a(t)\right)$$
$$= 0$$
$$\frac{\partial J}{\partial \boldsymbol{y}_a(t)} = 2\mathbf{R}_a^{-1}(t)H(t)\widetilde{\mathbf{P}}_a(t)\overline{\mathbf{S}}_a(t)\left(\mu(t) - \hat{\boldsymbol{x}}_a(t)\right)$$
$$+ 2\gamma\left(\mathbf{R}_a^{-1}(t)H(t)\widetilde{\mathbf{P}}_a(t)H^{\mathrm{T}}(t)\mathbf{R}_a^{-1}(t) - \mathbf{R}_a^{-1}(t)\right)\left(\boldsymbol{y}_a(t) - h(\hat{\boldsymbol{x}}_a(t)) - H(t)(\mu(t) - \hat{\boldsymbol{x}}_a(t)) - \frac{1}{2}\sum_{i=1}^{d_m}\phi_i^h tr\left[\left.\frac{\partial^2 h_i}{\partial x_a^2(t)}\right|_{\hat{\boldsymbol{x}}_a(t)}\overline{\mathbf{P}}_a\right]\right)$$
$$= 0$$

(A-42)

where

$$M(t) = \frac{\partial}{\partial \hat{\boldsymbol{x}}_a(t)}\left(\boldsymbol{y}_a(t) - h(\hat{\boldsymbol{x}}_a(t)) - H(t)(\mu(t) - \hat{\boldsymbol{x}}_a(t)) - \frac{1}{2}\sum_{i=1}^{d_m}\phi_i^h tr\left[\left.\frac{\partial^2 h_i}{\partial x_a^2(t)}\right|_{\hat{\boldsymbol{x}}_a(t)}\overline{\mathbf{P}}_a\right]\right) \quad \text{(A-43)}$$

Equation (A-42) are satisfied for the following values of $\hat{\boldsymbol{x}}_a(t)$ and $\boldsymbol{y}_a(t)$:

$$\hat{\boldsymbol{x}}_a(t) = \mu(t)$$
$$\boldsymbol{y}_a(t) = h(\hat{\boldsymbol{x}}_a(t)) + \frac{1}{2}\sum_{i=1}^{d_m}\phi_i^h tr\left[\left.\frac{\partial^2 h_i}{\partial x_a^2(t)}\right|_{\hat{\boldsymbol{x}}_a(t)}\overline{\mathbf{P}}_a\right] \quad \text{(A-44)}$$

Appendix III

Equation (A-44) can be substituted into (A-24), (A-25) and (A-27) to obtain the SOE H_∞ solution. To ensure that the optimized value of $\hat{\boldsymbol{x}}_a(t)$ gives the local minimum of J, the second derivative of J with respect to $\hat{\boldsymbol{x}}_a(t)$ must be positive. Now, consider (A-43). Using the derivatives property, we obtain

$$M(t) = \frac{\partial}{\partial \hat{\boldsymbol{x}}_a(t)}\left(\boldsymbol{y}_a(t) - h(\hat{\boldsymbol{x}}_a(t)) - H(t)(\mu(t) - \hat{\boldsymbol{x}}_a(t)) - \frac{1}{2}\sum_{i=1}^{d_m} \phi_i^h tr\left[\left.\frac{\partial^2 h_i}{\partial x_a^2(t)}\right|_{\hat{\boldsymbol{x}}_a(t)} \overline{\mathbf{P}}_a \right] \right)$$
$$= -\frac{\partial h(\hat{\boldsymbol{x}}_a(t))}{\partial \hat{\boldsymbol{x}}_a(t)} - \frac{\partial^2 h(\hat{\boldsymbol{x}}_a(t))}{\partial \hat{\boldsymbol{x}}_a^2(t)}\mu(t) + \frac{\partial^2 h(\hat{\boldsymbol{x}}_a(t))}{\partial \hat{\boldsymbol{x}}_a^2(t)}\hat{\boldsymbol{x}}_a(t) + \left.\frac{\partial h(\boldsymbol{x}_a(t))}{\partial \boldsymbol{x}_a(t)}\right|_{\hat{\boldsymbol{x}}_a(t)} \tag{A-45}$$

Ignore the term of third-order derivatives, since we use the second-order to approximate the nonlinear function $h(\cdot)$. Because $\hat{\boldsymbol{x}}_a(t) = \mu(t)$, we have $M(t) = 0$. Therefore, the value of γ must satisfy

$$\frac{\partial^2 J}{\partial \hat{\boldsymbol{x}}_a^2(t)} = 2\left(\overline{\mathbf{S}}(t) + \frac{1}{\gamma}\overline{\mathbf{S}}(t)\tilde{\mathbf{P}}(t)\overline{\mathbf{S}}(t) \right) > 0 \tag{A-46}$$

From (A-12) and (A-44), the instantaneous covariance matrix at time index t can be written as

$$\left(\boldsymbol{x}_a(t) - \hat{\boldsymbol{x}}_a(t)\right)\left(\boldsymbol{x}_a(t) - \hat{\boldsymbol{x}}_a(t)\right)^{\mathrm{T}} = \mathbf{P}_a(t)\boldsymbol{\lambda}(t)\boldsymbol{\lambda}^{\mathrm{T}}(t)\mathbf{P}_a^{\mathrm{T}}(t) \tag{A-47}$$

Therefore, the matrix $\overline{\mathbf{P}}_a$ can be approximated iteratively via the recursion

$$\overline{\mathbf{P}}_a(t+1) = \eta\overline{\mathbf{P}}_a(t) + (1-\eta)\mathbf{P}_a(t)\boldsymbol{\lambda}(t)\boldsymbol{\lambda}^{\mathrm{T}}(t)\mathbf{P}_a^{\mathrm{T}}(t) \tag{A-48}$$

where $0 < \eta \le 1$.

Consequently, according to (A-24), (A-25), (A-27) and (A-44), the SOE H_∞ solution can

be summarized as follows:

$$\begin{aligned}\hat{\boldsymbol{x}}_a(t+1) = f(\hat{\boldsymbol{x}}_a(t)) + \frac{1}{2}\sum_{i=1}^{d_s}\phi_i^f tr\left[\left.\frac{\partial^2 f_i}{\partial x_a^2(t)}\right|_{\hat{\boldsymbol{x}}_a(t)} \overline{\mathbf{P}}_a(t)\right] \\ + \mathbf{K}_a(t)\left(\boldsymbol{y}_a(t) - h(\hat{\boldsymbol{x}}_a(t)) - \frac{1}{2}\sum_{i=1}^{d_m}\phi_i^h tr\left[\left.\frac{\partial^2 h_i}{\partial x_a^2(t)}\right|_{\hat{\boldsymbol{x}}_a(t)} \overline{\mathbf{P}}_a(t)\right]\right)\end{aligned} \tag{A-49}$$

$$\mathbf{K}_a(t) = F(t)\mathbf{P}_a(t)\left[\mathbf{I} - \frac{1}{\gamma}\overline{\mathbf{S}}_a(t)\mathbf{P}_a(t) + H^{\mathrm{T}}(t)\mathbf{R}_a^{-1}(t)H(t)\mathbf{P}_a(t)\right]^{-1} H^{\mathrm{T}}(t)\mathbf{R}_a^{-1}(t) \tag{A-50}$$

$$\mathbf{P}_a(t+1) = F(t)\mathbf{P}_a(t)\left[\mathbf{I} - \frac{1}{\gamma}\overline{\mathbf{S}}_a(t)\mathbf{P}_a(t) + H^{\mathrm{T}}(t)\mathbf{R}_a^{-1}(t)H(t)\mathbf{P}_a(t)\right]^{-1} F^{\mathrm{T}}(t) + \mathbf{Q}_a(t) \tag{A-51}$$

$$\begin{aligned}\boldsymbol{\lambda}(t+1) = \left(F(t)F^{\mathrm{T}}(t) + \varepsilon I\right)^{-1} F(t)\left\{\left[\mathbf{I} - \frac{1}{\gamma}\overline{\mathbf{S}}_a(t)\mathbf{P}_a(t) + H^{\mathrm{T}}(t)\mathbf{R}_a^{-1}(t)H(t)\mathbf{P}_a(t)\right]\boldsymbol{\lambda}(t)\right. \\ \left. - H^{\mathrm{T}}(t)\mathbf{R}_a^{-1}(t)\left(\boldsymbol{y}_a(t) - h(\hat{\boldsymbol{x}}_a(t)) - \frac{1}{2}\sum_{i=1}^{d_m}\phi_i^h tr\left[\left.\frac{\partial^2 h_i}{\partial x_a^2(t)}\right|_{\hat{\boldsymbol{x}}_a(t)} \overline{\mathbf{P}}_a(t)\right]\right)\right\}\end{aligned} \tag{A-52}$$

$$\overline{\mathbf{P}}_a(t+1) = \eta\overline{\mathbf{P}}_a(t) + (1-\eta)\mathbf{P}_a(t)\boldsymbol{\lambda}(t)\boldsymbol{\lambda}^{\mathrm{T}}(t)\mathbf{P}_a^{\mathrm{T}}(t) \tag{A-53}$$

where $\overline{\mathbf{S}}_a(t) = \mathbf{C}_a^{\mathrm{T}}\mathbf{S}_a(t)\mathbf{C}_a$, $F(t) = \left.\frac{\partial f}{\partial x_a(t)}\right|_{\hat{\boldsymbol{x}}_a(t)}$ and $H(t) = \left.\frac{\partial h}{\partial \boldsymbol{x}_a(t)}\right|_{\hat{\boldsymbol{x}}_a(t)}$; ε is a positive scalar to prevent the term $F(t)F^{\mathrm{T}}(t)$ from being singular and $0 < \eta \le 1$. The value of γ must satisfy (A-46) to ensure the optimized value of $\hat{\boldsymbol{x}}_a(t)$ yields a local minimum of J.

Appendix IV

Since $\boldsymbol{\lambda}(N) = 0$, we have

$$\sum_{t=0}^{N} \boldsymbol{\lambda}^{\mathrm{T}}(t)\mathbf{P}_a(t)\boldsymbol{\lambda}(t) - \sum_{t=0}^{N-1} \boldsymbol{\lambda}^{\mathrm{T}}(t)\mathbf{P}_a(t)\boldsymbol{\lambda}(t) = 0 \tag{A-54}$$

Equation (A-54) can be written as

$$\begin{aligned} 0 &= \boldsymbol{\lambda}^{\mathrm{T}}(0)\mathbf{P}_a(0)\boldsymbol{\lambda}(0) + \sum_{t=1}^{N} \boldsymbol{\lambda}^{\mathrm{T}}(t)\mathbf{P}_a(t)\boldsymbol{\lambda}(t) - \sum_{t=0}^{N-1} \boldsymbol{\lambda}^{\mathrm{T}}(t)\mathbf{P}_a(t)\boldsymbol{\lambda}(t) \\ &= \boldsymbol{\lambda}^{\mathrm{T}}(0)\mathbf{P}_a(0)\boldsymbol{\lambda}(0) + \sum_{t=0}^{N-1} \boldsymbol{\lambda}^{\mathrm{T}}(t+1)\mathbf{P}_a(t+1)\boldsymbol{\lambda}(t+1) - \sum_{t=0}^{N-1} \boldsymbol{\lambda}^{\mathrm{T}}(t)\mathbf{P}_a(t)\boldsymbol{\lambda}(t) \\ &= -\gamma \left\| \lambda(0) \right\|^2_{\mathbf{P}_a(0)} - \gamma \sum_{t=0}^{N-1} \left(\boldsymbol{\lambda}^{\mathrm{T}}(t+1)\mathbf{P}_a(t+1)\boldsymbol{\lambda}(t+1) - \boldsymbol{\lambda}^{\mathrm{T}}(t)\mathbf{P}_a(t)\boldsymbol{\lambda}(t) \right) \end{aligned} \tag{A-55}$$